

Gas Sensing Study of Bi-Doped SnO₂ Thin Films Fabricated by Physical Vapor Deposition Technique

^{1*}Kashinath S. Thakare, ²Umesh. J. Tupe, ³R R. Ahire, ⁴Arun V. Patil

¹Department of Physics, MGV's Maharaja Sayajirao Gaikwad Arts, Science and Commerce College, Malegaon-Camp, Dist. - Nashik -423105, India.

²Department of Electronic Science, Vidya-Amrut Dnyan Pratishthan's Arts, Science and Commerce College, Shirsondi, Dist. Nashik 423208, India

³Sitaram Govind Patil Art's Science and Commerce College, Sakri, Dist. Dhule 424304, India

⁴Department of Physics, MGV's, Arts, Science and Commerce College, Surgana, Dist. Nashik 422211, India

Corresponding author: Kashinath S. Thakare

Abstract:

Gas sensing properties of Bi-doped SnO₂ thin films fabricated by Physical vapour deposition technique have been reported in this paper. Undoped and doped tin oxide semiconductors have applications in sensing many toxic gases and volatile organic compounds such as CO, CO₂, H₂S, Cl₂, Ethanol etc., For example, Ethanol sensors is used as a breath analyser, because the ethanol vapor in human breath can be correlated with its concentration in the blood. CO₂ being odourless, is difficult to be detected by smelling, requires smart sensors. Bismuth (Bi) is preferred as dopant material because the doping in SnO₂ produces a greater number of oxygen vacancies that act as active surface sites for the adsorption of oxygen. These oxygen vacancies excel response properties for a sensor material. Bi-doped SnO₂ may be used as CO₂ gas sensor. There are many reports in the literature that highlight the gas sensing properties of doped nano structured SnO₂.

Key words: Thin films, tin oxide, CO₂ sensor, doping, sensitivity, selectivity of sensor.

1. Introduction:

Since last few decades, among various oxides, SnO₂ (tin oxide) semiconductor films have been widely employed in recognition of volatile organic compounds as stable gas sensors. They are also used in monitoring the environment, industries etc. [1], as window layer in solar cells [2], as gas sensors to sense hazardous gases like CH₄, CO, NO_x, CNG etc.

[3-5]. SnO₂ and TiO₂ are promising gas sensors because [6-9] of their advantages like low cost, simple fabrication methods, and rapid response and recovery times [10].

Doping is one of the expected methods of enhancing the conductivity and stability of the sensor by incorporating an atom or ion into host material [11, 12]. Although numerous studies have been conducted on the electronic and optical properties of different semiconductor oxides doped with metals, only a few theoretical studies exist on metal-doped semiconductors oxides [13-15]. The present study aims to systematically study the effect of Bi doping concentration on the structural properties, conductivity and stability of SnO₂ by combining theoretical calculations with our experiments.

Gas monitoring devices are in demand for a rapidly growing range of applications. Sensors play an important role in the areas of emissions control, environment protection, public safety, and human health [16, 17]. Much more public concern today than ever before over serious environmental issues is further promoting the development of sensors with both high sensitivity and rapid response. Metal oxide based chemical sensors have been used extensively for the detection of toxic pollutant gases, combustible gases and organic vapours. The main advantages of chemical sensors are low price, small size, high sensitivity, and low power consumption. Ethanol is one of the most commonly used and wide spread alcohols, and thus there is a need to develop sensors for its detection. The most common application of ethanol sensors is as a breath analyser, since the ethanol vapor in human breath can be correlated with its concentration in the blood [18]. Bi was preferred as dopant material because the doping of Bi in SnO₂ produces number of oxygen vacancies. These vacancies act as active surface sites for the adsorption of oxygen which is very essential to possess excellent response properties for a sensor material. There are many reports in the literature that highlight the gas sensing properties of undoped and doped nano structured SnO₂. Q. He et. al. reported the effect of Bi doping on room temperature gas response properties of SnO₂ [19]. The physical synthesis method includes PVD. PVD is a form of thin film deposition, which is a vacuum-based process for coating the surfaces of different objects with pure materials. Coatings, also known as films, are commonly in the angstroms to microns thickness range and may be made up of a single material or a layered system of several materials. Thermal evaporation technique can be used to add pure atomic elements, such as metals and nonmetals, as well as molecules like oxides and nitrides. PVD is a vacuum coating process in which a coating material film is deposited atom by atom on a substrate by

condensation from the vapor to the solid phase. The basic operation principle of PVD is based on vacuum. During the deposition of thin film by vacuum evaporation following three steps are involved shown in Figure 1.

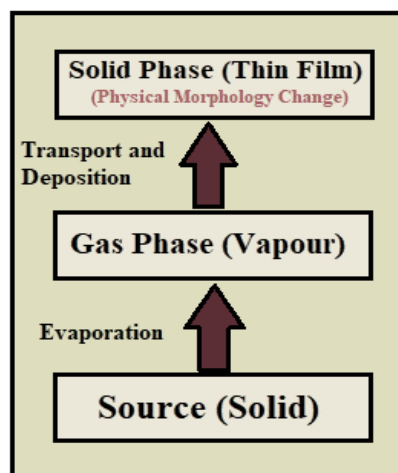


Fig. 1: Steps of thin film deposition in PVD

The aim of present work is to investigate the structural, morphological, electrical and gas sensing properties of Bi-doped SnO₂. We have successfully fabricated Bi-doped SnO₂ thin films on standard glass substrates by using Physical Vapour Deposition. The prepared film samples were analysed using X-ray diffraction (XRD), FESEM, EDAX, Static gas sensing system etc.

2. Materials and Method:

Commercially available SnO₂ and Bismuth Oxide nanoparticles (purity 99.99%) were used for the fabrications of Bi-doped SnO₂ thin films. Thin films were prepared by using PVD system. The system consist vacuum pump system, which was evacuated to 10⁻⁶-10⁻⁷ mbar pressure by rotary and diffusion pump appropriate arrangement shown in Figure 2. The molybdenum boat is used to hold the nanoparticles of SnO₂ and bismuth in evacuated glass chamber with appropriate arrangement of equipment like thermometer, power supply, high current transformer and others. The chamber was filled with vacuum and for deposition purpose clean glass substrates were used, the glass substrates were cleaned using acetone and IR lamp. Nanoparticles of SnO₂ and bismuth place in molybdenum boat by some standard arrangement and using maximum voltage power supply, which was used as the target for evaporation. Then, prepared thin film were annealed using muffle furnace at temperatures 400 °C and then used further study.

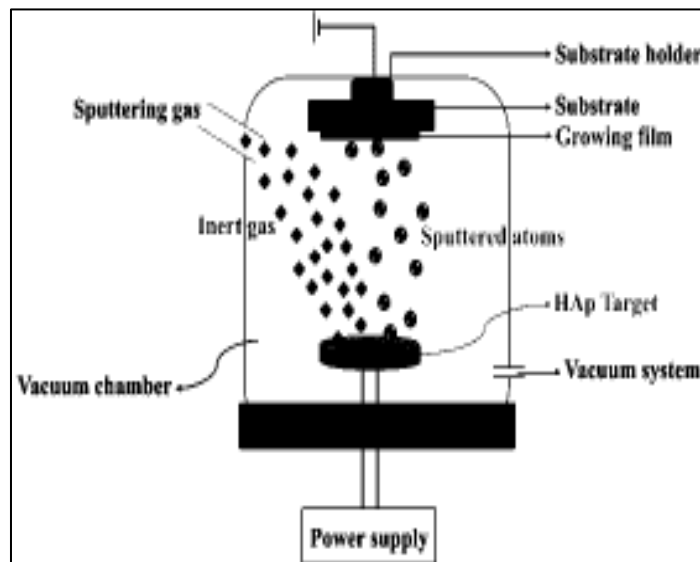


Fig. 2: Schematic diagram of physical vapour deposition method

The film thickness in the present work has been measured by weight difference method

within the error limited by the electronic balance used. The mass of the substrate was calculated before depositing of films. The material was deposited on rectangular glass substrate. The mass of the deposited thin film was again measured. The difference between two masses gave the net mass of the material deposited. Thickness of the films was calculated using the standard formula for the density, given by

$$t = \frac{\Delta m}{lb\rho} \quad \dots (1)$$

Where, Δm is weight difference of the material before and after deposition, l is length of the film deposited, b is breadth of the film and ρ is composite density of the deposited material. Thicknesses of most of the thin film samples calculated by this method were from 80 to 90 nm. The samples were characterized using X-ray diffraction i.e., XRD (D8 Advance Bruker-AXS with Cu $K\alpha 1$ source), FESEM (Hitachi-S-480-II) and Energy Dispersive Spectra. The electrical characteristics of the films were studied at varying temperature using a simple potential divider arrangement. Sample resistance was calculated by using the equation

$$R_{\text{film}} = R_{\text{ref}} \left(\frac{V_{\text{film}}}{V_{\text{ref}}} - 1 \right) \quad \dots (2)$$

Temperature coefficient of resistance (TCR), with room temperature resistance R_0 was calculated by using the relation,

$$\text{TCR} = \frac{1}{R_0} \frac{\Delta R}{\Delta T} \text{ } ^\circ\text{C} \quad \dots (3)$$

where, ΔR = change in resistance between temperature T_1 and T_2 , corresponding to temperature difference ΔT between T_1 and T_2 .

Activation energy (ΔE) of the electron transport in conduction band at high and low temperature regions was calculated from Arrhenius equation

$$R = R_0 e^{-\frac{\Delta E}{k_B T}} \quad \dots (4)$$

where, R_0 = room temperature resistance, k_B = Boltzmann constant and T = absolute temperature of film sample.

Gas sensing properties were studied in a gas sensing apparatus. The film samples were exposed to different gases such as Acetone (C_3H_6O), Ammonia (NH_3), Carbon Dioxide (CO_2), Chlorine (Cl_2), Ethanol (CH_4O) and Hydrogen Sulphide (H_2S) at varying gas concentrations and film resistance was measured (R_g). Gas concentration in ppm is given by the equation (5),

$$\text{Gas concentration (in ppm)} = \frac{\text{volume of injected gas in cc}}{\text{volume of bell-jar in cc}} \times 10^{-6} \quad \dots (5)$$

Resistance of the thin films was measured over the temperature range from $50^\circ C$ to $375^\circ C$ at the intervals of $25^\circ C$. Sensitivity (gas response) of the film samples is given by

$$\text{Sensitivity} = \left| \frac{R_a - R_g}{R_a} \right| = \frac{\Delta R}{R_a} \quad \dots (6)$$

Where, R_a = resistance of the sample in air and R_g = the resistance of sample in a particular gas ambience. Optimum temperature was found from the selectivity of the samples. At this temperature, CO_2 was tested for gas concentrations varying from 100 to 500 ppm in 25 lit. glass bell-jar.

3. Results and Discussion:

Structural Analysis by XRD

Figure 3 show the XRD patterns of Bi-doped SnO_2 thin film. Films were scanned over the range of 2θ from $20-80^\circ$. The (hkl) planes (120) and (111) correspond to orthorhombic phase of tin oxide. The data matched with that from the JCPDS data card [20] and the additional peaks (110) correspond to rhombohedral phase of bismuth. The observed data matched with JCPDS card [21]. The centred cubic phase of bismuth oxide γ phase according to JCPDS card no. 74-1375. Crystalline nature of the films is clearly seen from the data given in Table 1. The crystallite size of Bi-doped SnO_2 thin film was calculated using Debye sheerer formula and it was found to be 4.26 nm. The small size of crystallite particle is very

useful for gas sensing applications. Because the as crystallite size decreased the volume to surface area of particle is increased which provide more rate of adsorption of gas molecules on the surface of film.

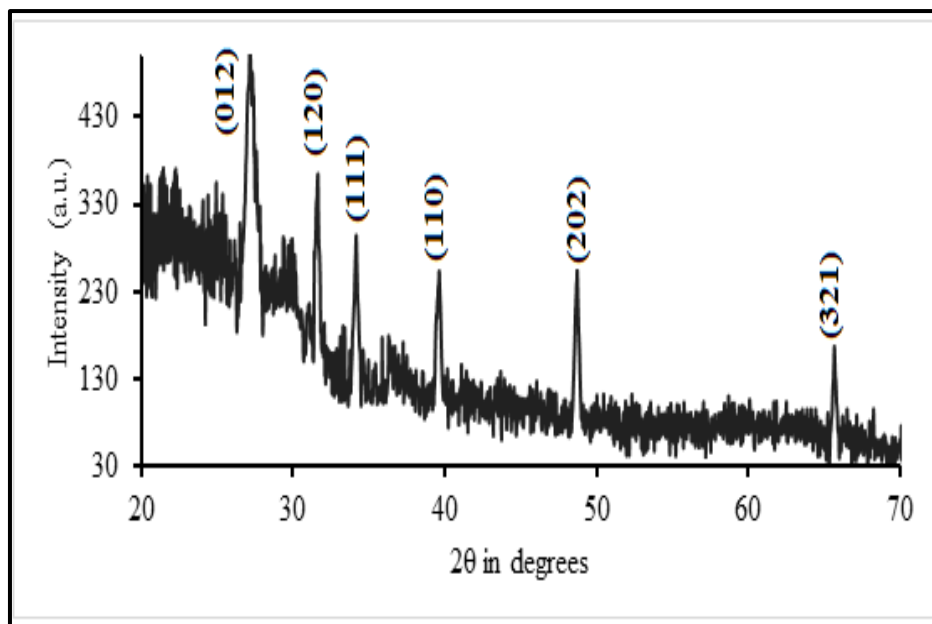


Fig. 3: XRD patterns of Bi-doped SnO₂ thin film

Table 1: Outcomes of Bi-doped SnO₂ from XRD pattern

Peak Position 2θ	(hkl) plane	FWHM (rad)	Crystallite size (nm)
27.16	012	0.03	4.26
31.63	120	0.01	11.01
34.15	111	0.02	10.27
39.61	110	0.01	10.83
48.70	202	0.01	19.39
65.62	321	0.01	24.25

Surface Morphology using FESEM

The surface morphologies of Bi-doped SnO₂ thin film obtained by using FESEM are shown in Figure 4. Average grain size Bi-doped film, were observed to be 65.61 nm. The compactness and agglomeration of the grains is clearly seen from the FESEM images of doped film. This is possibly due to annealing of the samples. The FESEM image of Bi-doped SnO₂ thin film shows the formation of spherical particles as well as the more porosity of

nanoparticles. The more porosity or voids are beneficial for gas sensing mechanism, these voids promote more reactive surface in presence of gas molecules.

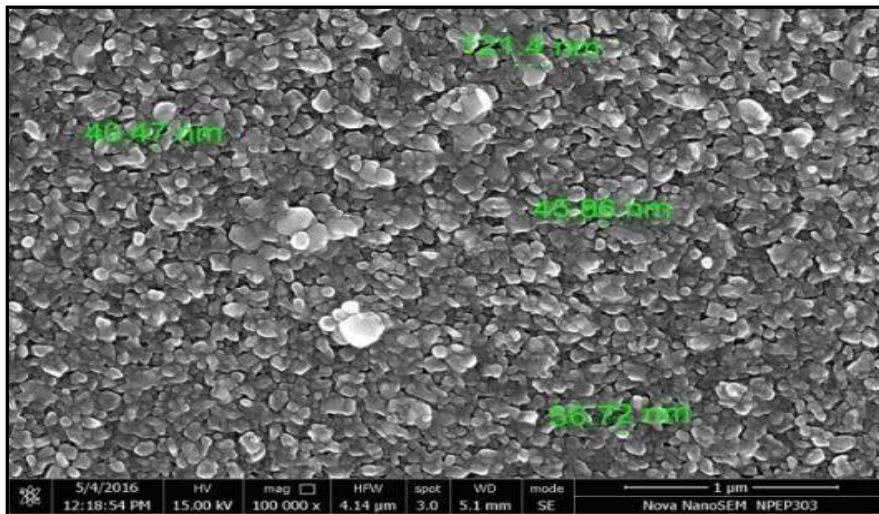


Fig. 4: FESEM image of Bi-doped SnO₂ thin film

EDAX Analysis

Figure 5 shows Energy Dispersive Spectra of Bi-doped SnO₂ thin film. Table 2 indicates the atomic and weight percentage of Sn, O and Bi. Non-stoichiometry of oxygen is seen from the data.

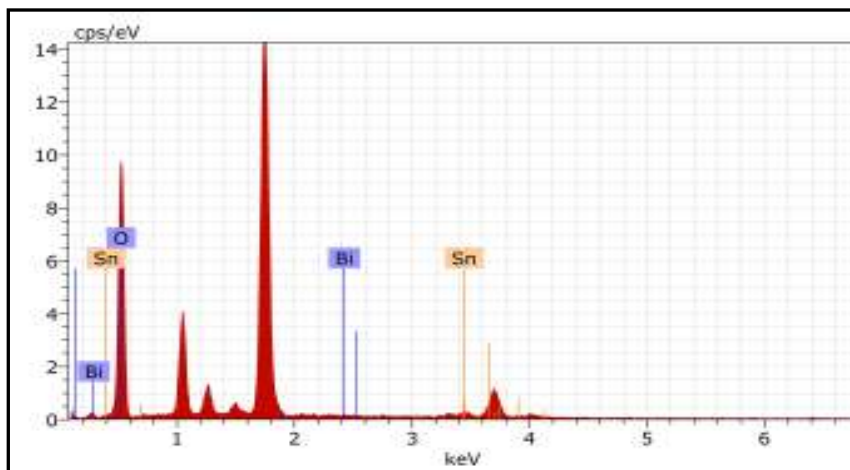


Fig. 5: EDAX spectra of Bi-doped SnO₂ thin film

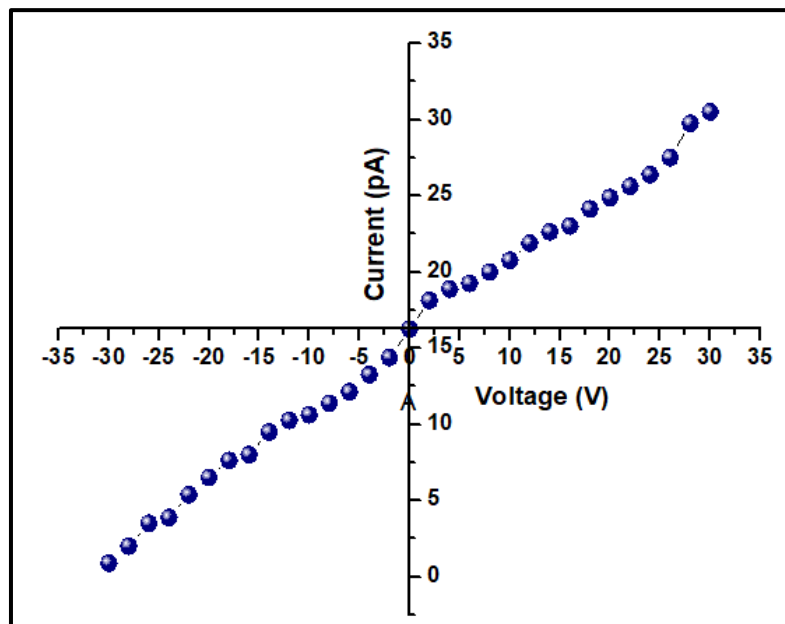
Table 2: Elemental Composition of Bi-doped SnO₂ from EDAX

Type of sample	Atomic Number	Element	Weight %	Atomic %
Bi-doped SnO ₂	50	Sn	12.48	01.89
	8	O	87.43	98.10
	83	Bi	0 0.09	00.01
		Total	100.00	100.00

Electrical Characteristics

A. I-V Characteristics

I-V characteristics of the of Bi-doped SnO₂ thin film were studied by simple series circuit constituting the sample in series with a regulated voltage source, a digital voltmeter and a picoammeter I-V characteristics for of Bi-doped SnO₂ thin film is shown in Figure 5.

**Fig. 5:** I-V characteristics of Bi-doped SnO₂ thin film

The resistance of the of Bi-doped SnO₂ thin films is observed to decrease. This is because of enhancement in the conduction due to doping. The characteristics also confirm ohmic nature of the of Bi-doped SnO₂ thin films.

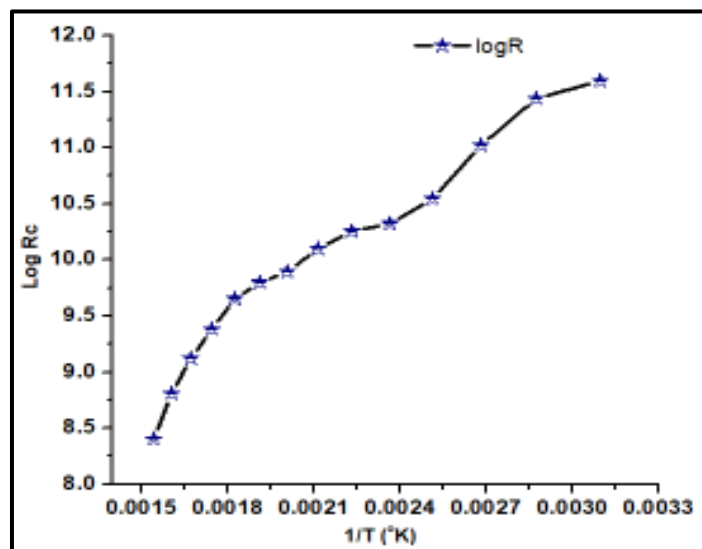


Fig. 6: Arrhenius plot of Bi-doped SnO₂ thin film

Fig. 6 represents variation in log R_c as a function of reciprocal of absolute temperature (Arrhenius plot) to estimate activation energy. Activation energy was estimated for low and high temperature regions. It was low in the low-temperature region since at lower temperatures supplied thermal energy was not enough to overcome the potential barrier. As the temperature increased, supplied energy also increased therefore in high-temperature region activation energy got altered. The activation energy is calculated at low temperature region was 0.08 eV and at high temperature region was 0.17 eV.

Gas Sensing Characterizations

The gas sensing behaviour of fabricated Bi-doped SnO₂ thin films was studied by using static measurement system. DC resistance measurement, by voltage divider method, was employed for sensitivity measurement as a function of temperature and target gas concentration. The Bi-doped samples were tested for acetone vapours, chlorine, carbon dioxide, ethanol vapours, hydrogen sulphide and ammonia for their concentrations in air ambience varying from 100 ppm to 500 ppm. The target gases were tested for temperature range varying from 50°C to 200°C. Figure 7 represents sensitivity versus temperature of Bi-doped SnO₂ thin films to selected target gases. It has been observed that the fabricated Bi-doped SnO₂ thin films shows maximum sensitivity to CO₂ gas at operating temperature 125 °C and gas concentration 300 was ppm. It was also found that films showed higher response to CO₂ over other gases. Gas response initially increases, reaches maximum to at 125 °C and then decreases for higher temperatures.

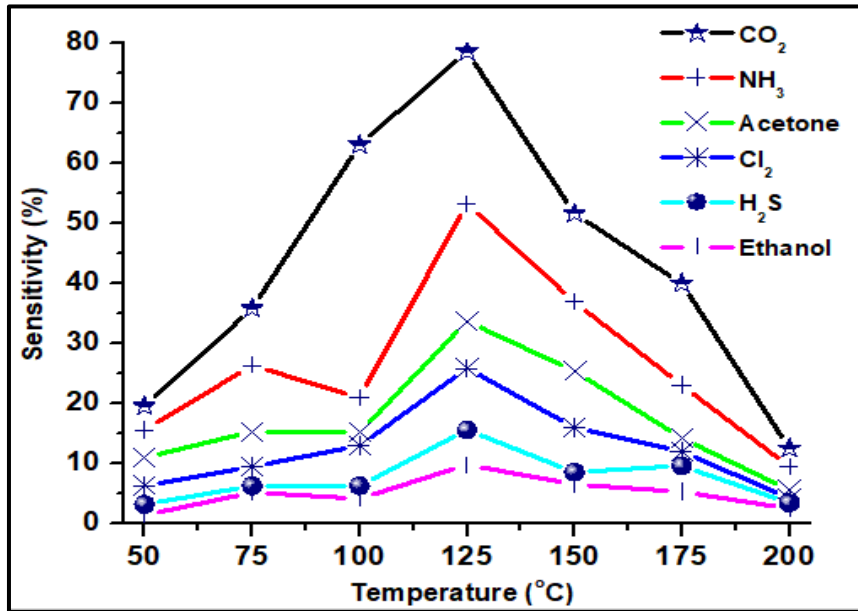


Fig. 7: Temperature versus sensitivity plot of Bi-doped SnO₂ thin film

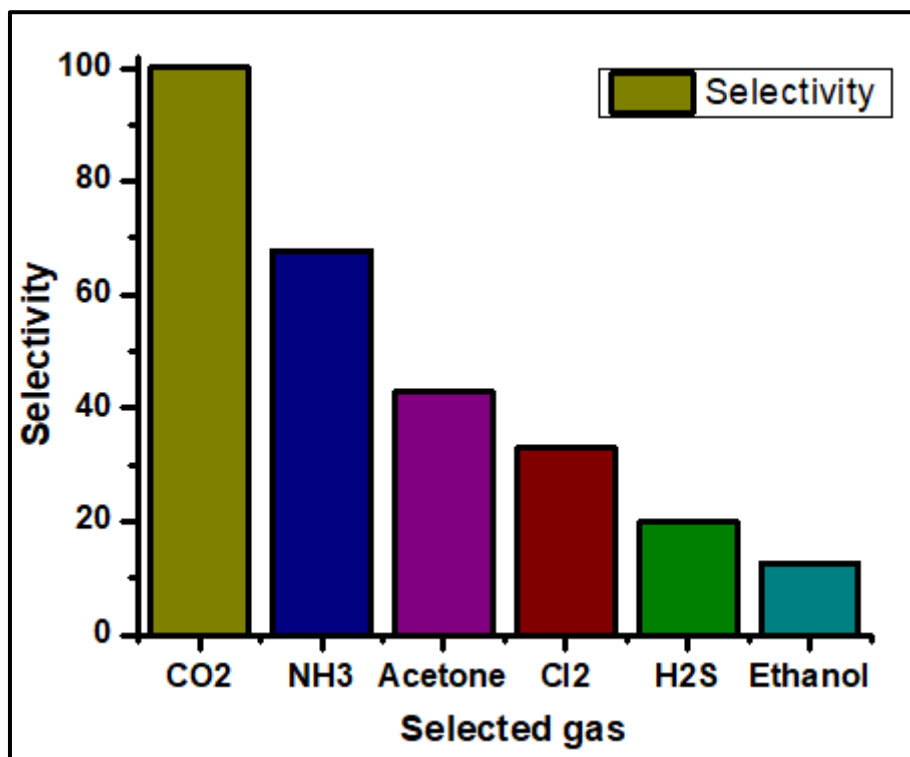


Fig. 8: Selectivity plot of Bi-doped SnO₂ thin film

Selectivity can be determine the response of particular analyte of gas among the mixture of gases. The selectivity plot of Bi-doped SnO₂ thin film is illustrate in Figure 8. The maximum selectivity was found to be CO₂ gas compared to other selected gases as shown in figure 8.

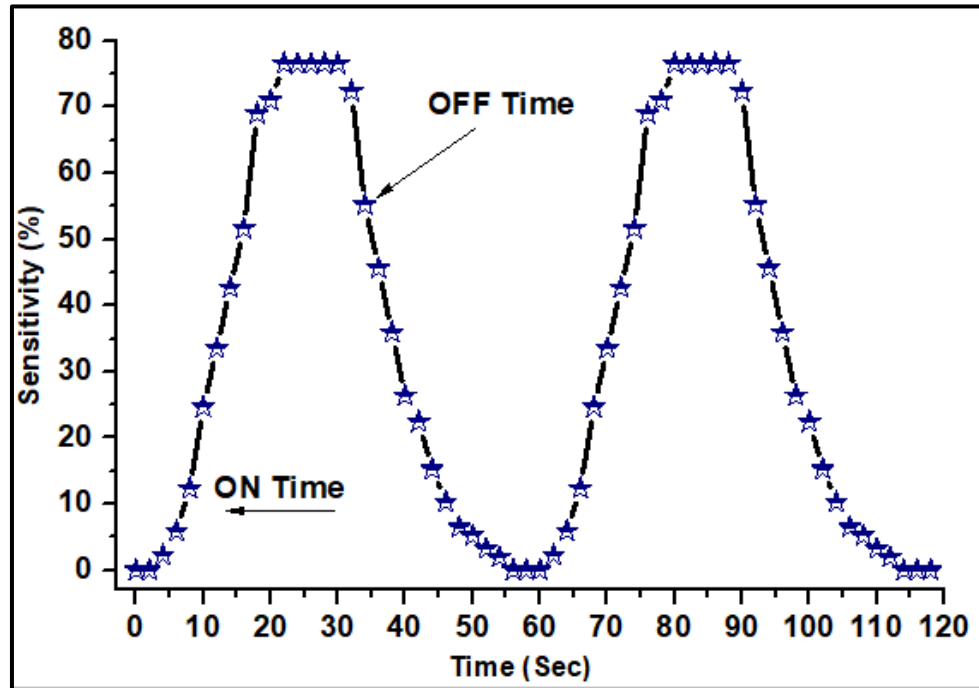


Fig. 9: Response time and recovery time plot of Bi-doped SnO₂ thin film

Response and recovery times are two important parameters of a gas sensor since their values determine the applicability of the sensor. In gas detection, response time is usually defined as the time taken to achieve 90% of the final change in conductance of the sensor in a given gas concentration [24]. Recovery time is the time taken to return from the conductance in a given gas concentration to 90% of initial conductance of the sensor [24]. The response time and recovery time were measured for CO₂ gas at operating temperature 125°C and concentration of 300 ppm of CO₂ gas as shown in Figure 9. The response and recovery times were observed to be ~9 s and ~33 seconds respectively. Any novel gas sensor has required low gas concentration and lower operating temperature. The ppm variations of CO₂ gas at operating temperature 125°C was carried out and the obtained result is revealed in Figure 10.

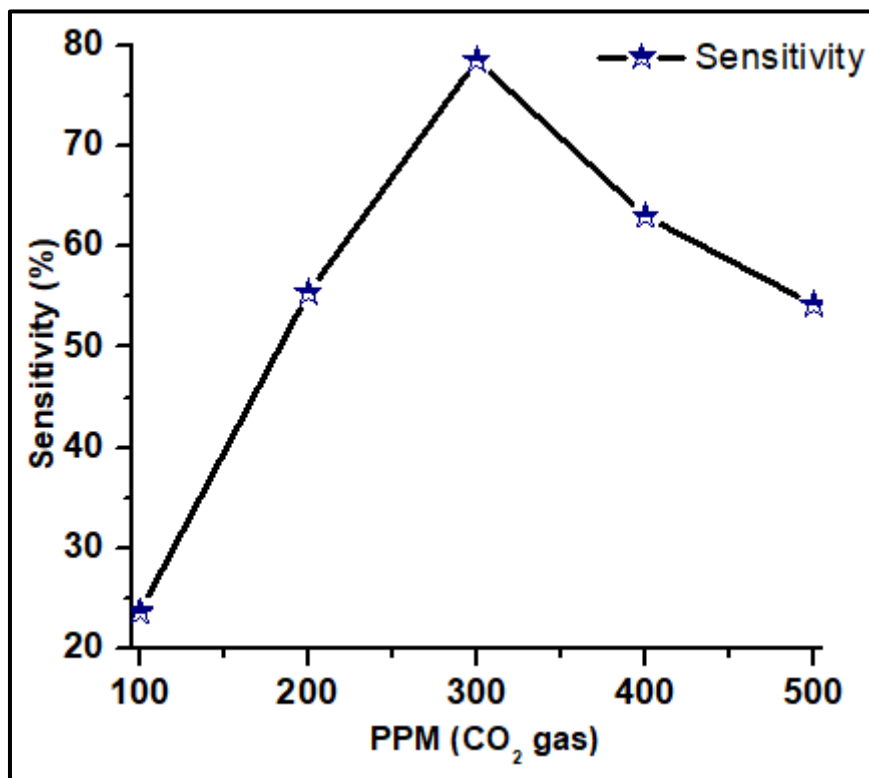
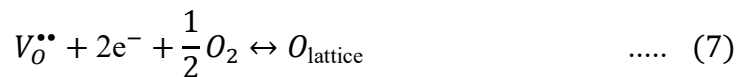


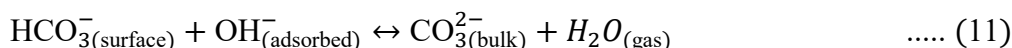
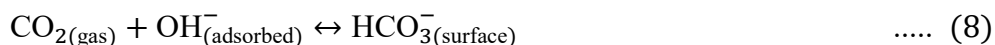
Fig. 10: CO₂ gas variation (ppm) versus sensitivity plot of Bi-doped SnO₂ thin film

Gas Sensing Mechanism

The metal oxide semiconductor gas sensors work on the principle of chemoresistance i.e., there is change in electrical conductivity of the film when exposed to a target gas. Thus, a gas molecule acts as either a donor or acceptor of charge carriers. Thus, chemoresistive property changes conductivity associated to adsorption and desorption of gas molecules on the surface of metal oxide. As lower layer of atmosphere is composed of nitrogen, oxygen and water molecules along with other gases in traces, metal oxide surface sensing depends upon wet and dry ambience on its surface. Water molecules have major role in wet conditions and oxygen plays a decisive role in dry atmosphere [27]. Thus, the response of metal oxide towards a specific target gas is a net change in resistance due to gas solid interaction in the ambient atmosphere. The following equation describes the adsorption process in case of oxygen deficient sites ($V_{O}^{\bullet\bullet}$) on the metal oxide surface. Oxygen from the ambient diffuses to the oxygen vacant sites in metal oxide surface by consuming one or two free electrons Eq. 7. Thus, the chemisorptions of oxygen molecules reduce the mobility of electrons leading to reduction in conductance in n-type materials and reduce the active sites for further adsorption.



Carbon dioxide molecule has linear bonded atoms and has no lone pair of electrons for bonding. Ostrick et. al. [28] have reported that at low temperatures, the dissociated hydroxyl and hydrogen ions from water molecules at the surface of metal oxide react with gaseous CO₂ to form carbonate ions (CO₃²⁻) as given in Eqns. (8) - (11), with the intermediate products, formate ions and bicarbonate ions [29]. At high temperatures, CO₂ molecules interact with the layered oxygen ions (O²⁻) directly to form carbonate ions [30] as given in Eqn. (12).



Besides the oxygen adsorption, CO₂ molecules further oxidized the metal oxide surface and increase the surface resistance (Fig.12). Following REDOX mechanism is proposed to explain

the interaction of oxygen and CO₂ on the metal oxide surface.



Since highly stable CO₂ gas showed poor response when reacted with pure SnO₂ metal oxide film, researchers prepared doped SnO₂ films to solve the challenge. Doping is one of the most effective techniques for an enhancement of gas response and selectivity of metal oxide gas sensors [31-34]. Different dopants were tried for this purpose [35].

Oxygen is adsorbed on the metal oxide surface when the film is heated in air. At lower temperatures, the surface reaction proceeds very slowly. The adsorption of oxygen forms ionic species including O₂⁻, O⁻ and O²⁻, which have acquired electrons from the conduction band. The adsorption kinematics is explained by the following reaction paths [36-38]. The oxygen ions O₂⁻, O⁻ and O²⁻ are stable below 100°C, between 100 and 300°C and above 300°C respectively [39].





They are correspondingly adsorbed from surface temperatures of 80°C, 130°C and 250°C respectively. The electron transfer from the conduction band to the chemisorbed oxygen leads to the decrease in the electron concentration in the film. For n-type semiconducting metal oxide, resistance of metal oxide film increases. The operating temperature dependence of sensing properties could result from changing adsorption and desorption rates of oxygen ions on metal-oxide surface [40].

The adsorption of O^- is very interesting step in metal oxide semiconducting gas sensor because the O^- ions assist the adsorbed oxidizing ions to take the electrons from the metal oxide surface. The concentration of electrons on the surface of metal oxide decreases and the resistance of n-type metal oxide layer increases accordingly [41]. The of Bi-doped SnO_2 thin films gas sensing mechanism is shown in figure 11.

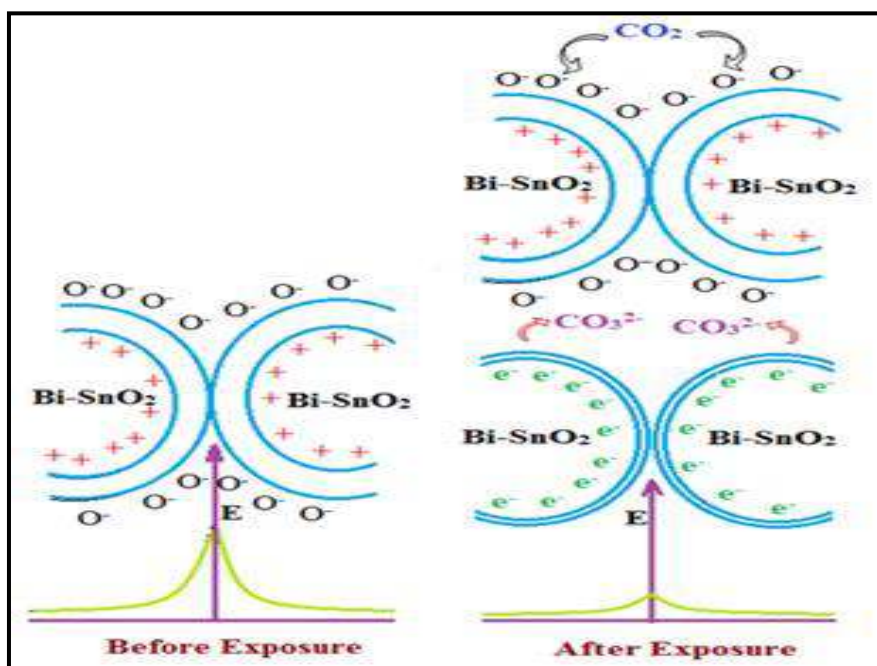


Fig. 11: Gas sensing mechanism of Bi-doped SnO_2 thin film before and after exposure to CO_2 gas

Conclusions

1. The Physical Vapour Deposition method can be used to fabricate of Bi-doped SnO_2 thin films.
2. Once the appropriate vacuum is obtained, a large number of uniform and contamination free thin films can be fabricated at room temperature by this method.
3. EDAX studies confirmed the nonstoichiometric of the Bi-doped SnO_2 thin films.

4. Surface properties have not changed appreciably. Electrical characterizations support the n-type semiconducting nature of the films deposited.
5. Since film samples showed maximum response at an operating temperature of 125°C to CO₂ gas, they can be used as CO₂ gas sensor.

Acknowledgement:

The authors are thankful to the Principal, MGV's, M. S. G. Arts, Commerce and Science College, Malegaon, Tal- Malegaon, Dist. Nashik, Maharashtra, India for providing required lab facilities for the present research work. Authors also thanks to of Head of department chemistry and CIF departments, SPPU, Pune for provided extensive support to SEM, EDS and XRD characterizations for this work.

Conflict of Interest: There are no any conflict of interest.

References:

1. G.W. Hunter, C.C. Liu, D. B. Makel and M. G. Hak (Ed), The MEMS Hand Book, CRC Press (2002) 1-22
2. A. Gotzberger and C. Helbing Sol. Energy Mater and Solar cells 62 (2000) 1
3. R. S. Niranjana and I. S. Mulla, Mater. Eng. B 103 (2003) 103
4. O. K. Varghese and L. K. Malhotra, Sensor & Actuators B 53 (1998) 19
5. N. S. Baik, G. Sakai, N. Muira and N. Tamajoe, Sensor & Actuators B 63 (2000) 74
6. Z. Wang and L. Liu: Mater. Lett. 63 (2009) 917-919
7. C. T. Wang and M. T. Chen: Mater. Lett. 63 (2009) 389-390
8. M. Hemissi, H. Amardjia-Adnani and J. C. Plenat: Current Appl. Phys. 9 (2009) 717-721
9. D. Zhang Y. Kim and Y. Kang: Current Appl. Phys. 6 (2006) 801- 804
10. Wen Zeng, Tianmo Liu and Zhongchang Wang–Materials Transactions, vol. 51, 2 (2010) 243-245
11. Y. Yang, Y. Jin, H. He, Q. Wang, Y. Tu, H. Lu and Z. Ye, Journal of the American Chemical Society 132 (2010) 13381
12. D. Fattakhova-Rohlfing, T. Brezesinski, J. Rathousky, A. Feldhoff, T. Oekermann, M. Wark and B.M. Smarsly, Advanced Materials 18 (2006) 2980
13. J. Osorio-Guillén, S. Lany and A. Zunger, Physical Review Letters 100 (2008) 036601

14. Z.Q. Li, Y.L. Yin, X.D. Liu, L.Y. Li, H. Liu and Q.G. Song, *Journal of Applied Physics* 106 (2009) 083701
15. W. Dong et al. *Electrochimica Acta* 132 (2014) 307–314
16. J. Park, X. Shen and G. Wang, *Sens. Actuators B* 136 (2009) 494–498
17. A. Kolmakov and M. Moskovits, *Ann. Rev. Mater. Res.* 34 15 (2004) 1–180
18. L.P. Chikhale, J.Y. Patil, F.I. Shaikh, A.V. Rajgure, R.C. Pawar, I.S. Mulla and S.S. Suryavanshi, *Materials Science in Semiconductor Processing* 27 (2014) 121–129
19. Q. He, W. Tu and J. Hu, *J. Mater. Sci.* 42 (2007) 8292–8297
20. JCPDS data card 01-075-9499
21. JCPDS data card 00-005-0519
22. R.C. Pawar, J.W. Lee, V.B. Patil and C.S. Lee, *Sens. Actuators B. Chem.* 187 (2013) 323–330
23. L.K. Bagal, J.Y. Patil, I.S. Mulla and S.S. Suryavanshi, *Ceram. Int.* 38 (2012) 4835–4844
24. T. Ishihara, K. Kometani, M. Hashada and Y. Takita, *J. Electrochem Soc.*, 138 (1991) 173
25. P. T. Moseley and B. C. Tofield, 'Solid state gas sensors', J. W. Arrow Smith, Britol, (1987) 56
26. C. Liewhiren and S. Phanichphant, *Sensors* 7 (2007) 1159-1184
27. Prabhakaran Shankar and John Bosco Balguru Rayappan, *Science Jet* (2015) 4:126
28. B. Ostrick, M. Fleischer, H. Meixner and C.D. Kohl, *Sens. Actuat. B* 68 (2000) 197
29. O. Wurzinger, G. Reinhardt, *Sens. Actuat. B* 103 (2004) 104
30. M. J. Madau and S. R. Morrison, Academic Press, San Diego (1989)
31. N. Butta, M. Meli and S. Pizzini, *Sensors and Actuators B* 2 (1990)151-161
32. K. D. Schierbaum, J. Geiger, U. Weimer and W. Göpel, *Sensors and Actuators B*, 13-14 (1993) 145-147
33. J. Mizsei, *Sensors and Actuators B* 15-16 (1993) 328-333
34. J. Tamaki, T. Maekawa, N. Miura and N. Yamazoe, *Sensors and Actuators B* 9 (1992) 197-203
35. A. Galdikas, V. Jasutis, S. Kaciulis, G. Mattogno, A. Mironas, V. Olevano, D. Senuliene and A. Setkus, *Sensors and Actuators B* 43 (1997) 140-146
36. A. Iabidi, E. Gillet, R. Delamare, M. Mareff and K. Aguir, *Sens. Actuators B: Chem.* 120 (2006) 338-345

37. R. S. Khadayate, M. T. Chaudhari, S. K. Disawal and P. P. Patil, *Invert. J. Sci. Technol.* 2 (2009) 185-189
38. P. P. Sahay and S. Tewari, *Sprayed ZnO thin films for ethanol sensors*, *J. Mater. Sci.* 40 (2005) 4791-4793
39. T. V. Belysheva, I. P. Bogovtseva, E. A. Kazachkov and N. V. Serebryakova, *J. Anal. Chem.* 58 (2003) 583-587
40. A. Z. Sadek, S. Choopun, W. Wlodarski, S. J. Ippolito and K. Kalantar-zadeh, *IEEE Sens. J.* 7 (2007) 919-924
41. K. Wetchakun, T. Samerjai, N. Tamaekong, C. Liewhiren, C. Siriwong, V. Kruefu, A. Wisitsoraat, A. Tuantranont and S. Phanichphant, *Sensors and Actuators B* 160 (2011) 580-591



Versatile synthesis of zinc oxide nanoparticles via chemical route: A review

Komal Bachhav^{a,b}, Arun S. Garde^{b,*}

^a Shri Vasantao Naik Arts, Science and Commerce College, Dhoni, Amravati 444702, India

^b M. S. G. Arts, Science and Commerce College Jalgaon camp, Jalgaon, Nark 423203, India

ARTICLE INFO

Keywords:
Nanotechnology
Sol-Gel
Co-Precipitation
Hydrothermal
Microemulsion
Solvotharmal

ABSTRACT

Nowadays, nanotechnology accomplishes a vital role in different sectors due to its applications, among the range of nanoparticles, metal oxide nanoparticles are potent candidates. Various metal oxide nanoparticles are significantly known today, and ZnO nanoparticles are extensively studied among them. ZnO nanoparticles are highlighted in several fields like pharmacy, optics, cosmetics, gas sensors, catalysis, electrochemistry, textile industries, polymer industries, and many more due to the availability of starting material, simple and efficient synthesis methods, and desired morphology. Numerous Physical, Chemical and Biological processes are trending and employed for synthesizing ZnO nanoparticles. This article reviews chemical route synthesis methods such as, Sol-Gel method, Co-Precipitation, Hydrothermal, Microemulsion, and Solvotharmal method for the synthesis of ZnO nanoparticles. It also focuses on ZnO NPs Characteristics, Characterizations and applications.

1. Introduction

Nanotechnology has attracted researchers in the last few years. Globally research and developments are concentrated around nanotechnology [1]. "There is plenty of room at the bottom" speech at Caltech in 1959 by the eminent theoretical physicist Richard P. Feynman gives vision and progression to nanotechnology [2-4]. The word 'nano' means size in terms of nanometre, particles having an atomic size between 1 and 100 nm are termed 'nanoparticles' (NPs) [5]. Nanomaterial particles display diverse properties due to their large surface area to volume ratio compared to bulk material [4,6]. Nanotechnology is gaining high attention worldwide due to its small size, higher efficiency, and simple synthesis method and applications of NPs in diverse sector [5,6]. Different factor affects the synthesis, morphology and materialistic properties of nanoparticles, which depends on numerous parameters [7-9]. It is conducive in different industrial fields such as optics, electrochemistry, catalysis, textile industries, various sensors, photocatalyst, optical devices, also applications in drug delivery, pharmaceutical, medical devices, food technology, cosmetics, and industry [10-20]. Numerous metal oxide has been practiced to the developed diverse gas sensor but among all zinc oxide is extensively used for the synthesis of gas sensors [21,22]. Increasing population increases the demand for all needy stuff with the sake of completing the requirement increase industrial production cause emission of numerous hazardous gases and pollutant directly dumped into the atmosphere. Gaseous

pollutant causes severe issues to human beings and also nature. To protect and preserve the environment and related problems faced by humans, it's important to detect and identify the hazardous gas and different constituent present in the atmosphere [15,23,24]. Metal oxide-based chemical sensor exhibits a noteworthy part in detecting and finding out the concentration of hazardous gases present in the atmosphere [25]. The synthesis of zinc oxide is attracted researchers and industries due to its versatile properties. It is an n-type of semiconductor having a wide bandgap (3.37 eV) with large exciton binding energy (60 meV) [26-28]. Zinc Oxide nanoparticles have been widely used nanoparticles with wide applications in numerous fields like gas sensors [29-31], solar cells [32], luminescent materials [33], photocatalysts [34], Paint [35], piezoelectric transducers [36], diode lasers [37]. Various synthetic routes are used to synthesize zinc oxide nanoparticles with desirable size, morphology, and orientation act as a key factor in the diverse application [29,38,39]. Synthesis of nanoparticles via different routes such as physical, biological, and chemical methods are depicted in Fig. 1. The prime objective of this review article is to give a perception of a synthesis of zinc oxide nanoparticles by numerous chemical methods and conditions to get desirable size nanoparticles with expected morphology.

2. Chemical methods for synthesis of nanoparticles

Wet chemical methods for the synthesis of nanoparticles are mainly

* Corresponding author.

E-mail address: asgarde1982@gmail.com (A.S. Garde).

<https://doi.org/10.1016/j.matpr.2023.08.269>

Received 14 June 2023; Received in revised form 15 August 2023; Accepted 22 August 2023

2214-7853/Copyright © 2024 Elsevier Ltd. All rights reserved. Selection and peer-review under responsibility of the scientific committee of the International Conference on Advances in Materials, Mechanics, Mechatronics and Manufacturing.

K. Bachhav and A.S. Gardi

categorized as bottom-up approach methods [40] in which particles, atoms, molecules, or ions in solution build up to form the desired shape, size, and dimensions of nanoparticles. It specifies the nucleation and growth of nano-size particles through bottom-up manufacturing [41]. Chemical synthesis of NPs can be achieved by the execution of a range of chemical reactions and several different thermodynamic parameters [42,43]. To reach a specific shape and size of NPs, the selection of reactants, reagents, reaction temperatures, solvents, catalytic entities, proportion and concentration of compositions, annealing rates, time and many influent factors comes into account. The properties of nanoparticles are depended very much on their size [44], so precise and meticulous synthesis of NPs becomes the most prominent attention. Choice of synthesis method of nanoparticles play a crucial role for nanoparticle properties such as surface structure, shape, size, physiological properties along with controlled reaction conditions such as temperature, pressure, solvent, which may affect nucleation and growth of the nanoparticles leads to change their properties [45-48]. Among the several advantages of the wet chemical synthesis method, some are, it is simple and economical with handy instruments [49]. Less temperature requirement for processing and the least energy input is an asset in choosing the chemical method [50]. Several chemical methods have been used to synthesize various NPs, enumerating as Sol-Gel method, Co-Precipitation method, Hydrothermal Synthesis, Microwave-assisted method, Emulsion / Microemulsion, Chemical Vapour deposition, and solvothermal among these methods, we focus on selective methods of synthesis of ZnO nanoparticles. The synthesis of nanoparticles via chemical routes is depicted in Fig. 2.

2.1. Sol - gel method

The chemical sol-gel method holds the preparation of the colloidal solution, which is the term Sol and converts sol into the aqueous acidic or alkaline phase term as Gel [51,52]. The process of sol to gel conversion requires divergent reactants and some capping agents followed

by different chemical reactions like hydrolysis, condensation, polymerization, etc. [3,52,53]. The most commonly used reactants are metal alkoxides $M(OR)_x$ M: Metal, or their chlorides by using an alcoholic or aqueous solvent. Researchers developed the synthesis of ZnO nanoparticles by a simple, effective, and expeditious route, with a range of sizes and shapes using dissimilar precursors. Spanhel et al. [54] were the first to come up with the idea of the chemical sol-gel method, Meulenkamp et al. [55] polished it afterward. Both of them used the sol-gel method to synthesize ZnO nanoparticles with zinc acetate as the precursor solution. M. Ristic et al. [56] used tetramethylammonium hydroxide (TMAH) as a surfactant to the zinc 2-ethylhexanoate using alcohol as a solvent. By performing XRD characterization they found crystallites with an average diameter of 25-30 nm and height of 35-45 nm with cylindrical morphology. TEM confirms the particle size of ZnO nanoparticles laying between 20 and 50 nm using this strategy. Yanping P. Gao et al. [57] synthesized ZnO aerogels using zinc nitrate alcoholic solution with propylene oxide to initiate the gelation process. They showed that the resulting alcogel when dried by using supercritical CO_2 it forms aerogel or if it is evaporated by ambient temperature, it forms xerogel. HRSEM results show 'flower-like morphology composed of thin flakes for aerogels and hexagonal platelets network of xerogel. P. Chandrasekaran and G. Viruthagiri et al. [38] have prepared ZnO nanoparticles using a sol-gel method with varying capping agents such as Tetraethyl-ammonium Bromide (TEABr), Ethylene diamine tetraacetic acid (EDTA) and Triethanolamine (TEA). They conclude from TEM and HRTEM result hexagonal structural morphology, which varies depending on the capping agent, but it does not vary much by changing their concentrations. Mariani A. Ciciliati et al. [58] reported improved sol-gel method synthesis of Fe-doped ZnO NPs in which water is taken as a peculiar solvent. The XRD pattern of this Fe-doped ZnO gives the wurtzite structure of ZnO with a hexagonal phase. The average grain size varies from 25 nm to 11 nm with an increase in the concentration of dopant Fe. Results confirm that dopant also affects the structure morphology. B. Manikandan et al. [59] synthesized ZnO NPs by using

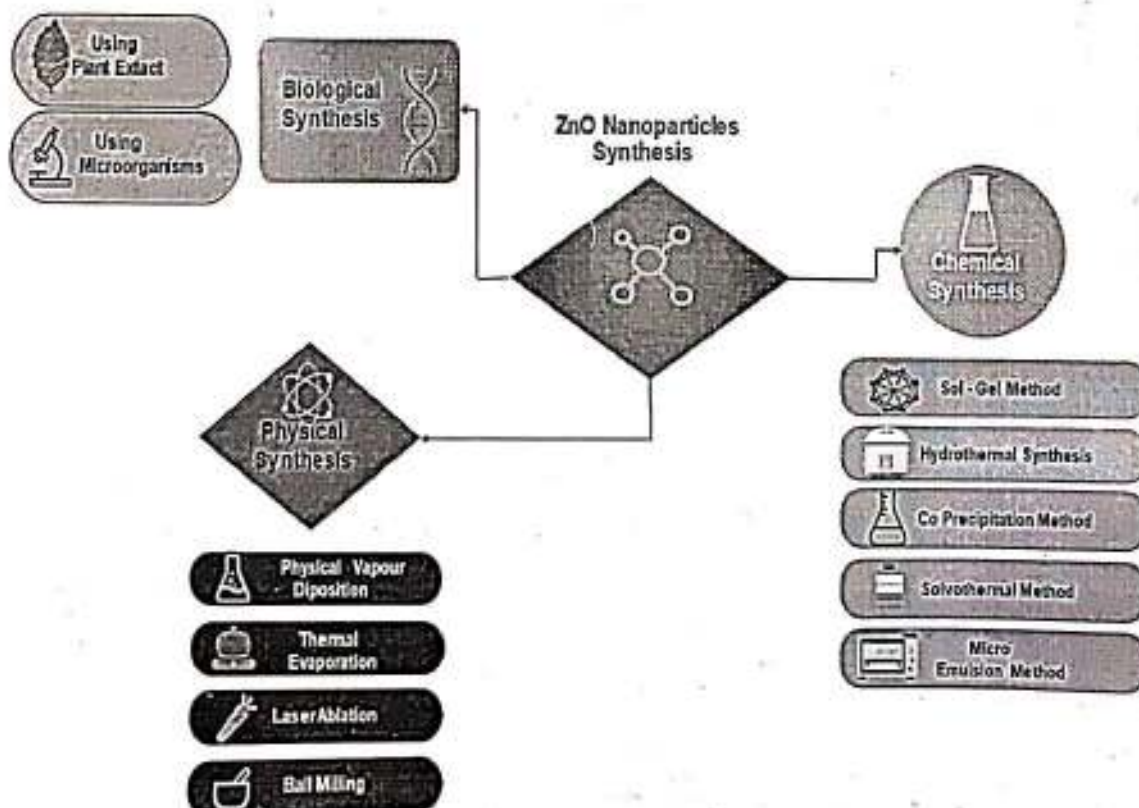


Fig. 1. Various Methods for Synthesis of ZnO Nanoparticles.

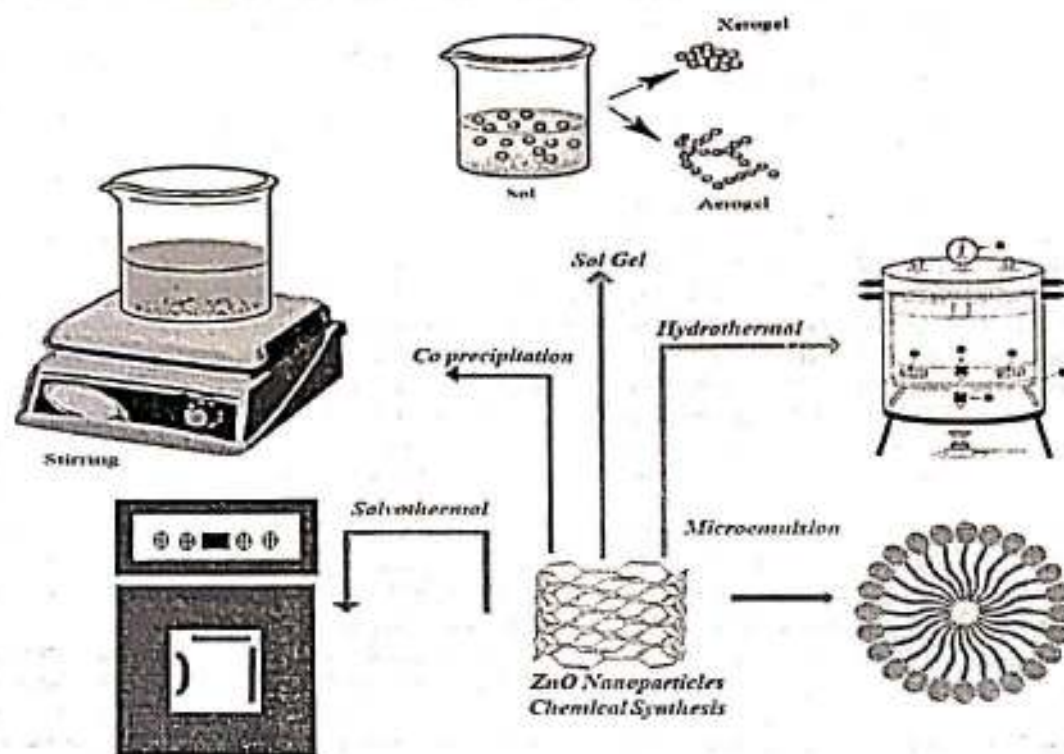


Fig. 2. Chemical Route Methods for Synthesis of ZnO Nanoparticles.

zinc acetate and sodium hydroxide under controlled pH conditions. They perform different characterizations such as XRD, FTIR, UV visible, FESEM, EDAX, and Raman spectroscopy. XRD pattern of ZnO nanoflakes confirms the presence of hexagonal wurtzite structure with 21.84 nm crystallite size, and FESEM shows flaky structural morphology with flat and irregular ZnO nanoflakes. The composition of elements in synthesized ZnO NPs containing Zinc (46.27%) and Oxygen (53.73%) confirm the purity of nanoparticles using EDAX. Behnam Khanizadeh et al. [60] introduced the synthesis and study of Mg and La-doped and co-doped ZnO nanoparticles using the sol-gel technique. The EDAX, TEM, and FESEM study shows the synthesized NPs have homogeneous spherical morphology. The study also reveals that the size of NPs is get affected by doping and co-doping processes and helps to find out the maximum photocatalytic activity for the removal of RhB. Anuj Kumar et al. [61] reported the preparation of ZnO nanoparticles as sol using zinc acetate and polyethylene glycol and transformed it into a gel using a surface reactant as NaOH. Numerous analytical techniques such as XRD, EDX, and TEM characterize synthesized nanoparticles, XRD confirms the hexagonal wurtzite structure with a size of 50 nm. The nanocomposite of ZnO and activated charcoal has formed by mixing, giving ZnO-AC nanocomposite electrodes for the application as a supercapacitor. He found the fabricated SC-Cell has relative capacitance as a single electrode. Anshika Nagar et al. [62] synthesized ZnO NPs and used them as an application of Field Emission Displays (FED's). The ZnO NPs were produced using x-100 into the zinc acetate solution as a precursor, followed by the addition of ammonia resulting in the precipitation of nanoparticles. FESEM results show ZnO nanoflower structure, and HRTEM found the closely packed ZnO NPs in the diameter of range from 30 nm to 60 nm. Obtained morphology of synthesized nanoparticles exhibits excellent field enhancement and the sharp edge of every petal of nanoflower act as a field emitter. Abid Zaman et al. [63] reported the ferromagnetic behaviour of Mn doped ZnO nanoparticles. In this study they have synthesized Mn doped ZnO nanoparticles by using Sol-Gel method and analysed the response of Mn doping by performing various characterisations. XRD analysis indicates the polycrystalline

nature and Wurtzite structure of ZnO nanoparticle after doping. They have studied the M-H loop that is the magnetic properties of Mn doped ZnO using vibrating sample magnetometer which confirms the ferromagnetic behaviour of Mn doped ZnO nanoparticles. The study also reveals that as the doping concentration reduces the size of ZnO from 38.42 nm to 27.54 nm. Auwal Yusha'u et al. [64] reported the photo-degradation of ZnO nanoparticles synthesized by chemical sol-gel method Zinc nitrate dihydrate ($Zn(NO_3)_2 \cdot 2H_2O$, 97%), nitric acid, oxalic acid dihydrate and Eriochrome Black T are the precursors to produce the ZnO nanoparticles. The XRD patterns shows the hexagonal wurtzite structure while SEM and TEM shows the spherical, oval shape morphology. The purity of ZnO is indicated by EDAX data and the obtained band gap is 3.28 eV for ZnO photocatalyst from Tauc's plot. The process such as photocatalysis, adsorption and photolysis are done to check photocatalytic activity of ZnO.

2.2. Hydrothermal method

The hydrothermal synthesis method as the name itself indicates synthesis of proposed NPs was carried out in the presence of aqueous condition which operated under high temperatures and pressures. This is a way of synthesis of nanoparticles suitable for the production and growth of nano crystallites using a simple scientific instrument, namely 'autoclave' [52]. The basic working principle of autoclaves is that the temperature difference is created in the growth chamber between its two ends. One is hotter and the other is cooler, the hot end forces the materials to get soluble on it, and the other end is desired material is got deposited [4]. It is a simple, efficient, effective, and user-friendly method for the synthesis of ZnO nanoparticles. Their behavioural study had to gain much attention in the field of research and development. Babita Baruwati et al. [65] introduced the synthesis of crystalline ZnO NPs using $Zn(NO_3)_2 \cdot 4H_2O$ as a precursor, followed by controlling the pH of the solution using ammonium hydroxide. Teflon-lined steel-coated autoclave operated at 1200 °C temperature for variable periods. The synthesized NPs are studied with different characterization

techniques such as XRD, TEM, UV-DRS, TG-DTA, Electric conductivity, and analyzed gas sensing properties. The XRD studies indicate the wurtzite phase of prepared crystallite, along with an average size of about 17 nm. The particles are found to be clustered in the results of TEM. The bandgap of prepared ZnO NPs is found to be 3.18 eV, their conductivity changes with temperature have been recorded, and find out the sensitivity of NPs towards LPG and EtOH. P. M. Anesh et al. [66] used the hydrothermal method to synthesize ZnO NPs from Zn $(\text{CH}_3\text{COO})_2 \cdot 2\text{H}_2\text{O}$ and NaOH in an alcoholic solution. XRD data confirms the average grain size of NPs was in the range of 7–24 nm; and their presence was confirmed through TEM, SAED, etc. In this study, the dependence of surface morphology on temperature was also elaborated. Due to Zn imperfection or vacancy of oxygen, they recorded green PL emission from UV visible spectra. Ying Zhou et al. [28] reported the synthesis of ZnO nanorods, in this method they used ZnO nanoparticle seeding which is coated on a glass substrate by using the sol-gel method followed by the addition of polyethyleneimine to prepare ZnO nanorods hydrothermally. The obtained nanoparticle has a wurtzite structure with different orientations, which grow vertically on a substrate confirmed by SEM and XRD. W.Z. Li et al. [67] synthesized ZnO NPs, with a Zn plate used as source as well as substratum. The substrates are burnished with sandpaper and ultrasonically cleaned with ethanol followed by distilled water. Zn plate is then deep in an autoclave filled with aqueous ammonia. With different operating temperatures and equal concentrations of ammonia, ZnO nanoparticles are prepared. XRD pattern and SEM results confirm the bitter-melon-like (BML) microstructure found on the Zn plate for two different samples. The average grain size from XRD data is also ranging from 29 nm to 32 nm with a sample as well as operating temperature. TEM data provide the BML with 1.7 μm width and diameter of spherical NPs as 200 nm. Kijung Yong et al. [68] developed a ZnO nanorod bundle sensor. To develop this sensor, synthesis of ZnO nanorods was carried out by using a solution of zinc chloride, distilled water, and NH_4OH as a starting material, then treated hydrothermally. To prepare the gas sensor, Au/Ti electrode, Ag paste, and ZnO nanorod bundle powder followed different systematic processes leading to the formation of the sensor. The sensing behavior of the ZnO sensor is analyzed against the H_2S gas using a furnace-type gas sensing system. Fubo Gu and Guangsheng Guo et al. [69] studied the sensing behavior of ZnO NPs synthesized by microwave hydrothermal technique in which prepared zinc nitrate solution is exposed to a microwave oven at 90 $^\circ\text{C}$ for 10 min. The generated precipitate is annealed and treated at a certain temperature and pressure. The structural, morphological study shows the polygon-shaped ZnO nanoflakes with an average size below 900 nm. By calcining precursor material, they found ZnO at 500 $^\circ\text{C}$ has the highest sensitivity for NO_2 gas in comparison to other operating temperatures. Yeon-Tae Yu et al. [70] introduce citrate-assisted hydrothermal synthesis of ZnO NPs, in which the prepared precipitate of $\text{Zn}(\text{OH})_2$ is dissolved in 35 ml of water in the presence of 1% trisodium citrate and followed by the hydrothermal reaction in an autoclave of Teflon line steel. The prepared ZnO nanoparticle-based gas sensor shows a better response for CO, ethanol, and aldehydes. It is dependent on the temperature and concentration of reducing gases. A noteworthy thing in the results that the response of gases depends on the electron exchange mechanism, which is found large in ethanol and acetaldehyde than in CO. Jianping Du and Jinping Li et al. [71] reported the o-phthalic acid-assisted synthesis of hexagonal grid-like ZnO lamellae (GZL). zinc acetate and urea are used as precursors added in deionized water with constant stirring followed by the addition of o-phthalic acid and the resultant solution is treated hydrothermally in an autoclave. Different ZnO nanoparticles are synthesized by varying proportions of the reactant with reaction time to study morphological behavior. By using an alumina ceramic cylindrical substrate and Ni-Cr wire, the ZnO sensor has been prepared. SEM result confirms GZL morphology, where small holes are detected in the lamellae. Furthermore, EDAX and HRTEM are also studied for prepared samples. K. Ramamurthi et al. [72] studied photocatalytic properties of ZnO NPs

prepared hydrothermally. A precursor solution of zinc chloride is get added by ammonium hydroxide dropwise to maintain its pH. The solution is then treated hydrothermally with the help of an autoclave, and the desired compound is obtained, entire process is repeated with maintaining a constant pH range of 9, 11, and 13. FESEM gives morphological changes concerning the pH value as for 7 pH it is a hexagonal cell with ZnO nanorods. While at 9 pH growth of nano disks occurred, porous nanorods were found at pH 11, whereas flower-shaped nanorods for 13 pH. High photocatalytic capacity has been observed for pH 9. Sonalika Agarwal and Kamendra Awasthia et al. [73] synthesized ZnO NPs using a hydrothermal technique using zinc acetate dihydrate and citric acid monohydrate as a reactant followed by the addition of NaOH and developed a gas sensor. For the fabrication of the Gas sensor, they used the micro drop coating method, alumina was the used substrate. The sensing properties of the respective sensor were studied against the pollutant gases such as CO, ethanol, and NO_2 . XRD pattern confirms wurtzite hexagonal structure. SEM study produces images of nanoflowers and packages of nanorods of ZnO. The average size data obtained from XRD for nanoflowers was 21 nm and for nanorods about 43 nm, having band gaps of 3.0 eV and 3.19 eV respectively. N. Srinivasan et al. [74] reported the preparation of nanocomposite with ZnO and the evaluation of a photocatalytic activity. At very first nano particles of C-doped ZnO and BiVO_4 were exclusively prepared hydrothermally using suitable precursors and reactants under desired conditions. Subsequently, the nanocomposite of C-ZnO/ BiVO_4 was prepared. The process was followed by mixing and sonicating with proper proportions at a suitable time. The range of characterizations was investigated for prepared nanoparticles and their composites separately such as XRD, morphological analysis (FESEM, TEM), UV, Raman study, photoluminescence, and photocatalytic activity. The maximum photocatalytic activity was found in C-ZnO/ BiVO_4 nanocomposite as compared to C-ZnO, ZnO, and BiVO_4 . Numerous parameters are responsible for the higher photocatalytic behavior of nanocomposite. Joon-Shik Park and Hoo-Jeong Lee et al. [75] proposed work leads to the preparation of 3D porous nanosheets of ZnO from the prepared precursor Zinc Hydroxide Carbonate (ZHC) which was calcinated at 500 $^\circ\text{C}$ with the help of muffle furnace. Proper resistive sensor fabricated by using Ti /Pt electrodes with sputter deposition technique on a silicon substrate. Synthesize material analyzed by different analytical techniques such as TGA-DTA, FE-SEM, TEM, BET, and XPS. The sensing behavior of the respective sensor is tested for different gases like acetone, CO, toluene, Nitrogen oxide, etc. The prepared sample has found greater sensitivity towards NO_x . Eman A. Mwafy et al. [76] synthesized ZnO nanoparticles with variable sizes using hydrothermal techniques operating at different temperatures. The dielectric properties of prepared samples are analyzed. The XRD, SEM, and UV-Visible spectra were studied and the proportionate dependence of sample irregularity with particle size was explained through morphological studies of particles. The absorption study helps to understand the relation between the effect of particle size and the shifting of wavelength. All the analytical techniques confirm the dielectric properties are found to depend on particle size. Praveen Sharma et al. [77] synthesized Nd doped ZnO nanoparticles by hydrothermal synthesis technique via ultrasonication of precursors. The XRD pattern of the fabricated samples indicate the purity and crystalline nature with fine peaks. An energy dispersive spectroscopy pattern (EDS) reflect zero contaminants. The optical properties of synthesized nanomaterial are done by UV-Vis Diffuse Reflectance Spectroscopy reveals the band gap ZnO and Nd-ZnO as 3.26 eV and 3.19 eV. The Photocatalysis of the prepared samples leads to photodegradation of Congo red dye solution under UV and Solar light respectively also results enhancement of photocatalytic activity with doping.

2.3. Co-precipitation method

Co-precipitation is one of the chemical route methods for the

synthesis of nanoparticles [78], it is the opportune, procurable, competent, and sophisticated method to yield nanoparticles. The mechanism of this method involves metal salts leading to the proposed nanomaterial dissolved in a suitable solvent. A precipitating agent is then added to the resultant solution such that an insoluble solid can be obtained [4]. Obtained precipitate followed the wash with a suitable solvent to remove impurities and heat treatment at a particular temperature to get desired metal oxide nanoparticles. Baibiao Huang et al. [79] utilized the coprecipitation technique to prepare ZnO/In₂O₃ nanoparticles. Zinc nitrate and indium nitrate are used as a precursor, which is dissolved in a suitable solvent followed by the addition of ammonia to maintain the pH of the solvent to obtain desired nanoparticles. Obtained compound goes through different washings and ranges of temperature. Photocatalytic activity of nanoparticles finds out by synthesizing nanomaterial with varying proportions of precursor. The photocatalytic study was investigated by methylene blue (MB) dye bleaching with the source of the Xe arc lamp, results showed excellent photocatalytic activity of nanoparticles. F. Giovannelli et al. [80] synthesized ZnO NPs with doping of Al with the help of the coprecipitation method. The solution prepared with zinc nitrate and aluminium chloride is centrifuged after the addition of NaOH to balance the pH of the precursor solution, obtained material is washed with demineralized water and at last, the yield was dried for further analysis. SEM morphology results, isotropic and platelets like Np with variable size. XRD patterns are recorded with different Zn /Al concentration ratios. Ravi Ganesan et al. [81] introduced Co-doped ZnO NPs synthesis considering the coprecipitation method into account. Starting with zinc acetate metal salt, ZnO NPs were prepared and cobalt acetate is added to zinc acetate solution to form Co-ZnO NPs. Crystallite size from XRD data changes from 35 nm to 29 nm due to the effect of Co incorporation to the ZnO parent material. FTIR study confirms that Co²⁺ acquires Zn²⁺ sites interstitially. The absorption study shows redshift due to the doping effect compared to pure ZnO NPs. Raman and magnetometer study of pure ZnO NPs show a diamagnetic effect whereas Co-doped ZnO NPs become ferromagnetic. A. N. El-Shazly et al. [82] prepared ZnO nanoparticles and evaluated their photocatalytic behavior. Nanoparticles are prepared from zinc sulfate heptahydrate and ammonium hydrogen carbonate as precursors using a dissimilar surfactant such as anionic, cationic, and PEG polymer. Different analytical techniques are used to identify and confirm the structure such as XRD, SEM, and HR-TEM. XRD confirms hexagonal wurtzite structure with 28 nm size and size 21 nm obtained due to the effect of surfactant, which causes a change in the size and shape of nanoparticles. The photocatalytic activity was observed maximum for nanoparticles obtained by using a cationic surfactant. Marcio Sousa Goes et al. [83] reported the synthesis of zinc oxide nanoparticles by employing ionic liquid. In this method, zincacetate dehydrate and TEA-PS, BF₄, and NaOH are used to obtain ZnO nanoparticles by the coprecipitation method. Ionic liquid affects the crystal structure of nanoparticles due to it behaves like a surfactant and studies their photoelectric properties. Rania E. Adam et al. [84] synthesized ZnO nanoparticles with zinc acetate dehydrate and Sodium hydroxide as a starting material and studied the degradation of congo red dye in the presence of solar radiation at various pH. Hexagonal wurtzite confirmed by XRD data and photocatalytic potential of nanoparticles evaluated at dissimilar pH influences decolonization of dye. Among the different pH, at pH 4 after 120 min, decomposition was found maximum in the presence of solar light as compared to other conditions. A. Kolodziejczak-Radzimska et al. [85] reported the synthesis using KOH and zinc acetate carried out at varying temperatures to obtain ZnO nanoparticles. Studies help to understand if variation in the proportion of starting material altered the shape, size and surface area of particles. Particle size increases with the increasing temperature of the reactant confirmed by the SEM data. Wang Jinxiao et al. [86] evaluated the gas sensing behavior of ZnO nanoparticles doped with Ni and activated by Au. zinc sulfate heptahydrate, nickel nitrate, ammonium acid carbonate, and HAuCl₄ solution are employed as a precursor.

XRD, SEM, TEM, XPS, FTIR, and Raman spectra were used to understand the structure, morphology, and surface element of synthesized particles. A ceramic substrate coated with ZnO containing Au electrode which leads to the formation of gas sensors. The sensing behavior of Au was found to be maximum as compared to Ni-doped ZnO and pure ZnO nanoparticles. Badal Kumar Mandal et al. [87] synthesized nanoparticles and evaluated their biological activity. zinc acetate dihydrate and sodium hydroxide are used as starting materials for the synthesis of material and are characterized by XRD, SEM-EDAX, and HR-TEM. XRD data confirms hexagonal structure with flower shape and which is effective against bacteria *Escherichia coli* and *Staphylococcus aureus*. Stephane Daniele et al. [88] reported synthesis of ZnO nanoparticles with enhanced visible emission. Nanoparticles are prepared by using different precursors such as zinc acetate dihydrate, zinc sulphate, solution in ethanol and precipitated using potassium hydroxide aqueous and LiOH respectively in alcoholic solution with different ratio following stirring, centrifuged and drying. Hexagonal wurtzite structure confirms by XRD obtained from different precursors which results average range of crystalline size as 15 nm – 25 nm. TEM results of the sample show the needle like structures which also confirms the crystalline size in the same range.

2.4. Microemulsion method

It is one of the simple chemical methods used to synthesize nanoparticles. Microemulsion name itself indicates it is a dispersion of two immiscible liquids having specific physicochemical properties like thermodynamically stable, isotropic, large interfacial area, and having the ability to solubilize the compound present in both phases [3,91]. These two immiscible phases are water (aqueous) and oil (hydrocarbon). There are two types of microemulsion methods, direct or water in oil (W/O) and reverse or oil in water (O/W), which are employed for the synthesis of numerous metal nanoparticles [3,91]. These methods are used to obtain desired and uniform-size nanoparticles. S. Hingorani et al. [91] reported the synthesis of ZnO nanoparticles using the microemulsion route and studied their varistor properties. Cetyl trimethyl ammonium bromide, 1-butanol, n-octane, zinc nitrate, and ammonium carbonate are employed for the synthesis of nanoparticles. In this method, zinc nitrate is a present aqueous layer of one emulsion added to another emulsion containing ammonium carbonate. In this process, ammonium carbonate was used to precipitate zinc in the form of zinc carbonate. The obtained carbonate material was calcinated to get zinc oxide nanoparticles. The calcination process is more smoothly understood by DSC and TGA. XRD confirms a hexagonal structure with 14 nm size which is smaller than the nanoparticles gained by other processes. Chun-Hua Yan et al. [92] synthesized one-dimensional ZnO nanostructures via microemulsion methods in which cetyltrimethylammonium bromide, n-hexanol, n-heptane, and Zn(OH)₂ as a precursor, carried out in Teflon-lined autoclave at a particular temperature. Obtained compound washed with ethanol and water, followed by centrifugation and dehydration gives the desired product. SEM images approve the formation of 1 D - structure which was a time-dependent study. Gaohong He et al. [93] introduced morphology control synthesis of ZnO nanoparticles. In this process, heptane, hexanol, polyoxyethylene *tert*-octylphenyl ether, Zn(NO₃)₂, PEG400, and NaOH are used to prepare two microemulsions. The first microemulsion of Zn(NO₃)₂ containing a diverse concentration of PEG-400 in an aqueous medium was added to the second microemulsion of aqueous NaOH with stirring. The obtained solution was processed in an autoclave followed by hydrothermal treatment for 15 h at 140 °C, and the product was obtained by centrifugation and dried at 60 °C. Various analytical methods such as SEM, TEM, TG-DTA, and FTIR are used. SEM confirms the morphology of nanoparticles such as hexagonal wurtzite with a size of less than 100 nm. Deepa Sarkara et al. [94] reported the synthesis of ZnO nanoparticles by employing Cyclohexane, ammonium hydroxide, Triton X-100, hexanol, zinc nitrate, and Sodium hydroxide as a precursor. Two

different microemulsions are, in which base-containing microemulsion solution was poured into zinc nitrate microemulsion with constant stirring to get a clear solution containing desired nanoparticles. Nanoparticles are obtained by centrifugation followed by washing and drying at a suitable temperature. XRD confirms hexagonal wurtzite structure, and TEM results confirm the spherical shape and average particle size is 25 nm. The study also reveals numerous parameters which affect the shape and size of particles prepared by microemulsion methods. Abbas Ali Khodadadi et al. [95] reported ZnO synthesis and evaluated sensitivity. In this method, hexanol, Cyclohexanol, triton X-100, ammonium hydroxide, Tetraethoxysilane, and zinc nitrate hexahydrate are used to prepare emulsions. Two-step microemulsion methods are used to prepare silica-ZnO nanoparticles and composite by one-step microemulsion method. Numerous analytical techniques such as FESEM, XRD, TEM, EDX, and BET are used to find the morphology, size, shape, and composition of elements. Construct sensor Si@ZnO-40 shows excellent sensitivity for ethanol at 350 °C as compared to methane, toluene, TCE, carbon monoxide, acetaldehyde, and propane. ZnO composition affects the reactivity of the sensor, and different parameters also play a vital role to sense the gases. Jianxi Yao et al. [96] induced synthesis of ZnO by photopolymerization using the microemulsion route. Precursor Triton X-100, azobisisobutyronitrile, ammonia, acrylamide, hexanol, zinc nitrate hydrate, and cyclohexanol. In this polymerization method, AIBN is used as a photoinitiator to obtain nanosheets. XRD data confirms hexagonal wurtzite ZnO, DSC and TGA help the fine decomposition of ZnO nanoparticles and nanosheets. ZnO nanosheets exhibited excellent electrochemical properties results as compared to marketable ZnO nanoparticles. Dejie Li and Jinling Chai et al. [97] reported the synthesis of ZnO nanoparticles by a surfactant-free microemulsion method and find out photocatalytic behaviour. In this method hexane, ammonium hydroxide, Propan-2-ol, zinc nitrate hexahydrate, and water were applied to prepare the emulsion solution. After completing the microemulsions process reaction mass is transferred to an autoclave heated at different temperatures. Zinc oxide nanoparticles are obtained by later centrifugation followed by several washings with water and ethanol. The photocatalytic evaluation indicates the performance of prepared nanoparticles is good as compared to commercial nanoparticles however the photocatalytic potential of particles prepared at 140 °C is more excellent than the particles prepared at 160 °C. Caner Durucan et al. [98] synthesized ZnO nanoparticles by reverse microemulsion method with variable particle size. Glycerol, sodium bis(2-ethylhexyl) sulfosuccinate, n-heptane, and zinc acetate dihydrate as precursors. Results also find that variation in calcination temperature also affects morphology and particle size. XRD, SEM, and TEM help to find out the size, shape, morphology, and thermal stability of compounds.

2.5. Solvothermal method

The concept of solvothermal used by Demazeau et al. this term covers all solvents [99–101]. In a solvothermal method of synthesis, nanoparticles are carried out in the presence of numerous organic solvents at high temperatures and pressure [102]. In this process, a solvent is used to synthesize diverse nanomaterials, and it is one of the vital methods of the wet chemical route [103]. Solvothermal synthesis of material plays a vital role in industries and research filed due to its potential to synthesize different morphological nanoparticles [101]. Okorn Mekasuwandumrong and Piyasan Praserttham et al. [103] reported the synthesis of ZnO nanoparticles using the solvothermal method. Aromatic solvents, alcohols, glycols, and n-alkanes were employed for the synthesis of nanoparticles at 250 °C by using zinc acetate as a precursor. Starting material was taken in a test tube containing 100 ml solvent, which was kept in an autoclave under a nitrogen atmosphere in an autoclave heated at certain pressure and temperature. Isolation of product after cooling the autoclave followed by washing and centrifugation. XRD, TEM, and SEM confirm hexagonal wurtzite structure with various particles size. The dielectric constant of solvent and

temperature relation understand using different solvents for the synthesis of nanoparticles. Wen-Feng Hsieh et al. [104] introduced the synthesis of ZnO nanowires by the solvothermal route and evaluated their activity for Dye-Sensitized Solar Cells. zinc nitrate hydrate, hexamethylenetetramine, and polyethylenimine were used for the synthesis of ZnO nanowires, and branched nanowires were grown by using ZnO nanowires. SEM, TEM, and XRD techniques are used to know the morphology, size, and shape of nanoparticles. The solar cell was prepared using ZnO nanowires, a glass substrate, and FTO substrates. Dye-Sensitized Solar Cells potential evaluation found excellent efficiency for branched ZnO nanowires than the ZnO nanowires. Samanta Cimitan and Stefania Albonetti et al. [105] studied In and Ga-doped ZnO nanoparticles with the help of the solvothermal method. In the synthesis process, the precursor solution of both dopants liquifies either in methoxy ethanol or ethanol only treated with the autoclave. The Dynamic Light Scattering (DLS) characterization has been done for the size measurements for which avalanche photodiode had used for detection purposes. The prepared sample was treated with a temperature range from 30 °C to 600 °C to record its TGA to detect the formation of and volatile by product with the effect of temperature. XRD data leads to spherical or ellipsoidal grains having diameters in the range of 15–20 nm. Yeon-Tae Yu et al. [106] synthesis of ZnO nanoparticles by solvothermal method from the zinc nitrate solution by maintaining its pH. The same method is repeated for zinc acetate and zinc chloride salts. The characteristic study has been done through XRD, TEM, HRTEM, UV Visible spectroscopy, and FTIR analysis. ZnO nanorods traced by TEM and HRTEM elaborate the nanorods as single crystalline. UV Visible spectra recognize the blue shift in absorption spectra. Finally, the prepared NPs were introduced as gas sensors for NO₂ gas, and obtained results showed ZnO nanorods exhibit excellent sensor activity as compared to ZnO nanoparticles, temperature, and concentration of gas also alter the sensing behavior. Lidia Santos and Elvira Fortunato et al. [107] introduced Gallium – Indium-Zinc-Oxide Nanoparticles (GIZO NPs) employing a solvothermal method using Gallium nitrate hydrate, indium acetate, zinc acetate, 2-methoxyethanol and ethanolamine are used to synthesize GIZO nanoparticles. Nanoparticles are well characterized by XRD, SEM, TEM, and EDS. Prepared GIZO film, electrolyte, and EGT characterized, the obtained results confirm that synthesized nanoparticles are applicable in EGT. Paulina Dreyse et al. [108] reported the preparation of ZnO nanoparticles by a combined process in which the precipitation process is solvothermal. ZnSO₄·7H₂O, NaOH, and K₂CO₃ are used as a precursor for the precipitation method and the obtained product is stirred at 80 °C in ethylene glycol water solution followed by treatment in a reactor at 200 °C, washing with a suitable solvent, drying and ultrasonic treatments to get desired nanoparticles. Nanoparticles obtained in this process exhibit different properties. I.A. Nagornova et al. [109] employed synthesis of ZnO nanoparticles and evaluated gas sensing potential. Zinc nitrate and acetylacetonate are used as a precursor to synthesize zinc acetylacetonate nanocrystals in aqueous conditions followed by treatment with ammonia hydrate at 60 °C. Ethylene glycol was used as a solvent for this process. Film of nanoparticles prepared on Al₂O₃-substrates by using the screen-printing technique at a certain temperature was employed to construct the film. Platinum electrodes and microheaters are used with Al₂O₃-substrate. Among the all-constructed film, Z2 film displays maximum sensing potential for NO₂ as compared to CH₄, H₂ and CO. Ankica saric et al. [110] reported synthesis, experimental and theoretical study of ZnO nanoparticle. Zinc acetylacetonate monohydrate, triethanolamine, ethanol, and 1-octanol are employed to synthesize nanoparticles by the solvothermal process. NPs are characterized by FESEM, XRD, IR, and UV-Visible spectroscopy and computational study by using the Gaussian 09 program. The obtained data from the study reveals that solvent ethanol affects the size, shape, and development of nanoparticles. Computational study and experimental study are found to be correlated and help to understand the role of surface relations of nanoparticles with solvent and their effect on the surface structure. Table.1 overviews

Table 1
Comparison of Chemical Synthesis Techniques.

Synthesis Method For ZnO Np's	Sol-Gel	Hydrothermal	Co-Precipitation	Solvothermal	Microemulsion
Reaction Mechanism / Parameters	Colloidal solution leads to Sol and Gel Formation Operating Temperature: 20°-500 °C	Aqueous solvents at high temperature and pressure treated in 'autoclave' Operating Temperature: 100°-1200 °C	Metal salts in solvents and precipitating agent is added to it Operating Temperature: 10°-100 °C	Organic Solvents treated at high temperature and pressure Operating Temperature: 30°-600 °C	Dispersion of two immiscible liquids Operating Temperature: 25°-150 °C
Structural Properties	Hexagonal, cylindrical morphology Average Particle Size: 10 nm-50 nm	Wurtzite Phase Structure Average Particle Size: 5 nm-35 nm	Hexagonal Wurtzite Average Particle Size: 20 nm-35 nm	Hexagonal Wurtzite Average Particle Size: 15 nm-30 nm	Hexagonal, Spherical Structure Average Particle Size: 30 nm-60 nm
Applications	Supercapacitor, Photovoltaic Devices, Gas Sensors	Gas Sensors	Gas Sensors, Photocatalyst	Gas Sensors, Solar Cell	Photocatalyst, Gas Sensors
References	[51-64]	[65-77]	[78-88]	[102-110]	[89-101]

comparative study of all the chemical synthesis methods cover in this review.

3. Conclusion

Metal oxide nanoparticles attracted the world due to the versatile properties of NPs, its easy, simple, and efficient method of preparation of nanoparticles made it more prominent. This review article mainly covers the synthesis of ZnO nanoparticles by chemical route methods including, Sol-Gel, Co-Precipitation, Hydrothermal, Microemulsion, and solvothermal methods. ZnO nanoparticles are an n-type of a semiconductor having a wide bandgap (3.37 eV) with large exciton binding energy making them suitable for diversified applications. Synthesized nanoparticles are characterized by numerous analytical methods such as XRD, DSC, TGA, FTIR, UV visible, FESEM, TEM, EDAX, and Raman spectroscopy. This synthetic way is an effective and efficient method to control morphology, size, shape, and crystal structure and make available numerous applications in diverse fields. In comparison with other nanoparticles, ZnO nanoparticles are the most studied nanoparticle due to the easy availability of precursor, simple synthetic route, easy isolation of product, and suitable for all chemical route methods.

CRediT authorship contribution statement

Komal Bachhav: Conceptualization, Methodology, Software, Validation, Formal analysis, Investigation, Resources, Writing – original draft, Writing – review & editing, Visualization. Arun S. Garde: Conceptualization, Methodology, Validation, Formal analysis, Resources, Data curation, Writing – review & editing, Supervision.

Declaration of Competing Interest

The authors declare that they have no known competing financial interests or personal relationships that could have appeared to influence the work reported in this paper.

Data availability

Data will be made available on request.

References

- [1] S.P. Paul, *Flux evaporation assisted green synthesis of metal nanoparticles: A mini review*, *Biotechnol. Rep.* 28 (2020) e00569.
- [2] R. Feynman, *Nanotechnology*, *Cultechs. Eng. Sci.* 23 (1960) 22-36.
- [3] A. Król, P. Pomastowski, K. Raflińska, V. Railean-Plugaru, B. Buzzewski, *Zinc oxide nanoparticles: Synthesis, entropic activity and toxicity mechanism*, *Adv. Colloid Interface Sci.* 249 (2017) 37-52, <https://doi.org/10.1016/j.cis.2017.07.033>.
- [4] T.A. Singh, J. Das, P.C. Sil, *Zinc oxide nanoparticles: A comprehensive review on its synthesis, anticancer and drug delivery applications as well as health risks*, *Adv. Colloid Interface Sci.* 286 (2020), 102317, <https://doi.org/10.1016/j.cis.2020.102317>.
- [5] S. Ahmed, S.A. Chaudhry, S. Ikram, *A review on biogenic synthesis of ZnO nanoparticles using plant extracts and microbes: a prospect towards green chemistry*, *J. Photochem. Photobiol. B Biol.* 166 (2017) 272-284, <https://doi.org/10.1016/j.jphotobiol.2016.12.011>.
- [6] H. Agarwal, S.V. Kumar, S. Rajeshkumar, *A review on green synthesis of zinc oxide nanoparticles-An eco-friendly approach*, *Resour. Eff. Technol.* 3 (2017) 406-413, <https://doi.org/10.1016/j.reft.2017.03.002>.
- [7] M.K. Alqafl, O.A. Abo Noga, F.Y. Alzoubi, *pH effect on the aggregation of silver nanoparticles synthesized by chemical reduction*, *Mater. Sci.-Pol.* 32 (2014) 107-111, <https://doi.org/10.2478/s13536-013-0166-9>.
- [8] Jitendra B. Arun G. *Influence of complexing agent, pH of solution and thickness on morphological and optical properties of ZnS particles layer prepared by electrochemical deposition technique*, *HanoverChem. J.* 2020, xabba, MareMarwa. 2020; 11:519-28. 10.17586/2220-8054-2020-11-5-519-528.
- [9] S.I. Sadovnikov, A.I. Gusev, *The effect of temperature on the particle sizes and the recrystallization of silver sulfide nanopowders*, *Phys. Solid State* 60 (2018) 1308-1315, <https://doi.org/10.1134/s1063780418070259>.
- [10] C.B. Ong, L.Y. Ng, A.W. Mohammad, *A review of ZnO nanoparticles as solar photocatalysts: Synthesis, mechanisms and applications*, *Rev. Renew. Sustain. Energy Rev.* 81 (2018) 536-551, <https://doi.org/10.1016/j.rser.2017.08.020>.
- [11] S. Faisal, H. Jan, S.A. Shah, S. Shah, A. Khan, M.T. Akbar, M. Rizwan, F. Jan, A. N. Waheedullah, A. Khattak, *Green synthesis of zinc oxide (ZnO) nanoparticles using aqueous fruit extracts of Myristica fragrans: their characterizations and biological and environmental applications*, *ACS Omega* 6 (9709-22) (2021), <https://doi.org/10.1021/acsomega.1c00310>.
- [12] Ramades J. *Nanotechnology: an introduction*. William Andrew; 2016.
- [13] S. Hasan, *A review on nanoparticles: their synthesis and types*, *Int. J. Recent Sci.* 2277 (2015) 2502.
- [14] H. Mirzaei, M. Darroudi, *Zinc oxide nanoparticles: Biological synthesis and biomedical applications*, *Ceram. Int.* 43 (2017) 907-914, <https://doi.org/10.1016/j.ceramint.2016.10.051>.
- [15] R. Kumar, O. Al-Dessary, G. Kumar, A. Umar, *Zinc oxide nanostructures for NO2 gas-sensor applications: A review*, *Nano-Micro Lett.* 7 (2015) 97-120, <https://doi.org/10.1007/s40820-014-0023-3>.
- [16] L. Al-Naamani, S. Dobretsov, J. Dutta, *Chitosan-zinc oxide nanoparticle composite coating for active food packaging applications*, *Innov. Food Sci. Emerg. Technol.* 38 (2016) 231-237, <https://doi.org/10.1016/j.ifset.2016.10.010>.
- [17] A.G. Rad, H. Abbasi, M.H. Afzali, *Gold nanoparticles: synthesising, characterizing and reviewing novel application in recent years*, *Phys. Procedia* 22 (2011) 203-208, <https://doi.org/10.1016/j.phpro.2011.11.032>.
- [18] A.S. Garde, *Electrical and humidity sensing properties of WO3 thick film resistor prepared by screen printing technique*, *Sens. Lett.* 15 (2017) 915-923, <https://doi.org/10.1166/asl.2017.3698>.
- [19] B.R. Saekapal, H.B. Gajare, S.S. Karade, R.R. Salunkhe, D.P. Dubal, *Zinc oxide encapsulated carbon nanotube thin films for energy storage applications*, *Electrochim. Acta* 192 (2016) 377-384, <https://doi.org/10.1016/j.electacta.2016.01.193>.
- [20] S. Bagheri, N.M. Julkapil, *Modified iron oxide nanomaterials: functionalization and application*, *J. Magn. Magn. Mater.* 416 (2016) 117-133, <https://doi.org/10.1016/j.jmmm.2016.08.042>.
- [21] M.J. Spencer, *Gas sensing applications of 1D-nanostructured zinc oxide: Insights from density functional theory calculations*, *Prog. Mater. Sci.* 57 (2012) 437-486, <https://doi.org/10.1016/j.pmatsci.2011.06.001>.
- [22] Y. Kang, F. Yu, L. Zhang, W. Wang, L. Chen, Y. Li, *Review of ZnO-based nanomaterials in gas sensors*, *Solid State Ion.* 360 (2021), 115544, <https://doi.org/10.1016/j.ssi.2020.115544>.
- [23] A.S. Garde, *Humidity sensing properties of WO3 thick film resistor prepared by screen printing technique*, *J. Alloy. Compd.* 617 (2014) 367-373, <https://doi.org/10.1016/j.jallcom.2014.07.073>.
- [24] Sodeghi B. *Synthesis and characterization of ultrafine Ag/ZnO nanotetrapods (AZNTP) for environment humidity sensing*, *Avicenna J Environ Health Eng* 2018; 5:115-9. 10.15171/ajehe.2018.15.

- [25] H.T. Tran, M.J. Spencer, Zinc oxide for gas sensing of formaldehyde: Density functional theory modelling of the effect of nanostructure morphology and gas concentration on the chemisorption reaction, *Mater. Chem. Phys.* 193 (2017) 274–284, <https://doi.org/10.1016/j.materchemphys.2017.02.031>.
- [26] D. Chu, Y. Maruda, T. Ohji, K. Kato, Formation and photocatalytic application of ZnO nanorods using aqueous solution, *Langmuir* 26 (2010) 2811–2815, <https://doi.org/10.1021/lb902566a>.
- [27] J.H. Choy, E.S. Jang, J.H. Won, J.H. Chung, D.J. Jang, Y.W. Kim, Soft solution route to directionally grown ZnO nanorod arrays on Si wafer; room-temperature ultraviolet laser, *Adv. Mater.* 15 (2003) 1911–1914, <https://doi.org/10.1002/adma.200310277>.
- [28] Y. Zhou, W. Wu, G. Hu, H. Wu, S. Cai, Hydrothermal synthesis of ZnO nanorod arrays with the addition of polyethyleneimine, *Mater. Res. Bull.* 43 (2008) 2113–2118, <https://doi.org/10.1016/j.materresbull.2007.09.024>.
- [29] Z. Fan, D. Wang, P.C. Chang, W.Y. Tseng, J.G. Lu, ZnO nanowire field-effect transistor and oxygen sensing property, *Appl. Phys. Lett.* 85 (2004) 5923–5925, <https://doi.org/10.1063/1.1836870>.
- [30] Q. Zhang, C. Xie, S. Zhang, A. Wang, B. Zhu, L. Wang, Z. Yang, Identification and pattern recognition analysis of Chinese liquors by doped nano ZnO gas sensor array, *Sens. Actuators B Chem.* 110 (2005) 370–376, <https://doi.org/10.1016/j.snb.2005.02.017>.
- [31] S. Kanaparthi, S.G. Singh, Chemiresistive sensor based on zinc oxide nanoflakes for CO₂ detection, *ACS Appl. Nano Mater.* 2 (2019) 700–706, <https://doi.org/10.1021/acsnano.8b01763>.
- [32] R. Vimal, K.C. Hu, Zinc oxide based dye-sensitized solar cells: A review, *Renew. Sustain. Energy Rev.* 70 (2017) 920–935, <https://doi.org/10.1016/j.rser.2016.11.273>.
- [33] J. Zhang, W. Yu, L. Zhang, Fabrication of semiconducting ZnO nanobelts using a halide source and their photoluminescence properties, *Phys. Lett. A* 299 (2002) 276–281, [https://doi.org/10.1016/S0375-9601\(02\)00622-9](https://doi.org/10.1016/S0375-9601(02)00622-9).
- [34] A. Raja, S. Ashokkumar, P.R. Marthandan, J. Jayachandran, C.P. Kothiwada, G. R. Rajendran, M. Srinivasan, Eco-friendly preparation of ZnO NPs using *Tetrahymena dihalata* and its photocatalytic and antimicrobial activity, *J. Photochem. Photobiol. B* (2017).
- [35] Z. Fereidouni, M.R. Loghman-Estarki, R.S. Razzavi, M. Taheran, Template synthesis of zinc oxide nanoparticles entrapped in the zeolite Y matrix and applying them for thermal control paint, *Mater. Sci. Semicond. Process.* 16 (2013) 547–553, <https://doi.org/10.1016/j.mssp.2012.08.005>.
- [36] S.C. Minne, S.R. Manalis, C.F. Quate, Parallel atomic force microscopy using cantilevers with integrated piezoresistive sensors and integrated piezoelectric actuators, *Appl. Phys. Lett.* 67 (1995) 3918–3920, <https://doi.org/10.1063/1.115317>.
- [37] S. Chu, M. Olmedo, Z. Yang, J. Kong, J. Liu, Electrically pumped ultraviolet ZnO diode lasers on Si, *Appl. Phys. Lett.* 93 (2008), 181106, <https://doi.org/10.1063/1.3012579>.
- [38] P. Chandrasekaran, G. Viruthagiri, N. Srinivasan, The effect of various capping agents on the surface modifications of sol-gel synthesized ZnO nanoparticles, *J. Alloy. Compd.* 540 (2012) 89–93, <https://doi.org/10.1016/j.jallcom.2012.06.032>.
- [39] Awasthi K. General introduction of zinc oxide nanomaterials. In *Nanostructured Zinc Oxide*, Elsevier 2021, p. 1–19.
- [40] N. Rajpat, Methods of preparation of nanoparticles—a review, *Int. J. Adv. Eng. 7* (2015) 1806.
- [41] G.K. Weldegerbreal, Synthesis method, antibacterial and photocatalytic activity of ZnO nanoparticles for azo dyes in wastewater treatment: A review, *Inorg. Chem. Commun.* 120 (2020), 108140, <https://doi.org/10.1016/j.inoche.2020.108140>.
- [42] A.V. Nikam, B.L. Prasad, A.A. Kulkarni, Wet chemical synthesis of metal oxide nanoparticles: a review, *CritEngComm* 20 (2018) 5091–5107, <https://doi.org/10.1039/C8CE00487K>.
- [43] Gardi AS. Large scale synthesis and characterization of cadmium sulfide nanoparticles by simple chemical route. *Hançerleşimci Önemli, Zinçoks, MareMarma.* 2020; 11:434–42. [10.17586/2220-8054-2020-11-4-444-452](https://doi.org/10.17586/2220-8054-2020-11-4-444-452).
- [44] B.R. Cuenya, Synthesis and catalytic properties of metal nanoparticles: Size, shape, support, composition, and oxidation state effects, *Thin Solid Films* 518 (2010) 3127–3150, <https://doi.org/10.1016/j.tsf.2010.01.018>.
- [45] M. Vijayakumar, K. Priya, R.T. Nancy, A. Noorlidah, A.B.A. Ahmed, Biosynthesis, characterization and anti-bacterial effect of plant-mediated silver nanoparticles using *Artemisia nilagirica*, *Ind. Crop. Prod.* 41 (2013) 235–240, <https://doi.org/10.1016/j.indcrop.2012.04.017>.
- [46] B. Knoll, F. Keilmann, Near-field probing of vibrational absorption for chemical microscopy, *Nature* 399 (1999) 134–137, <https://doi.org/10.1038/20154>.
- [47] Wiley, Benjamin, Yungang S, Younan X. Synthesis of silver nanostructures with controlled shapes and properties. *Accounts of chemical research* 2007; 40:1067–1076. [10.1021/ar700097a](https://doi.org/10.1021/ar700097a).
- [48] S. Sengupta, D. Eavarone, I. Capila, G. Zhao, N. Watson, T. Kiziltepe, R. Sasisekharan, Temporal targeting of tumour cells and neovasculature with a nanoscale delivery system, *Nature* 436 (2005) 568–572, <https://doi.org/10.1038/nature03794>.
- [49] H. Van den Hul, D. Mondelaers, M.K. Van Bael, J. Mullens, Water-based wet chemical synthesis of (doped) ZnO nanostructures, *J. Sol-Gel Sci. Technol.* 39 (2006) 41–47, <https://doi.org/10.1007/s10971-006-6322-5>.
- [50] Rao BG, Mukherjee D, Reddy BM. Novel approaches for preparation of nanoparticles. In *Nanostructures for novel therapy*, Elsevier; 2017, p. 1–36.
- [51] K.J. Klabunde, R.M. Richards (Eds.), *Nanoscale materials in chemistry*, John Wiley & Sons, 2009.
- [52] R.L. Manjunatha, K.V. Usharani, H. Naik, Synthesis and characterization of ZnO nanoparticles: A review, *J. Pharmaceut. Biotechnol.* 5 (1) (2019) 1095–1100.
- [53] M. Parashar, V.K. Shukla, R. Singh, Metal oxides nanoparticles via sol-gel method: a review on synthesis, characterization and applications, *J. Mater. Sci. Mater. Electron.* 31 (2020) 3729–3749, <https://doi.org/10.1007/s10854-020-02994-8>.
- [54] L. Spanhel, M.A. Anderson, Semiconductor clusters in the sol-gel process: quantized aggregation, gelation, and crystal growth in concentrated zinc oxide colloids, *J. Am. Chem. Soc.* 113 (1991) 2826–2833, <https://doi.org/10.1021/ja00004a004>.
- [55] E.A. Meulenkamp, Synthesis and growth of ZnO nanoparticles, *J. Phys. Chem. B* 102 (1998) 5566–5572, <https://doi.org/10.1021/jp98220h>.
- [56] M. Blätel, S. Musil, M. Ivanda, S. Popović, Sol-gel synthesis and characterization of nanocrystalline ZnO powders, *J. Alloy. Compd.* 397 (2005) L1–L4, <https://doi.org/10.1016/j.jallcom.2005.01.045>.
- [57] Y.P. Guo, C.N. Sikk, L.J. Hope-Weeks, A sol-gel route to synthesize monolithic zinc oxide aerogels, *Chem. Mater.* 19 (2007) 6007–6011, <https://doi.org/10.1021/cm0719419>.
- [58] M.A. Cicillini, M.F. Silva, D.M. Fernandes, M.A. de Melo, A.A. Hechenbleitner, E. A. Pineda, Fe-doped ZnO nanoparticles: synthesis by a modified sol-gel method and characterization, *Mater. Lett.* 159 (2015) 84–86, <https://doi.org/10.1016/j.matlet.2015.06.023>.
- [59] B. Manikandan, T. Endo, S. Kaneko, K.R. Murali, R. John, Properties of sol gel synthesized ZnO nanoparticles, *J. Mater. Sci. Mater. Electron.* 29 (2018) 9474–9485, <https://doi.org/10.1007/s10854-018-0981-3>.
- [60] B. Khanizadeh, M. Khorzavi, M.A. Behnajady, A. Shamel, B. Vahid, Mg and La Co-doped ZnO nanoparticles prepared by sol-gel method: synthesis, characterization and photocatalytic activity, *Period. Polyttech., Chem. Eng.* 64 (2020) 61–74, <https://doi.org/10.3311/PPCH.12959>.
- [61] A. Kumar, Sol gel synthesis of zinc oxide nanoparticles and their application as nano-composite electrode material for supercapacitor, *J. Mol. Struct.* 1220 (2020), 128654, <https://doi.org/10.1016/j.molstruc.2020.128654>.
- [62] A. Nagar, A. Kumar, S. Parveen, A. Kumar, H. Dhasmana, S. Husain, A. Verma, V. K. Jain, Zinc oxide nanoflowers synthesized by sol-gel technique for field emission displays (FEDs), *Mater. Today: Proc.* 32 (2020) 402–406, <https://doi.org/10.1016/j.matpr.2020.02.087>.
- [63] S. Kanwal, M. Tahir Khan, V. Tirth, A. Algahtani, T. Al-Mughanam, A. Zaman, Room-temperature ferromagnetism in Mn-doped ZnO nanoparticles synthesized by the sol-gel method, *ACS Omega* 8 (2023) 28749–28757, <https://doi.org/10.1021/acsomega.2c03418>.
- [64] Yusha'u A, Darma MS, Isah KA. Sol-gel synthesis of ZnO nanoparticles for optimized photocatalytic degradation of Eriochrome Black T under UV irradiation. *Algerian Journal of Engineering and Technology* 2023; 8:117–30. [10.57056/ajet.v8i1.100](https://doi.org/10.57056/ajet.v8i1.100).
- [65] B. Baruwat, D.K. Kumar, S.V. Manorama, Hydrothermal synthesis of highly crystalline ZnO nanoparticles: a competitive sensor for LPG and EtOH, *Sens. Actuators B Chem.* 119 (2006) 676–682, <https://doi.org/10.1016/j.snb.2006.01.028>.
- [66] Madathil AN, Vanaja KA, Jayaram MK. Synthesis of ZnO nanoparticles by hydrothermal method. In *Nanophotonic materials IV 2007*; 6639: 47–55. SPIE, [10.1117/12.730364](https://doi.org/10.1117/12.730364).
- [67] L. Kamari, W.Z. Li, C.H. Vansoy, R.M. Leblanc, D.Z. Wang, Zinc oxide micro-and nanoparticles: synthesis, structure and optical properties, *Mater. Res. Bull.* 45 (2010) 190–196, <https://doi.org/10.1016/j.materresbull.2009.09.021>.
- [68] J. Kim, K. Yong, Mechanism study of ZnO nanorod-bundle sensors for H₂S gas sensing, *J. Phys. Chem. C* 115 (2011) 7218–7224, <https://doi.org/10.1021/jp110129f>.
- [69] M. Chen, Z. Wang, D. Han, F. Gu, G. Guo, Porous ZnO polygonal nanoflakes: synthesis, use in high-sensitivity NO₂ gas sensor, and proposed mechanism of gas sensing, *J. Phys. Chem. C* 115 (2011) 12763–12773, <https://doi.org/10.1021/jp201810d>.
- [70] P. Rai, Y.T. Yu, Citrate-assisted hydrothermal synthesis of single crystalline ZnO nanoparticles for gas sensor application, *Sens. Actuators B Chem.* 173 (2012) 58–65, <https://doi.org/10.1016/j.snb.2012.05.068>.
- [71] J. Du, R. Zhao, S. Chen, H. Wang, J. Li, Z. Zhu, Self-assembly of gridlike zinc oxide lamellae for chemical-sensing applications, *ACS Appl. Mater. Interfaces* 7 (2015) 5870–5878, <https://doi.org/10.1021/am509139f>.
- [72] N. Kumaresan, K. Ramamurthi, R.R. Babu, K. Sathuraman, S.M. Babu, Hydrothermally grown ZnO nanoparticles for effective photocatalytic activity, *Appl. Surf. Sci.* 418 (2017) 138–146, <https://doi.org/10.1016/j.apsusc.2016.12.231>.
- [73] S. Agarwal, P. Rai, E.N. Gao, E. Llobet, F. Güell, M. Kumar, K. Awasthi, Gas sensing properties of ZnO nanostructures (flowers/rods) synthesized by hydrothermal method, *Sens. Actuators B Chem.* 292 (2019) 24–31, <https://doi.org/10.1016/j.snb.2019.04.083>.
- [74] N. Srinivasan, M. Anbuchezhlyan, S. Harish, S. Ponvasamy, Hydrothermal synthesis of C doped ZnO nanoparticles coupled with BiVO₄ and their photocatalytic performance under the visible light irradiation, *Appl. Surf. Sci.* 494 (2019) 771–782, <https://doi.org/10.1016/j.apsusc.2019.07.093>.
- [75] S. Nundy, T.Y. Eom, K.Y. Song, J.S. Park, H.J. Lee, Hydrothermal synthesis of mesoporous ZnO microspheres as NO_x gas sensor materials—Calcination effects on microstructure and sensing performance, *Ceram. Int.* 46 (2020) 19354–19364, <https://doi.org/10.1016/j.ceramint.2020.04.279>.
- [76] M.M. ElFaham, A.M. Mostafa, E.A. Mwofy, The effect of reaction temperature on structural, optical and electrical properties of tunable ZnO nanoparticles

- synthesized by hydrothermal method, *J. Phys. Chem. Solid* 154 (2021), 110089, <https://doi.org/10.1016/j.jpcs.2021.110089>.
- [77] M. Lal, P. Sharma, C. Ram, Optical, structural properties and photocatalytic potential of Ni-ZnO nanoparticles synthesized by hydrothermal method, *Results Opt. 10* (2023), 100371, <https://doi.org/10.1016/j.reso.2023.100371>.
- [78] Baboaram K. Novel solution routes to ferroelectrics and relaxors. In *Handbook of Advanced Dielectric, Piezoelectric and Ferroelectric Materials*, Woodhead Publishing, 2008, p. 852-883.
- [79] Z. Wang, B. Huang, Y. Dai, X. Qin, X. Zhang, P. Wang, H. Liu, J. Yu, Highly photocatalytic ZnO/ta2O3 heterostructures synthesized by a coprecipitation method, *J. Phys. Chem. C* 113 (2009) 4612-4617, <https://doi.org/10.1021/jp510760j>.
- [80] F. Giovannelli, A.N. Ndimba, P. Diaz-Chao, M. Motellón-Helino, F.I. Raynal, C. Autret, F. Delorme, Synthesis of Al doped ZnO nanoparticles by aqueous coprecipitation, *Powder Technol.* 262 (2014) 203-208, <https://doi.org/10.1016/j.powtec.2014.04.065>.
- [81] V. Gandhi, R. Ganesan, H.H. Abdulrahman Syedahamed, M. Thalyan, Effect of cobalt doping on structural, optical, and magnetic properties of ZnO nanoparticles synthesized by coprecipitation method, *J. Phys. Chem. C* 118 (18) (2014 May 8) 9715-9725, <https://doi.org/10.1021/jp411194i>.
- [82] A.N. El-Shazly, M.M. Rashad, E.A. Abdel-Aziz, I.A. Ibrahim, M.F. El-Shahat, A. E. Shaban, Nanostructured ZnO photocatalysts prepared via surfactant assisted Co-Precipitation method achieving enhanced photocatalytic activity for the degradation of methylene blue dyes, *J. Environ. Chem. Eng.* 4 (2016) 3177-3184, <https://doi.org/10.1016/j.jece.2016.06.018>.
- [83] S.A. Argenteo, C. Stanhaus, J.C. Padilha, L.P. Cabeca, J.L. Ferrari, M.S. Goes, Use of ionic liquid TEA-PS. BF4 as media synthesis of ZnO based on coprecipitation method, *J. Alloy. Compd.* 810 (2019), 151835, <https://doi.org/10.1016/j.jallcom.2019.151835>.
- [84] R.E. Adam, G. Pozina, M. Willander, O. Nur, Synthesis of ZnO nanoparticles by co-precipitation method for solar driven photodegradation of Congo red dye at different pH, *Photonics Nanostruct. Fundam. Appl.* 32 (2018) 11-18, <https://doi.org/10.1016/j.photonics.2018.05.005>.
- [85] A. Kolesnyczak-Rudzińska, T. Jesionowski, A. Krystalkiewicz, Obtaining zinc oxide from aqueous solutions of KOH and Zn (CH3COO) 2, *Physicochem. Probl. Miner. Process.* 44 (2010) 93-102.
- [86] W. Jimiao, Y. Jun, H. Niag, Y. Jianfeng, Acetone gas sensing properties of Au-activated Ni-doped ZnO nanoparticles prepared by Coprecipitation method, *Rare Met. Mater. Eng.* 47 (2018) 1602-1608, [https://doi.org/10.1016/S1875-5372\(18\)30150-4](https://doi.org/10.1016/S1875-5372(18)30150-4).
- [87] K.M. Kumar, B.K. Mandal, E.A. Naidu, M. Sinha, K.S. Kumar, P.S. Reddy, Synthesis and characterization of flower shaped zinc oxide nanostructures and its antimicrobial activity, *Spectrochim. Acta - A: Mol. Biomol.* 104 (2013) 171-174, <https://doi.org/10.1016/j.saa.2012.11.025>.
- [88] A. Apostolák, Y. Zhu, P. Gaultier, A. Valette, J.M. Bluet, T. Cornier, B. Massenelli, S. Dastide, Improved visible emission from ZnO nanoparticles synthesized via the Co-precipitation method, *Materials* 16 (2023) 5400, <https://doi.org/10.3390/ma16155400>.
- [89] Leung R, Hou MJ, Shah DO. Microemulsions: formation, structure, properties, and novel applications. In *Surfactants in Chemical/Process Engineering*, Routledge 2017, p. 315-368.
- [90] Zielińska-Jurek A, Reszczyńska J, Grabowska E, Zaleska A. Nanoparticles preparation using microemulsion systems. *Microemulsions-an introduction to properties and applications*. 2012, p. 229-50.
- [91] S. Hingorani, V. Pillai, P. Kumar, M.S. Multani, D.O. Shah, Microemulsion mediated synthesis of zinc-oxide nanoparticles for varistor studies, *Mater. Res. Bull.* 28 (1993) 1303-1310, [https://doi.org/10.1016/0025-5408\(93\)90178-G](https://doi.org/10.1016/0025-5408(93)90178-G).
- [92] J. Zhang, L.D. Sua, X.C. Jiang, C.S. Liao, C.H. Yan, Shape evolution of one-dimensional single-crystalline ZnO nanostructures in a microemulsion system, *Cryst. Growth Des.* 4 (2004) 309-313, <https://doi.org/10.1021/cg034142z>.
- [93] X. Li, G. He, G. Xiao, H. Liu, M. Wang, Synthesis and morphology control of ZnO nanostructures in microemulsions, *J. Colloid Interface Sci.* 333 (2009) 465-473, <https://doi.org/10.1016/j.jcis.2009.02.029>.
- [94] D. Sarkar, S. Tikku, V. Thapar, R.S. Srinivasa, K.C. Khilar, Formation of zinc oxide nanoparticles of different shapes in water-in-oil microemulsion, *Colloids Surf. A Physicochem. Eng. Asp.* 381 (2011) 123-129, <https://doi.org/10.1016/j.colsurfa.2011.03.011>.
- [95] F.H. Saboor, A.A. Khodadadi, Y. Mortazavi, M. Asgari, Microemulsion synthesized silica/ZnO stable core/shell sensors highly selective to ethanol with minimum sensitivity to humidity, *Sens. Actuators B Chem.* 238 (2017) 1070-1083, <https://doi.org/10.1016/j.snb.2016.07.127>.
- [96] Y. Ding, J. Xu, L. Chen, J. Yao, S. Dai, J. Wu, T. Hayat, A. Alsaedi, Pierced ZnO nanowires via a template-free photopolymerization in microemulsion, *J. Alloy. Compd.* 787 (2019) 779-785, <https://doi.org/10.1016/j.jallcom.2019.02.107>.
- [97] X. Zhang, Y. Han, W. Liu, N. Pan, D. Li, J. Chal, A novel synthesis of hexagonal cylinder-like ZnO with an excellent performance by a surfactant-free microemulsion-hydrothermal method, *Ind. Eng. Chem. Res.* 97 (2021) 326-336, <https://doi.org/10.1016/j.iecr.2021.02.019>.
- [98] O.A. Yildirim, C. Durucan, Synthesis of zinc oxide nanoparticles elaborated by microemulsion method, *J. Alloy. Compd.* 506 (2010) 944-949, <https://doi.org/10.1016/j.jallcom.2010.07.125>.
- [99] Demazeau G, Morrel O., Devalette M., Verdon E. 1987. European Patent, EP 238367.
- [100] Cuney M, Cathelineau M, editors. Proceedings of the 4th International Symposium on Hydrothermal Reactions: Nancy (France), Institut Lorrain des Geosciences; 1993.
- [101] G. Demazeau, Solvothermal and hydrothermal processes: the main physico-chemical factors involved and new trends, *Res. Chem. Intermed.* 37 (2011) 107-123, <https://doi.org/10.1007/s11164-011-0240-z>.
- [102] Feng SEI, Li GEI. Hydrothermal and solvothermal syntheses. In *Modern inorganic synthetic chemistry*, Elsevier; 2017, p. 73-104.
- [103] S. Kunjara Na Ayudhya, P. Tonto, O. Mekasuwandumrong, V. Pavarajarn, P. Praserttham, Solvothermal synthesis of ZnO with various aspect ratios using organic solvents, *Cryst. Growth Des.* 6 (2446-50) (2006), <https://doi.org/10.1021/cg050345z>.
- [104] H.M. Cheng, W.H. Chiu, C.H. Lee, S.Y. Tsai, W.F. Hsieh, Formation of branched ZnO nanowires from solvothermal method and dye-sensitized solar cells applications, *J. Phys. Chem. C* 112 (2008) 16359-16364, <https://doi.org/10.1021/jp805239k>.
- [105] S. Cimban, S. Albonetti, L. Forni, F. Peri, D. Lazzari, Solvothermal synthesis and properties control of doped ZnO nanoparticles, *J. Colloid Interface Sci.* 329 (2009) 73-80, <https://doi.org/10.1016/j.jcis.2008.09.060>.
- [106] P. Rai, W.K. Kwak, Y.T. Yu, Solvothermal synthesis of ZnO nanostructures and their morphology-dependent gas-sensing properties, *ACS Appl. Mater. Interfaces* 5 (2013) 3026-3032, <https://doi.org/10.1021/am302611a>.
- [107] L. Santos, D. Nunes, T. Calmeiro, R. Branquinho, D. Salgueiro, P. Barquinha, L. Pereira, R. Martins, E. Fortunato, Solvothermal synthesis of gallium-indium-zinc-oxide nanoparticles for electrolyte-gated transistors, *ACS Appl. Mater. Interfaces* 7 (2015) 638-646, <https://doi.org/10.1021/am506814c>.
- [108] B. Navas, A. Balleza, I. González, J.L. Palma, P. Dreyse, Controlled dispersion of ZnO nanoparticles produced by basic precipitation in solvothermal processes, *Heliyon* 6 (2020) e05821.
- [109] I.A. Nagornov, A.S. Mokrushin, E.P. Simonenko, N.P. Simonenko, P.Y. Gorbenov, V.G. Sevastyanov, N.T. Kuznetsov, Zinc oxide obtained by the solvothermal method with high sensitivity and selectivity to nitrogen dioxide, *Ceram. Int.* 46 (2020) 7756-7766, <https://doi.org/10.1016/j.ceramint.2019.11.270>.
- [110] A. Šarić, I. Despotović, G. Stefančić, Solvothermal synthesis of zinc oxide nanoparticles: A combined experimental and theoretical study, *J. Mol. Struct.* 1178 (2019) 251-260, <https://doi.org/10.1016/j.molstruc.2018.10.025>.

Structural, Thermal, and Optical Properties of Synthesized Cobalt Ferrite Nanoparticles

Yogeshwari J. Bhadane & Arun S. Garde

Research Centre in Physics, M S G Arts, Science & Commerce College Malegaon camp
Dist. Nashik 423 105

Corresponding Author: arungarde@yahoo.co.in

Abstract :

The Cobalt spinel ferrite nanoparticles were prepared by hydrothermal technique. This paper aims to study the behaviour due to the effect of temperature on the nanoparticles sintered at 200°C for 60 minutes in an air atmosphere. The optimal hydrothermal treatment was performed at 180°C and pH 10 for 4 hr. The CO-Fe₂O₄ nanoparticles were characterized by X-ray diffraction (Structural), and patterns showed that CO-Fe₂O₄ nanoparticles have a cubic structure. The synthesized cobalt ferrite nanoparticles were heated from 100°C to 900°C under flowing N₂ and changes in mass losses are recorded. The UV-vis absorption spectrum shows an absorption band at 259 nm and 261nm due to CO-Fe₂O₄ nanoparticles sintered at 200°C. IR shows the absorption peak of synthesized CO-Fe₂O₄ nanoparticles was observed in 416cm⁻¹ attributed to the stretching Fe-O bonds respectively. This IR suggests no hydrogen bonding is observed in synthesized CO-Fe₂O₄ hydrogen bonding is observed at 3414 cm⁻¹. The results also revealed that the as-prepared spinel cobalt ferrite nanoparticles have an estimated optical band gap energy in the range of 2.5 to 4.5eV. For that CO-Fe₂O₄ nanoparticles is suitable for Biomedical application.

1. Introduction :

Nowadays ferrites are in the scientific field as well as commercial Progressing. Until now ferrites were seen in optics, electronics, mechanics, and other fields. But currently, ferrites have started making progress in the medical field, cobalt ferrite is a good example of that. Cobalt ferrites do their best in the biomedical field. Cancer is the most deadly disease in present times. Cobalt ferrites have proven their quality in cancer treatment. Because in the treatment of cancer, when the drug is delivered into the body, it not only treats cancer cells but also harms other innocent cells. Cobalt ferrites are coming in handy to stop this. Cobalt ferrites nanoparticles have been synthesized using various synthesis methods such as mechanical milling, laser ablation, co-precipitation, plasma synthesis, hydrothermal, auto-combustion, microwave, sol-gel, and microemulsion.^[1,2,3] The synthesis of cobalt ferrite hydrothermal method is used because pure and highly crystalline nanoparticle is obtained using this method. The chemical co-precipitation results in the product of perfect stoichiometry. So we are using the chemical route method (such as hydrothermal) to synthesize pure and rare earth metal doped iron oxide semiconducting nanoparticles.

2. Methodology :

2.1 Materials and Reagents :

Ferric nitrate (Fe(NO₃)₃.9H₂O), cobalt nitrate (CO(NO₃)₂.6H₂O), and sodium hydroxide(NaOH) were purchased from LOBA Chemie, India, Distilled Water

2.2 Preparation of Cobalt ferrite nanoparticles :

Cobalt ferrite nanoparticles were synthesized by a hydrothermal method. This was performed by ferric nitrate (25.96gm) and cobalt nitrate (9.2gm) separately dissolving in 60 ml

distilled water by maintaining the ratio of nitrates (g): water (ml) as 1:3, then both solutions were mixed with stirring. After that NaOH solution (6gm, 50ml distilled water) was added dropwise. The mixture was allowed to stir at 70 °C until the pH of the mixture reached 10 and a brown reaction occurred. Then after that, this solution was transferred to a Teflon-lined autoclave. The autoclave was then sealed and placed in an oven set up at 180 °C for 4h. Then the temperature of the autoclave comes to room temperature, separate the black precipitate, and wash it with bi-distilled water and ethanol. Dry the separated precipitate and sinter it at 200 °C for 1 hour. The as-prepared powder is characterized using a UV – visible spectrophotometer, FT-IR spectrophotometer, X-ray diffractometer, and thermo gravimetric analysis for structural, optical, and thermal properties respectively.

3. Characterization :

3.1 Structural analysis :

3.1.1 X-ray diffraction (XRD) pattern of the spinel cobalt ferrite nanoparticles :

The X-ray diffraction (XRD) pattern of the spinel type cobalt ferrite nanoparticles synthesized via hydrothermal method is shown in Fig. 1. These are well indexed at 2θ values of 18.2° (111), 30.08° (220), 35.4° (311), 43.05° (400), 53.4° (422), 56.9° (511), 62.5° (440), and 74.01° (533). The peaks are indexed based on the JCPDS (#22-1086) [4, 5]. These reflections belong to the cubic structure of f.c.c. type. No extra peak other than these reflections is observed in the XRD pattern. The analysis of the XRD pattern confirms the single-phase cubic spinel structure of the prepared samples. The most intense peak (311) of the XRD pattern was considered to estimate the crystallite size. The crystallite size was calculated by the well-known Debye-Scherrer's formula $D = \frac{K\lambda}{\beta \cos\theta}$ [6,7,8] which is found to be 21.6 nm confirming the nanocrystalline nature of the prepared CoFe_2O_4 samples.

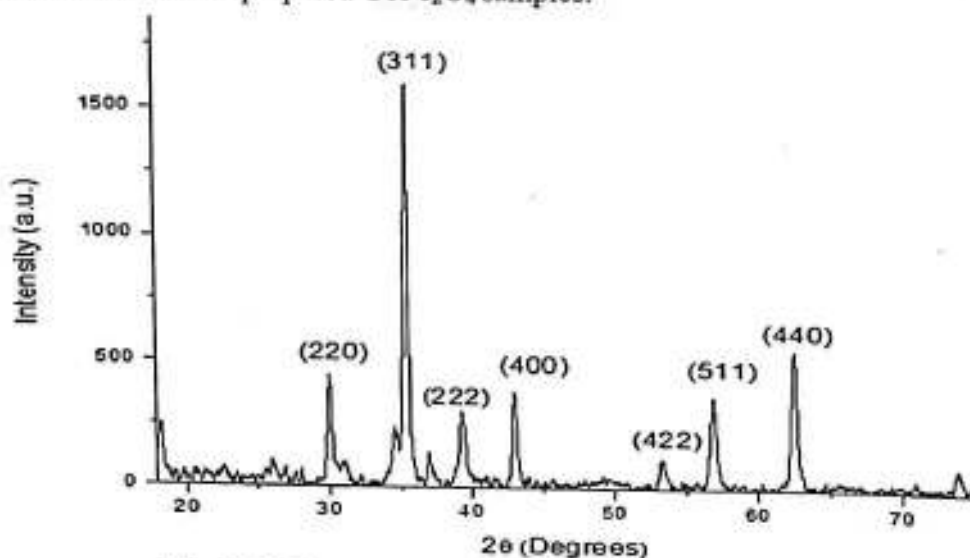


Fig 1. XRD patterns of the CoFe_2O_4 nanopowder

3.1.2 TGA :

Thermo gravimetric analysis (TGA) of synthesized cobalt ferrite nanoparticles is shown in Fig. 2. The synthesized cobalt ferrite nanoparticles were heated from 50°C to 800°C under flowing N_2 and changes in mass losses are recorded. The initial weight loss at the temperature range of 50–150°C was due to the evaporation of absorbed water and the primary breakdown of

the complex. The weight loss observed between 150–550°C with a mass loss of 12.6%, was due to dehydration of the hydroxyl group in the spinel structure and formation of semi-organic carbon materials/metal oxides^[10]. The other stage in sudden weight loss at the temperature range of 550–640°C is due to the formation of spinel phase metal oxide. After 640°C, no further distinguishable weight loss was detected, indicating that all organic constituents were eliminated.

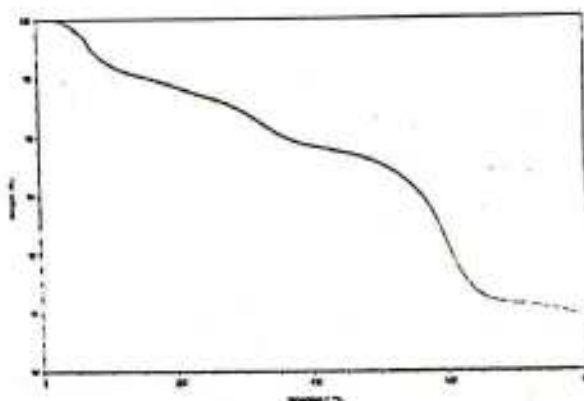


Fig.2 Thermo gravimetric analysis of CoFe_2O_4

3.1.3 FT-IR :

Figure 3 shows the FTIR spectrum of CoFe_2O_4 nanoparticles^[13]. Infrared studies were carried out in order to ascertain the purity and nature of the cobalt ferrite nanoparticles. The FTIR spectra of CoFe_2O_4 showed transmittance at 579cm^{-1} relates to the Fe-O bond. The transmittance at 462 and 411cm^{-1} determines the metal oxide bond (Co-O) in the nanoparticles. The peak observed at 3511cm^{-1} is assigned to the OH group and 3364cm^{-1} confirms the OH stretching and deformation in the bare CoFe_2O_4 nanoparticles. The CoFe_2O_4 confirms the metal oxide bands in the spinel structure.

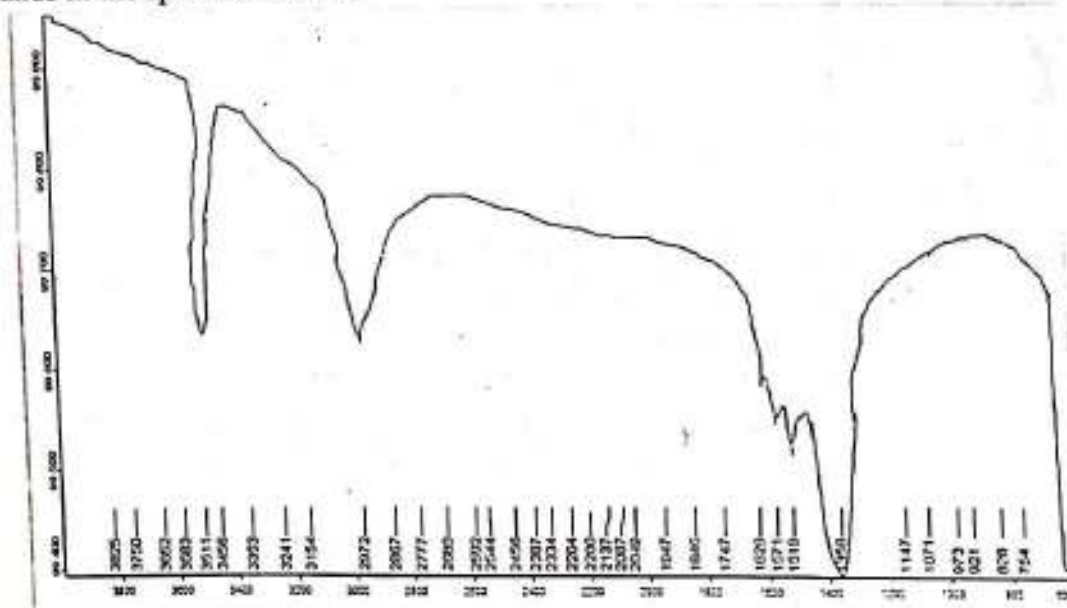


Fig 3. FTIR Spectra of CoFe_2O_4 nanoparticles

3.1.4 UV visible spectra :

The UV-Vis absorption spectrum for CoFe_2O_4 is shown in Fig. 4. As shown in the recorded UV-Vis absorption spectrum shows that the maximum absorption was observed at 416 nm

wavelength. The presented CoFe_2O_4 was stable for more than 6 days and without any phase separation and sedimentation^[14]. The band gap is calculated by using

$$\therefore \epsilon = \frac{hc}{\lambda}$$

This formula, where ϵ is the energy band gap, hc is photon energy and λ is 416×10^{-9} ; after solving this we get an energy band gap is 2.9eV.

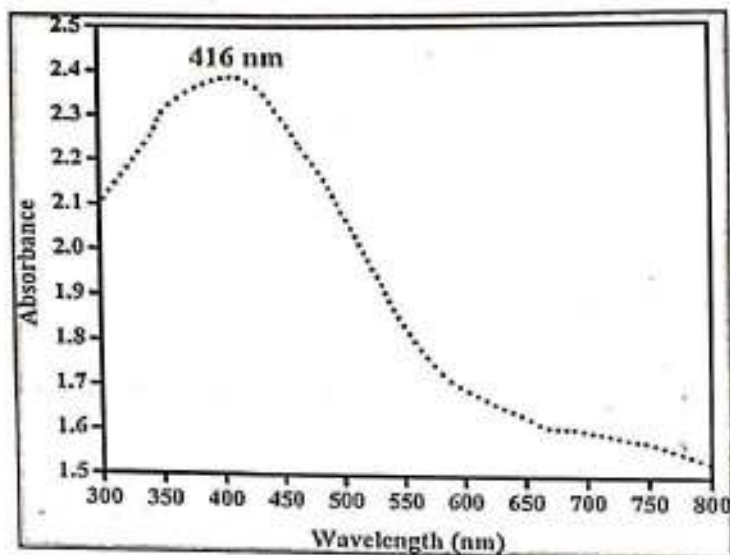


Fig. 4: UV visible spectra of CoFe_2O_4 nanoparticles

4. Conclusion :

In this study, cobalt ferrite nanoparticles were successfully synthesized using the hydrothermal method and comprehensively characterized. The findings confirmed the nanocrystalline nature, structural integrity, optical properties, and thermal behaviour of the nanoparticles. The results suggested promising applications in targeted drug delivery, cancer treatment, and biomedical imaging. Further research and development in this field are necessary to harness the full potential of cobalt ferrite nanoparticles for biomedical purposes.

References :

1. M. Y. Nassar and M. Khatab, Cobalt ferrite nanoparticles via a template-free hydrothermal route as an efficient nano-adsorbent for potential textile dye removal, *RSC Adv.*, 2016, 6, 79688 —79705
2. B. Debnath, H. G. Salunke and S. Bhattacharyya, Spin Disorder and Particle Size Effects in Cobalt Ferrite Nanoparticles with Unidirectional Anisotropy and Permanent Magnet-like Characteristics, *J. Phys. Chem. C*, 2020, 124, 25992 —26000
3. E. P. Muniz, L. S. D. de Assunção, L. M. de Souza, J. J. K. Ribeiro, W. P. Marques, R. D. Pereira, P. S. S. Porto, J. R. C. Proveti and E. C. Passamani, On cobalt ferrite production by sol-gel from orange fruit residue by three related procedures and its application in oil removal, *J. Clean. Prod.*, 2020, 265, 121712
4. P. A. Asogekar, S. K. Gaonkar, A. Kumar and V. M. S. Verenkar, Influence of Co over magnetically benign Zn ferrite system and study of its structural, dielectric, super paramagnetic and antibacterial efficacy, *Mater. Res. Bull.*, 2021, 141, 111330.

5. Nedaa M. Refat, Mostafa Y. Nassar and Sadeek A. Sadeek, Acontrollable one-pot hydrothermal synthesis of spherical cobalt ferrite nanoparticles: synthesis, characterization, and optical properties, *RSC Advance*, 2022, 12, 25081
6. Shyamaldas, M. Bououdina and C. Manoharan, Dependence of structure/morphology on electrical/magnetic properties of hydrothermally synthesised cobalt ferrite nanoparticles, *J. Magn. Mater.*, 2020, 493, 165703.
7. M. Y. Nassar, I. S. Ahmed and H. S. Hendy, A facile one-pot hydrothermal synthesis of hematite (α - Fe_2O_3) nanostructures and cephalixin antibiotic sorptive removal from polluted aqueous media, *J. Mol. Liq.*, 2018, 271, 844– 856.
8. R. Jenkins and R. L. Snyder, *Instruments for the Measurement of Powder Patterns, in Introduction to X-ray Powder Diffractometry*, John Wiley & Sons, Inc., 1996, pp.173–203.
9. S. Kanagesana, M. Hashima, S. Tamilselvanb, N.B. Alitheenb, I. Ismaila, M.Syazwana, M.M.M. Zuikimia, Sol-gel auto-combustion synthesis of cobalt ferrite and it's cytotoxicity properties, *Digest Journal of Nanomaterials and Biostructures*, Vol. 8, No. 4, October – December 2013, p. 1601 – 1610
10. L. Guo, X. Shen, X. Meng, Y. Feng, *J. Alloys Compd.* 490, 301 (2010).
11. M. Sivakumar, S. Kanagesan, R. Suresh Babu, S. Jesurani, R. Velmurugan, C. Thirupathi, T. Kalaivani, *J Mater Sci: Mater Electron* 23, 1045 (2012)
12. P. Sivakumar, R. Ramesh, A. Ramanand, S. Ponnusamy, C. Muthamizhchelvan, *Materials 1610 Research Bulletin* 46, 2204 (2011).
13. Augustin Maria Joseph, Balu Thangaraj, Rejith Selvamony Gomathi, Anto Arockia Raj Adaikalam, Synthesis and characterization of cobalt ferrite magnetic nanoparticles coated with polyethylene glycol, *AdvNanoBioM&D*: 2017: 1(1):71-77, ISSN: 2559 – 1118
14. Prashant B. Kharat, Apparao R. Chavan, Ashok V. Humbe, K. M. Jadhav, Evaluation of thermo acoustics parameters of CoFe_2O_4 -ethylene glycol nanofluid using ultrasonic velocity technique, *Journal of Materials Science: Materials in Electronics* <https://doi.org/10.1007/s10854-018-0386-1>
15. P Chitra and E Ranjith Kumar and Pushpagiri and Anath Steephen, "Size and Phase Purity Dependent Micro structure and Magnetic Properties of Spinel Ferrite Nanoparticles." *Journal of Superconductivity and Novel Magnetism* (2021) <https://doi.org/10.1007/s10948-021-05831-Z>
16. Gayatri Sivaraman and S. Kalainathan, "Synthesis and microstructure of gallium substituted cobalt ferrite nanoparticles by hydrothermal method." *Int. J. Nanoparticles*, Vol. 9(1)2016, pp.11-18.
17. Wei Wang, Zui Ding, Xiruo Zhao, Sizhu, Feng Li, Ming Yue and J Ping Liu, "Microstructure and magnetic properties of MFe_2O_4 (M= Co, Ni, and Mn) ferrite nanocrystals prepared using colloid mill and hydrothermal method," *Journal of Applied Physics* 117, 17A328(2015), ppl-4.
18. R.W. Chantrell, K. O'Grady, et al., *Journal of Physics D: Applied Physics* 18(1985) 2505.
19. H. Shenker, *Physical Review* 107 (1957) 1246.
20. D.J. Craik, E.D. Isaac, *Proceedings of the Physical Society* 76 (1960) 160.

Study the Luminescence Properties of Ce Doped $Ba_2Al_2SiO_7$ Phosphor

Ms. Sweta Dipakraj Kapade¹, Prof (Dr) R. N. Shelar², Prof. Dr. Sushma Kulkarni³, Dr. Dinesh S. Bobade⁴

¹ MGV's MSG College, Malegaon

² MGV's MSG College, Malegaon

³ MGV's MSG College, Malegaon

⁴ RNC Arts, JDB Commerce and NSC Science College, Nashik Road, Nashik,

Abstract:

$Ba_2Al_2SiO_7$, a long-lasting afterglow phosphor, was prepared at high temperature using a solid-state reaction in a weak reductive atmosphere. UV-visible spectroscopy, infrared spectroscopy, X-ray diffraction (XRD), scanning electron microscope (SEM), energy dispersive spectrum (EDS), and photoluminescence (PL) were used to characterize the prepared powder samples. The XRD analysis of the prepared $Ba_2Al_2SiO_7$ host and Ce^{3+} doped $Ba_2Al_2SiO_7$ phosphors revealed a hexagonal crystal structure. The band gap energies of prepared undoped and Ce^{3+} doped $Ba_2Al_2SiO_7$ nano-phosphors were calculated using UV spectroscopy. The FT-IR technique was used to study the bonding nature of the prepared samples. The crystal structure of the prepared Ce^{3+} doped $Ba_2Al_2SiO_7$ phosphors was calculated using the XRD technique, and it was found to be hexagonal axes with cell parameters $a=4.7636A^0$, $c=15.5820 A^0$, and particle size 28.776nm. The optical band gap energies of $Ba_2Al_2SiO_7$ host and Ce^{3+} doped $Ba_2Al_2SiO_7$ were calculated using UV spectroscopy. The PL spectra showed the maximum intensity for Ce^{3+} doped $Ba_2Al_2SiO_7$ Y at 282 and 443 nm under 600 nm excitation. The CIE color coordinates of the Ce^{3+} doped $Ba_2Al_2SiO_7$ Y are calculated using the radiant imaging color calculator program and refer to the 1931 CIE Standard Source C.

Keywords: muffle furnace, Solid state diffusion method, spectrophotometer technique

1. Introduction:

Rare earth element activated phosphor materials have been studied for the past 30 years and used in a variety of applications. These rare earth elements piqued people's interest because of their characteristic emission in the visible and near-visible (ultraviolet) regions. The visible emissions are attributed to the $5d \rightarrow 4f$ transition. Researchers are particularly interested in europium ion activated phosphors because of their characteristic emission of europium ions in the visible region. The europium ion activated phosphors have been used in a variety of applications, including display devices, solid state lighting, radiation dosimetry, x-ray imaging, CRO tubes[1-4]., LEDs, and Hg discharge lamps [5-8]. The luminescence property of the europium ion is known to be strongly influenced by its surrounding crystal field and the symmetry it acquires. Basically, silicates have appropriate.

Properties from an application standpoint include excellent temperature stability, water resistance, and the ability to exhibit luminescence when doped with rare earth and transition elements such as europium (Eu) and cerium (Ce). The emission of rare earth elements is affected by the size, charge, and strength of the ligand-metal ion bonding caused by the surrounding ligands. This emission, known as the $5f \rightarrow 4d$ transition [9-10], is a broad band emission that ranges from ultraviolet to yellow.

Recently, various silicate phosphors activated with Cerium ions have been studied and investigated. As a result, we can conclude that barium doped silicate phosphor has potential applications in a variety of lighting fields.

In this paper, we will present the synthesis and characterization of Ce doped $Ba_2Al_2SiO_7$ nano phosphor using UV-Visible, FT-IR, X-ray powder diffraction, FE-SEM, EDS, and spectrophotometer techniques.

2. Method of Preparation:

We used the solid state diffusion method to prepare Ce doped $Ba_2Al_2SiO_7$. Solid state reactions use a diffuse reaction mechanism, necessitating repeated grinding and heating. So, the reaction is grind for 15-20 minutes and heat the solid powder mixture (calcination) at elevated temperatures in air using a muffle furnace ($750^{\circ}C$) for 24 hours of $Ba_2Al_2SiO_7$, the material cooled down for 24 hours, and repeated grinding and heating the powder at $750^{\circ}C$ for 6 hours in a controlled atmosphere is required to master the valence of the activator and the stoichiometry of the

host lattice. As a result, doping 1-3% of the activator in the oxide host has been delicate. Again, samples are stored in glass bottles with proper labeling. These samples are used for further characterization.

3. _ Characterization of cerium doped $Ba_2Al_2SiO_7$:

UV-visible spectroscopy, FT-IR spectroscopy, X-ray powder diffraction, FESEM, EDS-spectroscopy, and spectrophotometer techniques are used to characterize the prepared Ce doped $Ba_2Al_2SiO_7$ samples.

3.1 UV-visible spectra (UV):

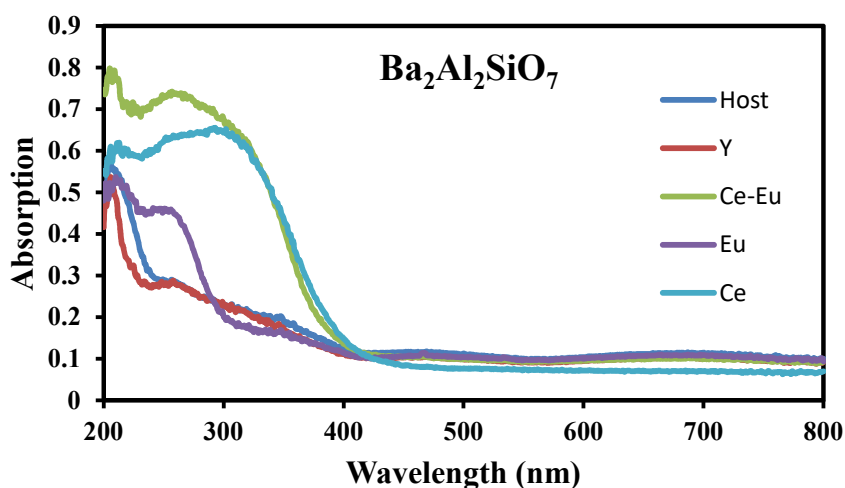


Fig.1.1 Band gap energy of $Ba_2Al_2SiO_7$

Table no 1.1: band gap energy of the prepared sample of $Ba_2Al_2SiO_7$ are enlisted below.

	Energy(ev)
Host	5.04
Y	5.18
Ce	3.43

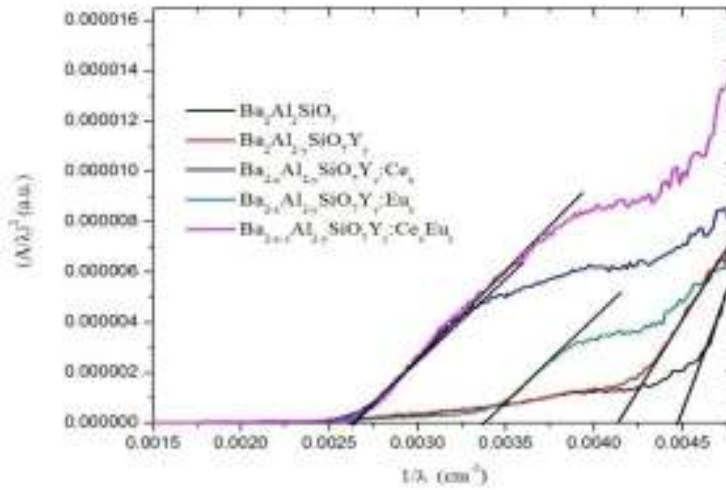


Fig.1.2 Band gap energy of $Ba_2Al_2SiO_7$

1.2 IR-Spectroscopy

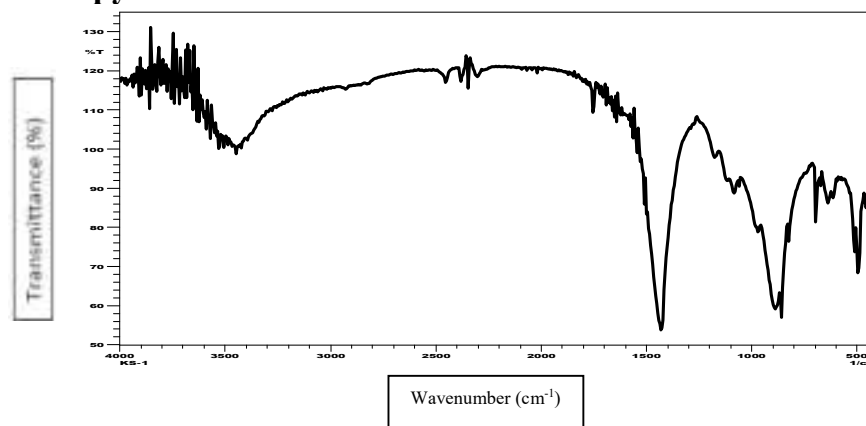


Figure.(1.3a): IR spectra transmittance $Ba_2Al_2SiO_7$: Host

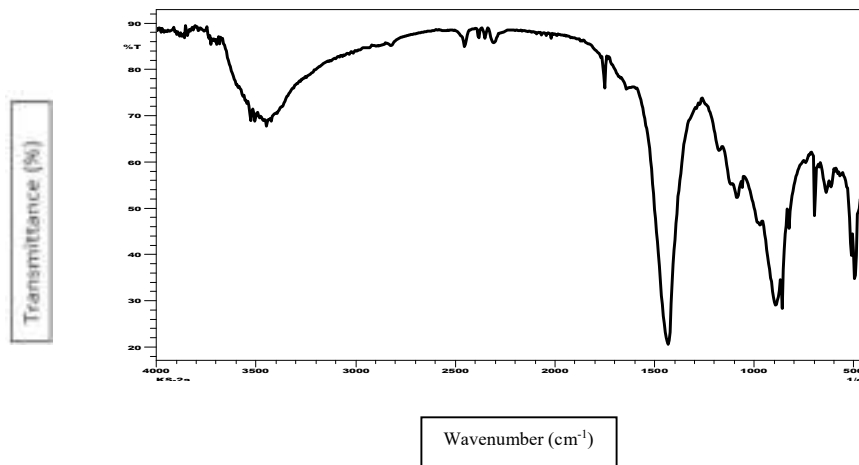


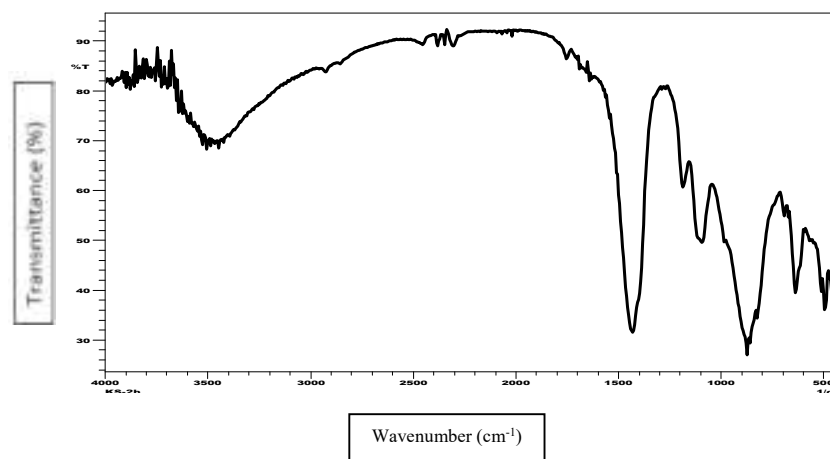
Figure.(1.3b): IR spectra transmittance $\text{Ba}_2\text{Al}_2\text{SiO}_7 : \text{Y}$ Figure.(1.3c): IR spectra transmittance $\text{Ba}_2\text{Al}_2\text{SiO}_7 : \text{Ce}$

Table. 1.2: IR Vibrations

Vibrations	Bonds	Nature of Vibrations
1400	Ba – O	Vibrations
1200 – 800	Si–O–Si Si–O–Al	Stretching Vibrations in SiO_4
935	Si-O	Terminal Stretching Vibrations
750 – 600	Al-O, Si-Si, Si-Al	Stretching Vibrations
600 – 300	Si-O-Si, Si-O-Al	Bending Vibrations

The IR spectra are shown in the figure. (1.3a)(1.3b)(1.3c). The presence of broad bands in the spectrum indicates that the sample is amorphous. A broad band centered at 950 cm^{-1} in the $1200\text{-}800 \text{ cm}^{-1}$ region indicates asymmetric vibrations of Si-O [11-13] within different Si structural units. An intense broad band in the $300\text{-}600 \text{ cm}^{-1}$ range is attributed to the bending vibration of Si-O-Si linkages in various structural units. The symmetric stretching of Si-O and Si-O-Si units results in a less intense band between 600 and 800 cm^{-1} . The presence of crystalline phases is represented by the

splitting of the broad bands into a number of sharp bands at approximately 1010, 970, 900, 830, 662, 600, 482, and 452 cm^{-1} . Thus, as with XRD, FTIR indicates the start of the crystallization phase. With increasing temperature and dwell time, these vibration bands become sharper and more intense, reflecting an increase in the crystalline phase in glass-ceramic materials. Some additional bands appear around 1060, 930, 706, 625, and 550 cm^{-1} , becoming more intense as dwell time and temperature increase. According to the literature, these vibrational bands are typical of the $\text{Ba}_2\text{Al}_2\text{SiO}_7$ crystalline phase. With a longer dwell time at higher temperatures, these bands become more sharp and intense, implying an increase in the amount of $\text{Ba}_2\text{Al}_2\text{SiO}_7$ crystalline phase. A number of sharp and intense vibrational bands, corresponding to both crystalline phases, are present.

3.3 X-Ray Diffraction (XRD):

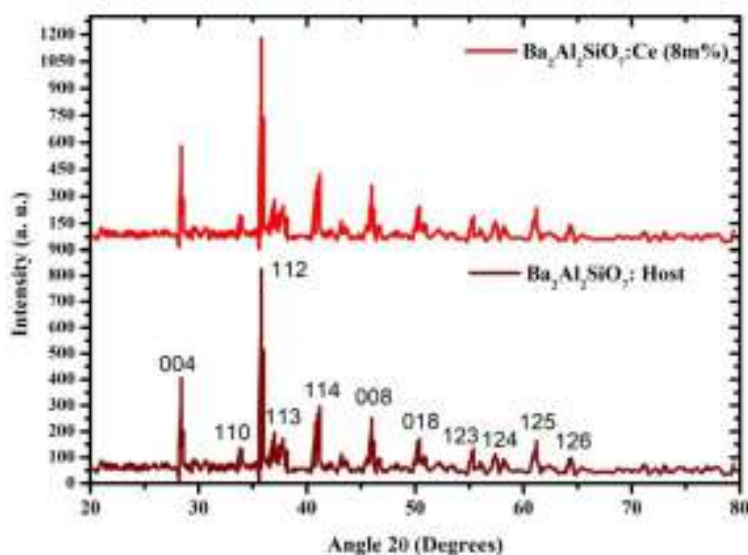


Fig (1.4) - XRD spectrum for Ce doped in $\text{Ba}_2\text{Al}_2\text{SiO}_7$

The XRD pattern of $\text{Ba}_2\text{Al}_2\text{SiO}_7$ is shown in Figure (1.4). The XRD pattern of $\text{Ba}_2\text{Al}_2\text{SiO}_7$ matches ICDD file no. 96-900-1420. It has hexagonal axes structure with cell parameter $a=4.7636\text{\AA}$ and $c=15.5820\text{\AA}$ [11-13].

The XRD pattern shows peaks with high intensity, confirming the high crystalline nature of the prepared host $\text{Ba}_2\text{Al}_2\text{SiO}_7$ sample. The particle size from the XRD data is calculated using a formula and is found to be 28.776nm.

$$d = \frac{0.9\lambda}{\beta \cos\theta}$$

3.4 Scanning Electron Microscope (SEM):

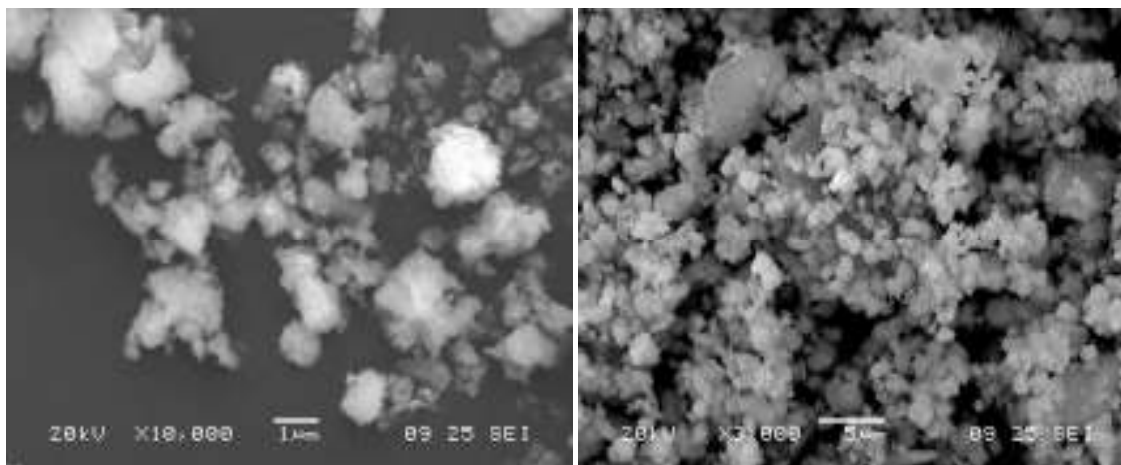
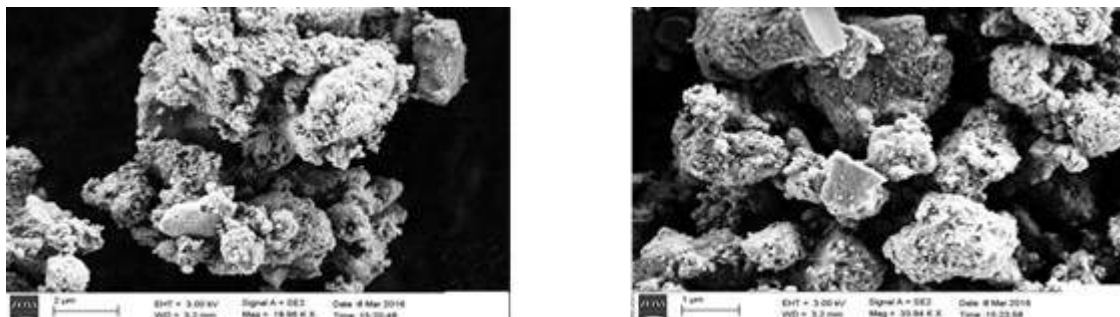


Fig (1.5a) - SEM for 1micrometer size

Fig. (1.5b)- SEM for 5 micrometer size

Figures (1.5a) and (1.5b) show SEM micrographs at various magnifications, demonstrating the presence of surface crystallization. The figure also depicts the dendrite growth of crystals. Figure depicts two distinct types of crystallites in the microstructure. So, we use FESEM for the particle.

3.5 Field Emission Scanning Electron Microscopy (FESEM):



Figures 1.6: Field Emission Scanning Electron Microscope.

FE-SEM images of the host $Ba_2Al_2SiO_7$ (fig.1.6) show that the host sample has a nanostructure on the order of 50 to 100 nm.

3.6 Energy Dispersive Spectrum (EDS):

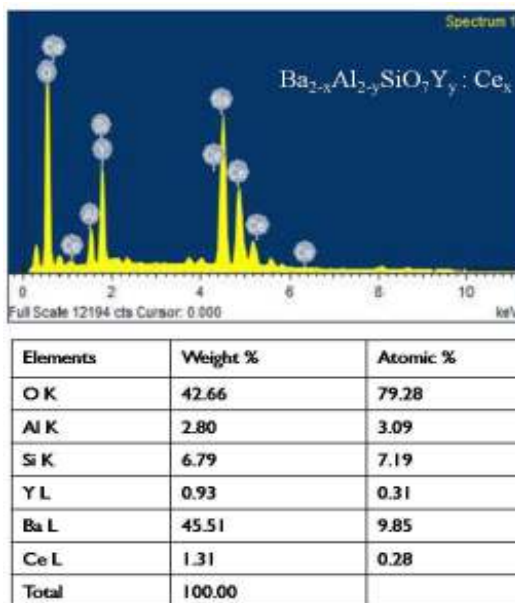


Figure 1.7 Energy dispersive spectrum of $Ba_{2-x}Al_{2-y}SiO_7Y_y: Ce_x$

Figure (1.7) shows the EDS spectrum and elemental composition of $Ba_2Al_2SiO_7$. The EDS spectrum of $Ba_2Al_2SiO_7$ shows signals for Ba, Al, Si, and O in the prepared host material. These observations, combined with XRD analysis, confirm the successful preparation of $Ba_2Al_2SiO_7$ phosphors.

3.7 Photoluminescence (PL)

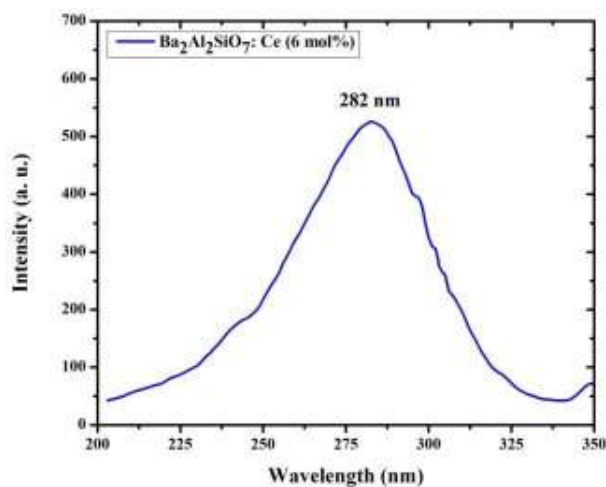


Fig.(1.8)- Excitation spectra of $Ba_2Al_2SiO_7: Ce$ phosphor

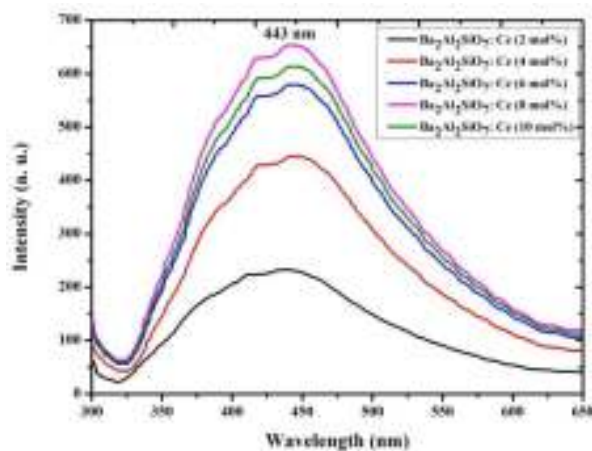


Fig (1.9) - Emission spectra of $\text{Ba}_2\text{Al}_2\text{SiO}_7:\text{Ce}$ phosphor

We measured photoluminescence spectra for $\text{Ba}_2\text{Al}_2\text{SiO}_7:\text{Ce}^{3+}$. Figure 1.8 shows the excitation spectra for $\text{Ba}_2\text{Al}_2\text{SiO}_7:\text{Ce}^{3+}$. The excitation spectra are carried out at the 450nm emission wavelength. It shows only one peak at 282 nm, which serves as the excitation wavelength for the sample's emission spectrum [15-17].

The emission spectrum is shown in figure (1.9) above. It had a broad emission peak at 443 nm and other low intensity peak at 423nm. The broad emission peak at 443nm is used for the excitation spectrum.

As a result, the prepared sample of $\text{Ba}_2\text{Al}_2\text{SiO}_7:\text{Ce}^{3+}$. can be used in UV excitation and emission LEDs.

3.8 Color Co-Ordinates

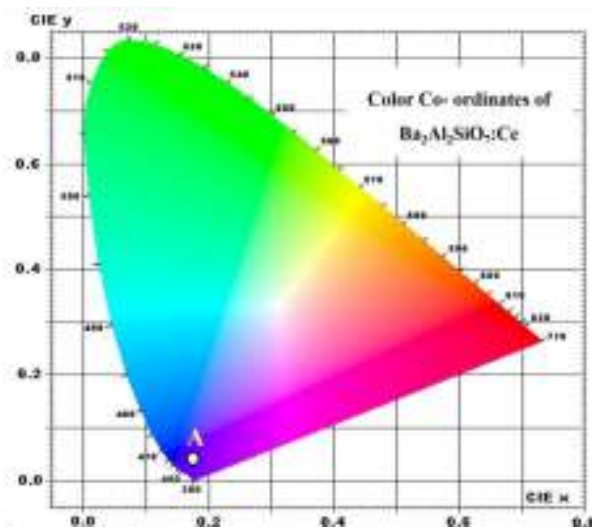


Fig.1.10: Color co-ordinates of $\text{Ba}_2\text{Al}_2\text{SiO}_7:\text{Ce}^{3+}$

A 2-D chromaticity diagram similar to the one in Figure 1.10 can be used to express the chromaticity coordinates [20-22]. This graphic displays the spectral wavelengths of the major single frequency colors as well as all the hues that a typical observer would be able to perceive for different (x,y) pairs. The white point on this diagram is represented by the A point.

The chromatic coordinates (x, y) was calculated using the color calculator program radiant imaging refer to the 1931 CIE Standard Source C (illuminant Cs (0.3101, 0.3162)) [22]. The coordinates of the Ce³⁺ doped Ba₂Al₂SiO₇ phosphors of strong blue color (x_0.8535, y_0.3852) for emission at 443 nm and are shown in Figure 8 by points A (white circle). This indicates that the color properties of the phosphor powder prepared by combustion synthesis do approaching requirements of solid state lighting.

4. _ Conclusions:

A solid-state reaction used to prepare the cerium ion doped Ba₂Al₂SiO₇ phosphor. The XRD measurements show that the prepared phosphor has a hexagonal structure. The band gap energies are calculated using UV spectroscopy and are 3.43 eV, 5.18 eV, and 5.04 eV for pure Ba₂Al₂SiO₇, 0.1 m% Ce³⁺ doped Ba₂Al₂SiO₇, and 0.5 m% Ce doped Ba₂Al₂SiO₇, respectively. PL measurements show the highest intensity at 443 nm, these phosphors are appropriate for lighting applications.

5. _ References:

- [1]. Wang, K., He, Q., Yang, D., & Pi, X. (2023, January 9). *Highly Efficient Energy Transfer from Silicon to Erbium in Erbium-Hyperdoped Silicon Quantum Dots*. *Nanomaterials*. <https://doi.org/10.3390/nano13020277>
- [2]. Wu, J., Liu, Q., Gao, P., Wang, J., Qi, Y., Li, Z., Li, J., & Jiang, T. (2023, August 30). *Design, Synthesis, and Characterization of a Novel Blue-Green Long Afterglow BaYAl₃O₇:Eu²⁺, Nd³⁺ Phosphor and Its Anti-Counterfeiting Application*. *Nanomaterials*. <https://doi.org/10.3390/nano13172457>
- [3]. Emen, F. M., Külçü, N., & Yazıcı, A. N. (2010, March 31). *Synthesis, characterization and luminescence properties of long afterglow Phosphor Ba₄Al₁₄O₂₅:Eu,Dy*. *European Journal of Chemistry*. <https://doi.org/10.5155/eurjchem.1.1.28-32.8>
- [4]. García Ramírez, V. M., García Murillo, A., Carrillo Romo, F. D. J., Alvarez González, R. I., & Madrigal Bujaidar, E. (2023, July 29). *A New Ultrafine Luminescent La₂O₃:Eu³⁺ Aerogel*. *Gels*, 9(8), 615. <https://doi.org/10.3390/gels9080615>
- [5]. Achari, A. M., Perumalsamy, V., Swati, G., & Khare, A. (2023, November 21). *SrAl₂O₄:Eu²⁺,Dy³⁺ Long Afterglow Phosphor and Its Flexible Film for Optomechanical Sensing Application*. *ACS Omega*, 8(48), 45483–45494. <https://doi.org/10.1021/acsomega.3c05222>
- [6]. Piotrowski, W., Trejgis, K., Maciejewska, K., Ledwa, K., Fond, B., & Marciniak, L. (2020, September 9). *Thermochromic Luminescent Nanomaterials Based on Mn⁴⁺/Tb³⁺ Codoping for*

- Temperature Imaging with Digital Cameras. *ACS Applied Materials & Interfaces*, 12(39), 44039–44048. <https://doi.org/10.1021/acsami.0c11730>
- [7]. https://www.irjmets.com/uploadedfiles/paper//issue_10_october_2023/45540/final/fin_irjmets1698239554.pdf. (2023, October 27). *International Research Journal of Modernization in Engineering Technology and Science*. <https://doi.org/10.56726/irjmets45540>
- [8]. Sipina, E. V., Spassky, D. A., Krutyak, N. R., Morozov, V. A., Zhukovskaya, E. S., Belik, A. A., Manylov, M. S., Lazoryak, B. I., & Deyneko, D. V. (2023, February 7). Abnormal $\text{Eu}^{3+} \rightarrow \text{Eu}^{2+}$ Reduction in $\text{Ca}_{9-x}\text{Mn}_x\text{Eu}(\text{PO}_4)_7$ Phosphors: Structure and Luminescent Properties. *Materials*, 16(4), 1383. <https://doi.org/10.3390/ma16041383>
- [9]. Vaidyanathan, S. (2023). Recent progress on lanthanide-based long persistent phosphors: an overview. *Journal of Materials Chemistry C*, 11(26), 8649–8687. <https://doi.org/10.1039/d2tc05243a>
- [10]. Zhang, T., Guo, H., Shi, Q., Qiao, J., Cui, C., Huang, P., & Wang, L. (2023). Investigation of a Novel Pr^{3+} -Activated Liygeo4 Phosphor with Red Long-Persistent Luminescence. <https://doi.org/10.2139/ssrn.4600163>
- [11]. Zheng, M., Li, X., Bai, Y., Tang, S., Li, P., & Zhu, Q. (2023, June 6). Sunlight-Activated Long Persistent Luminescent Coating for Smart Highways. *Coatings*, 13(6), 1050. <https://doi.org/10.3390/coatings13061050>
- [12]. Verma, A., Bisen, D., Brahme, N., Sahu, I. P., & Barik, P. (2023, September 1). Long Lasting Persistent Photo-Luminescence Properties of $\text{EuM}_1-x\text{MgAl}_10\text{O}_17$ ($M = \text{Ba, Ca, Sr, Zn}$) Phosphors. *Journal of Physics: Conference Series*, 2576(1), 012011. <https://doi.org/10.1088/1742-6596/2576/1/012011>
- [13]. Castaing, V., Lozano, G., & Míguez, H. (2022, April 26). Transparent Phosphor Thin Films Based on Rare-Earth-Doped Garnets: Building Blocks for Versatile Persistent Luminescence Materials. *Advanced Photonics Research*, 3(7). <https://doi.org/10.1002/adpr.202100367>
- [14]. Lee, C. Y., Wu, C. C., Li, H. H., & Yang, C. F. (2022, August 6). Synthesis and Luminescence Properties of Eu^{2+} -Doped $\text{Sr}_3\text{MgSi}_2\text{O}_8$ Blue Light-Emitting Phosphor for Application in Near-Ultraviolet Excitable White Light-Emitting Diodes. *Nanomaterials*, 12(15), 2706. <https://doi.org/10.3390/nano12152706>
- [15]. Etafo, N. O. (2024, January 10). A Novel Warm Red-Emission of $\text{SrLa}_0.9\text{Eu}_0.1\text{AlO}_4$ Phosphor obtained by Combustion Method. *Journal of Engineering Research*, 4(1), 2–12. <https://doi.org/10.22533/at.ed.1317412409015>
- [16]. Farooq, M., Rafiq, H., Shah, A. U. I., & Rasool, M. H. (2023, December 1). Review— On the Development of Phosphors for Luminescent Materials: Synthesis, Characterization, Applications and Evolution of Phosphors as White-Light-Emitting Diodes. *ECS Journal of Solid State Science and Technology*, 12(12), 126002. <https://doi.org/10.1149/2162-8777/ad1062>
- [17]. Kuriyan, N. S., Ghosh, P., Arya, A., & Sabeena, M. (2023, August). Site preference-based luminescence studies in Eu doped calcium magnesium silicate phosphor: A combined experimental and DFT approach. *Journal of Luminescence*, 260, 119901. <https://doi.org/10.1016/j.jlumin.2023.119901>
- [18]. Bidwai, D., Parauha, Y. R., Sahu, M. K., Dhoble, S. J., Jayasimhadri, M., & Swati, G. (2022, June). Synthesis and luminescence characterization of aqueous stable $\text{Sr}_3\text{MgSi}_2\text{O}_8$: Eu^{2+} , Dy^{3+} long afterglow nanophosphor for low light illumination. *Journal of Solid State Chemistry*, 310, 123089. <https://doi.org/10.1016/j.jssc.2022.123089>
- [19]. Krushna, B. R., Sharma, S., Prasad, B. D., Sridhar, C., Varalakshmi, S., George, A., Francis, D., Sivashanmugam, T., Manjunatha, K., Wu, S. Y., & Nagabhushana, H. (2024, February). A new strategy to boost luminescent markers for LFP detection and anti-counterfeiting applications using flux assisted $\text{BaLa}_2\text{ZnO}_5$: Eu^{3+} phosphor. *Materials Research Bulletin*, 170, 112561. <https://doi.org/10.1016/j.materresbull.2023.112561>

- [20]. Chen, N., Lin, T., Liu, Z., Liu, R., Zhang, J., Fu, X., & Zhang, H. (2024, January). Ultraviolet and visible persistent luminescence from Sr₃MgSi₂O₈:Pr³⁺. *Ceramics International*, 50(1), 1891–1897. <https://doi.org/10.1016/j.ceramint.2023.10.290>
- [21]. Kumar, P., Singh, D., Gupta, I., & Kumar, H. (2023, November). Synthesis, crystallographic structure, down shifting luminescence of Er(III) activated GdSr₂AlO₅ nanophosphors: An efficient green emitter for solid state lighting. *Materials Science in Semiconductor Processing*, 167, 107765. <https://doi.org/10.1016/j.mssp.2023.107765>
- [22]. Yang, X., Tang, B., & Cao, X. (2023, July). The roles of dopant concentration and defect states in the optical properties of Sr₂MgSi₂O₇:Eu²⁺, Dy³⁺. *Journal of Alloys and Compounds*, 949, 169841. <https://doi.org/10.1016/j.jallcom.2023.169841>
- [23]. Color Calculator Version 2, A Software from Radiant Imaging, Inc. (2007).



Integrated Approach to the Optimization, Synthesis, Fabrication, and Application of ZnO-Based Sensors for Portable LPG Leakage Detection Systems

V.T. Salunke¹, S.C. Kulkarni¹, Sajid Naeem^{2✉}, A.D. Shaligram³, R.Y. Borse⁴, P.B. Buchade⁵

¹Department of Electronic Science, MSG Arts, Science & Commerce College, Malegaon Camp 423203, Maharashtra, India

²Department of Applied Sciences, Maulana Mukhtar Ahmad Nadvi Technical Campus, Malegaon 423203, Maharashtra, India

³Department of Electronic Science, SPPU Pune 411007 Maharashtra, India

⁴MJM Arts, Commerce & Science College, Karanjali (Peth) 422208, Maharashtra, India

⁵MES Abasaheb Garware College, Pune 411004, Maharashtra, India

Received November 20, 2023

Revised March 22, 2024

Accepted April 15, 2024

Published online: 28 June 2024

Keywords

ZnO

Sensor

Energy

Metal Oxide

LPG Gas

Material Science

Abstract: Liquefied petroleum gas (LPG) is used for cooking as well as in vehicles in the form of compressed natural gas (CNG) and in industries. As gas is volatile, there is the possibility of leakage which will be turned into take explosion or fire. It is a keen need to use the detection system for gas leakage for security purposes. ZnO thick film sensor was synthesized and fabricated by using the standard screen-printing method. The XRD pattern revealed that the ZnO thick film was polycrystalline, with an average crystallite size of around 27.1174 nm. The SEM scan revealed a ZnO particle size of around 1.88 μ m. Additionally, electrical and thermal properties were examined. This paper discussed the synthesized ZnO thick film LPG gas leakage detector prototype using Arduino ATMEGA8.

© 2024 The authors. Published by Alwaha Scientific Publishing Services SARL, ASPS. This is an open access article under the CC BY license.

1. Introduction

The main source of fuel in this era is liquefied petroleum gas (LPG) not only in urban areas but also in rural areas. Compared to traditional fuel material LPG is clean and easy to handle. Because of the different government schemes most of the families in the rural areas benefited from using LPG. Today gas sensors are marked and demanded chemical sensors (Shankar and Rayappan 2015). Gas detection and indicators are widely needed in industries, industrial safety, monitoring and controlling environmental conditions, and processing control. The change in any one or more properties for instance resistance, temperature, humidity, etc. in the presence of a gas environment identifies the detection of gas leakage (Sowmya et al.

2021). The working of a metal oxide-based thick film gas sensor is based on the reaction of gas molecules with the surface of a thick film (Gusdevi et al. 2021). In this Oxygen, ions absorb on the surface by removing the electrons from bulk material and creating the barrier which limits the electron movement and results in the conductivity of the sensor (Hussain et al. 2017). For the detection of gas by metal oxide semiconducting material smaller grain size, stability, and good structural and electrical properties are the most important parameters (Bhavithra et al. 2021). The structural and electrical properties can be changed and improved by adding the additive and or dopant material (Ménil et al. 2005). Metal oxide materials are widely used for different applications such as solar cells, sensors, supercapacitors, optoelectronics, cosmetics,

✉ Corresponding Author: sajidnaeem@mmnctc.edu.in

piezoelectric, etc. (Naeem et al. 2023). For commercial purposes, LPG is considered fuel in all countries (Devi et al. 2006). Today LPG is vastly and primarily used in different applications, mostly for cooking and recently in vehicles since it is clean and convenient (Shinde et al. 2007). The LPG gas is stored as a liquid at high pressure and low temperatures thus the gas converts into liquid in the cylinder which is used for cooking purposes (Arshak and Gaidan 2005). LPG means Liquefied Petroleum Gas having a mixture of different hydrocarbon elements and originating from natural gas (Singh et al. 2023). For commercial use, LPG is stored in a cylinder whereas the LPG storage area uses strong and not easily leak gas tubes (Patil et al. 2023). But we know that LPG is a flammable gas so the main issue of the leakage problem of LPG is a serious problem for home security and residential area. Many commercial gas sensors are available in the market. Out of that MQ series metal oxide-based gas sensors are used widely. Use of MQ gas sensor for detecting different reducing gases like LPG, smoke methane, and butane directly or with Arduino from 200 to 10000 ppm gas (Singh and Yadav 2023). This gas sensor cannot identify which gas was leaked, if a mixture of gas is present in the air, it detects the gas having the highest ppm. Similarly, most of the research was done on metal oxide semiconducting-based gas sensors (Reshma et al. 2023). The adsorption properties of the gas sensor change with respective changes in temperature and simultaneously noted the change in resistance value (Ingale et al. 2023). The sensitivity of the gas sensor depends on the gas molecules distributed on the surface of the sensor material, the morphology of the surface of the sensor, the grain size of the material, the surface area, etc (Panwar et al. 2023). The oxide materials like tin oxide, iron oxide, zinc oxide, cadmium oxide, aluminum oxide, molybdenum oxide, nickel oxide, and tungsten oxide, were studied for a long time as gas sensors. However, these oxide materials are sensitive to gas at very high temperatures (Shkir, 2023).

Zinc oxide (ZnO)-based gas sensors have become increasingly popular due to their rapid response, low detection limits, high selectivity, reliable performance, and cost-effectiveness. ZnO offers additional advantages such as biocompatibility, chemical stability, environmental friendliness, and low synthesis costs, making it a focal point in research for detecting toxic and harmful gases. A comparative analysis of a developed ZnO sensor prototype with available ones would involve evaluating sensitivity,

selectivity, response time, detection limit, stability, reliability, manufacturing cost, environmental impact, and long-term performance. This analysis helps researchers understand the strengths and weaknesses of the developed sensor and identify areas for improvement, ultimately advancing the field of gas sensing technology. The comparison aims to highlight the prototype's performance against existing sensors, showcasing its potential for practical applications. Researchers analyze various parameters, including sensitivity, selectivity, and response time, to gauge the prototype's effectiveness. By addressing these aspects, the study contributes valuable insights to enhance ZnO-based gas sensor technology.

Nowadays, interfacing of commercially available gas sensors with Arduino is widely used for sensing various gases and indicating the leakage of gas. Many researchers continuously work on thin/thick film semiconductor material gas sensors and try to improve the sensitivity, response, and recovery time but very few used the material for a working model. In this paper ZnO is used as a gas sensor prototype for LPG gas sensing using Arduino has been discussed. The advantage of this prototype system is that we can change the thick film sensor as well as the operating temperature (less than or equal to 300 °C) for the different gases as studied in characterization.

2. Experimental details

The methodology includes different stages, an experimental technique for the synthesis of ZnO powder, fabrication of thick film sensor, structural characterization of thick film sensor, electrical and gas sensing characteristics of thick film, and prototyping of ZnO thick film using Arduino.

2.1. Synthesis of ZnO

The ZnO powder was prepared by using the high-temperature self-combustion sol-gel method (Nehru et al. 2016). In this method, the precursors are Zinc nitrate hexahydrate as a source material and Dextrose as a fuel was used. The mixture of source material and fuel was dissolved in water and kept on a hot plate. As the solution becomes gel-type it was kept in a pre-heated muffle furnace at 550 °C for 5 to 10 minutes. The solution boils, ignites, and after completion of the reaction yields an amorphous-like powder. The powder was calcinated at 650 °C to get pure ZnO. The XRD of the powder proves the formation of ZnO.

2.2. Fabrication of ZnO thick films

The ZnO thick films were fabricated using a well-known screen-printing technique. For making the paste and for fabrication the ratio of organic to inorganic material was 70:30 throughout the work. For the formation of proper paste, in inorganic material ZnO powder and glass powder as a permanent binder were used. Whereas the inorganic part contains Ethyl cellulose as a temporary binder and Butyl Carbitol Acetate as a vehicle. The prepared paste was printed on the alumina substrate using the screen-printing technique. After drying the films in air and under an IR lamp the films were fired at 700 °C for 1 hour to remove the organic vehicle and stick the film material evenly on the surface of the alumina substrate. To decrease the wake-up time of the sensor of thick films one can mix the smaller amount (1 to 10%) of the different oxide material additives like Al₂O₃ and TiO₂ are added to the ZnO powder (Lamdhade 2015). And then analyze the electrical and gas sensing characteristics of the sensor films. The flow chart of the fabrication process shows the detailed method. Fig. 1 shows the block diagram of the process of fabrication of ZnO thick films.

3. Results and Discussion

3.1 Structural and morphological analysis

The structural characteristics of ZnO films were studied using X-ray diffraction (XRD) and morphology characteristics were studied using a scanning electron microscope (SEM). ZnO thick film was prepared at 550 °C



Fig. 1. Block Diagram of preparation and fabrication of thick film samples.

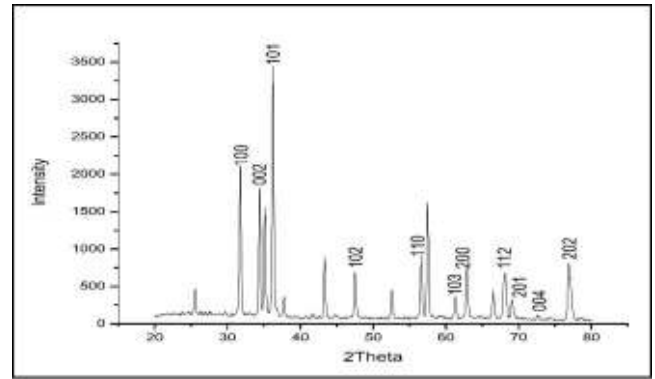


Fig. 2. XRD pattern of ZnO thick film.

temperature. Fig. 2 shows the XRD pattern of ZnO thick film.

The nature of the ZnO thick film was polycrystalline from the XRD pattern. To find the crystallite size Scherrer's formula was used below Eq. (1).

$$\text{Crystallite size (D)} = \frac{k\lambda}{\beta \cos\theta} \quad (1)$$

Where λ is the wavelength of X-ray radiation and β is the FWHM.

Fig. 3 shows the SEM image of the ZnO thick film. The grains were agglomerated with space in between. The ZnO particle size of about 1.88 μ m was observed by SEM image. The specific surface area of the spherical particles of ZnO thick film material was derived by using the following Eq. (2).

$$S_w = \frac{6}{\rho d} \quad (2)$$

Where ρ the density and d is the diameter of the particles.

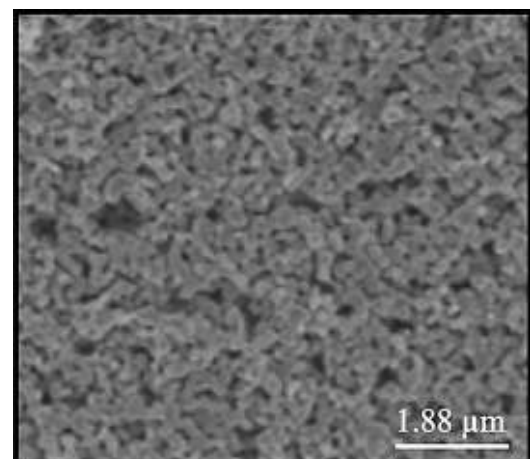


Fig. 3. SEM image of ZnO thick film.

Table 1 Crystallite size from XRD and Particle size, specific surface area from SEM.

Sr. No.	2θ	Plane (hkl)	Observed Values				
			2θ	d(A°)	Intensity (I/I ₀)	FWHM (β)	D (nm)
1	31.78	100	31.80	2.81	62.50	0.2553	34.1529
2	34.44	002	34.41	2.61	53.71	0.2551	34.4118
3	36.26	101	36.26	2.48	100.00	0.3130	28.1908
4	47.55	102	47.48	1.92	20.21	0.3023	30.3037
5	56.62	110	56.57	1.63	27.60	0.3600	26.4517
6	62.88	103	61.27	1.51	11.71	0.3375	28.8766
7	63.40	200	62.84	1.48	22.10	0.3867	25.4112
8	67.98	112	66.48	1.41	12.92	0.3946	25.4082
9	69.12	201	68.15	1.38	20.60	0.5101	19.8468
10	72.59	004	69.08	1.36	8.95	0.4183	24.3368
11	76.98	202	76.84	1.24	23.64	0.5121	20.9004

Table 1 contains the standard values of XRD data of ZnO from JCPDS 36-1451 card and calculated values of 2θ, d, FWHM, and peaks (hkl). The estimated crystallite, particle size, and specific surface area from XRD characterization. The average size of crystallite is about 27.1174 nm.

3.2 Electrical and Thermal Characterization

The electrical and gas sensing characteristics of prepared ZnO thick film were studied in the presence of air and LPG gas environments with respective changes in temperature. As the temperature rises, the decrease in sensor resistance takes place because of desorption of hydroxyl groups indicates the increase in sensitivity (Nehru et al. 2016). The gas sensing characteristics were observed in the presence of 1000 ppm LPG gas. Figure 4(a) shows the variation of resistance of prepared ZnO thick film concerning the change in temperature from room temperature to 400 °C. As the temperature increases the resistance of ZnO film decreases. Also, it was clear that the resistance of the film was lower in the presence of a gas environment. Fig. 4 (b) shows the graph for finding the operating temperature. The operating temperature is the temperature at which the thick film sensor senses the gas and changes its resistance. The operating temperature was calculated using the ratio of the resistance of the film in the air to the resistance of the film in a gas environment.

The ZnO gas sensors require a higher temperature (between 200 °C to 400 °C) to sense and respond to the reducing or oxidizing gases is the main disadvantage. Figure 5 clearly shows the two different peaks at temperatures 170 °C and 240 °C with the sensitivity of 3.5 and 4.29, respectively. The sensitivity increases with an increase in temperature.

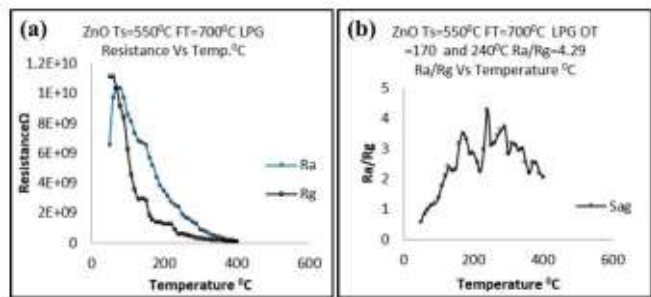


Fig. 4. (a) Electrical characteristics of ZnO thick film in the presence of air and LPG gas (b) Response curve of Film resistance V/s Operating temperature.

3.3 ZnO thick film-based LPG gas sensor prototype

As metal oxide-based gas sensors work at higher temperatures the heater and its temperature are the most important parameters while designing a prototype gas sensor. In this study, a Nichrome wire wound around a ceramic core having 1Ω resistance was used as a heater with a high power rating from 50 to 100 watts. The size of the heater is 10 X 10 X 30 mm. The Maximum working surface temperature of the heater is up to 400 °C. To power up the heater 12V power supply was provided. To control and maintain the operating temperature thermocouple is used. The output of the thermocouple is connected to the ADC through the AD595 instrumentation amplifier. The Atmel ATmega8A board is used to interface and to show the result on an LCD screen. Figure 5 shows the circuit diagram of ZnO thick film-based LPG gas sensor prototype.

This circuit can be used for different types of thin/thick metal oxide-based gas sensors. The sensor film can be removed and replaced for testing of different gases. Once the heater is ON, it increases the surface temperature so that ZnO thick film temperature. As soon as the heater

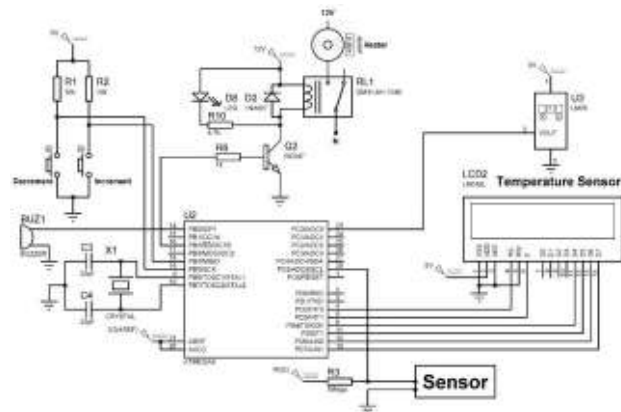


Fig. 5. Circuit diagram of ZnO thick film-based LPG gas sensor prototype.

temperature reaches the operating temperature heating stops and maintains the temperature. Buzzer used to indicate the heater temperature reached up to operating point temperature. Once this buzzer is ON, the circuit is ready for testing gas leakage. The buzzer starts only once initially when the circuit is powered up and the heater starts to heat up to the operating point temperature after that control circuit maintains the operating temperature and heater ON and OFF as per requirement. It takes different times for different operating temperatures. It takes around 4 minutes to reach a temperature of 150 °C. At this temperature around 50 mW power is required to the circuit. After exposure of LPG gas, the surface of the sensor reacts with LPG result to drop the resistance of sensor gradually.

The change in the sensor resistance is displayed on the LCD screen indicates the leakage of gas. This sensor circuit i.e prototype gas sensor works for different type of thick/thin films at variable operating temperatures by simply exchanging the first sensor film with the other sensor film. The maximum temperature of the heater is 300 °C so one can use it for an operating point up to 300 °C. Fig. 6 (a) shows the sensing circuit with display (portable prototype sensor kit) Fig. 6 (b) shows the actual circuit's internal connection with Arduino and Portable prototype kit.

Figure 7 (a) and (b) shows the complete prototype sensor under testing condition. The screen displays the heater's real-time temperature means sensor temperature by the word 'TMP', the operating temperature of the sensor by the word 'SET', and the resistance of the sensor by the word 'REST'. Two push buttons are used for setting the operating temperature as per requirement one for increasing and the other for decreasing the set temperature. After power on the circuit first set the operating temperature and the power on the heater, it increases to the set point, and the heater is automatically off. If the heater temperature decreases or increases,

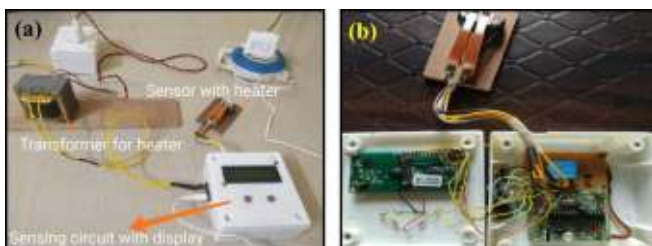


Fig. 6 (a) Portable Prototype gas sensor kit (b) Internal view interfacing with Arduino.

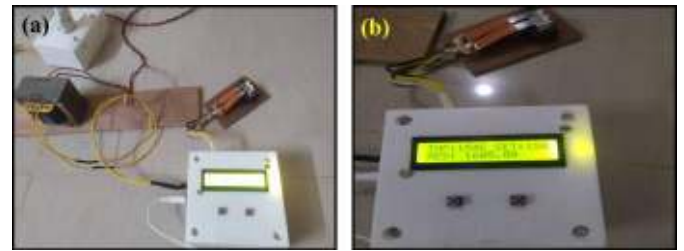


Fig. 7 (a) Portable Prototype ZnO gas sensor kit under testing condition (b) Output LCD display for readings.

control the circuit ON and OFF the heater and maintains the operating point. This complete process is completed in 5-7 minutes. After that, if LPG exposes on the surface of the thick film sensor it is indicated on display by decreasing the value of resistance.

4. Conclusion

The usual screen-printing approach was used to synthesize and produce a ZnO thick film sensor. According to the XRD pattern, the ZnO thick film is polycrystalline, with an average crystallite size of roughly 27.1174 nm. The SEM scan revealed that the ZnO particle size was approximately 1.88μm. Electrical and thermal properties have also been investigated. A prototype LPG gas leakage detector based on ZnO film sensor and Arduino ATMEGA8 has been constructed and tested successfully. Petroleum liquefied gas LPG is used not just for cooking but also in vehicles as compressed natural gas (CNG) and in industry. Because gas is flammable, there is a risk of leakage, which could result in an explosion or fire. It is critical to use a gas leak-detecting system for security reasons.

Disclosures

Free Access to this article is sponsored by SARL ALPHA CRISTO INDUSTRIAL.

Declaration

Contribution of the authors

All authors contributed equally to the preparation of this manuscript. All authors reviewed the manuscript.

Conflict of Interest

This research work has been done by all the listed authors with mutual interest. All the data used in this research work are cited in the manuscript. Therefore, no conflict of interest related to any person or agency for this manuscript.

Funding: Not Applicable

Acknowledgement:

We'd like to thank Dr. R.Y. Borse (Head, Department of Electronics, MSG College Malegaon) for overseeing and inspiring us to work on the experimental and characterization-based research article mentioned above.

References

- Arshak, K., & Gaidan, I. (2005). Development of a novel gas sensor based on oxide thick films. *Materials Science and Engineering: B*, 118(1-3), 44-49.
- Bhavithra, S., Sushmitha, B., Venkatesan, T., & Sankar, P. A. G. (2021). Intelligent Lpg Gas Leak Detection and Automatic Gas booking Alert System Using Pic Microcontroller. *International Journal of Engineering Science Technologies*, 5, 1-8.
- Devi, G. S., Subrahmanyam, V. B., Gadkari, S. C., & Gupta, S. K. (2006). NH₃ gas sensing properties of nanocrystalline ZnO based thick films. *Analytica Chimica Acta*, 568(1-2), 41-46.
- Gusdevi, H., Ade Setya, P., Zulaeha, P. H., & No, J. S. H. (2021). Prototype of LPG gas leakage detector using flame sensor and MQ-2 sensor. *APTİKOM Journal on Computer Science and Information Technologies (CSIT) Vol. 5 No. 1 March 2020*, 2, 28.
- Hussain, S., Liu, T., Javed, M. S., Aslam, N., & Zeng, W. (2017). Highly reactive OD ZnS nanospheres and nanoparticles for formaldehyde gas-sensing properties. *Sensors and Actuators B: Chemical*, 239, 1243-1250.
- Ingale, R. S., Shinde, S. G., Khamkar, K. A., Ahire, S. A., & Patil, I. J. (2023, February). The Al³⁺ doped modified ZnO sensor material: Fabrication, characterization and gas sensing characteristics of some environmental pollutant and greenhouse gases. In *Journal of Physics: Conference Series* (Vol. 2426, No. 1, p. 012050). IOP Publishing.
- Lamdhade, G.T. (2015). Tin Oxide And Titanium Dioxide Based CO₂ Gas Sensor, *Journal of Electron Devices*, Vol. 21, 2015, pp. 1849-1853.
- Ménil, F., Debéda, H., & Lucat, C. (2005). Screen-printed thick-films: from materials to functional devices. *Journal of the European ceramic society*, 25(12), 2105-2113.
- Naeem, S., A.V. Shaikh, U.P. Shinde, & A.V. Patil . (2023) Electrochemical Deposition, Synthesis, and Characterization of Dopant-Free Cobalt Hydroxide as an Enhanced Electrode Material for Supercapacitors. *ES Energy & Environment*, 2023, 21, 915.
- Naeem, S., Ali, A., Memon, K., Bavluwala, M., Shinde, U. P., & Patil, A. V. (2023). A review of flexible high-performance supercapacitors for the internet of things (IoT) and artificial intelligence (ai) applications. *Energy and Thermofluids Engineering*, 3, 1-9.
- Naeem, S., Shaikh, A. V., Rasool, A., Husain, D., Alam, M. T., & Patil, A. V. (2024). Enhancing supercapacitor performance through electrodeposition of cobalt hydroxide thin film: structural analysis, morphological characterization, and investigation of electrochemical properties. *Ionics*, 30(1), 399-405.
- Naeem, S., Shinde, U. P., & Patil, A. V. (2024). Cobalt hydroxide-based electrodes for supercapacitors: Synthesis, characterization, and electrochemical performance optimization. *Energy Storage*, 6(1), e516.
- Nehru, L.C., C. Sanjeeviraja (2016) Zinc Oxide Nanoparticles Synthesized by Microwave-Assisted Combustion Method and Their Potential for Ethonal Gas Detection. *International Journal of Materials Engineering* 2016, 6(5): 166-172.
- Panwar, S., Kumar, V., & Purohit, L. P. (2023). Influence of Gd doping on gas sensing performance of Gd-(ZnO/TiO₂) nanocomposites. *Optical Materials*, 141, 113919.
- Patil, S. D., Nikam, H. A., Sharma, Y. C., Yadav, R. S., Kumar, D., Singh, A. K., & Patil, D. R. (2023). Highly selective ppm level LPG sensors based on SnO₂-ZnO nanocomposites operable at low temperature. *Sensors and Actuators B: Chemical*, 377, 133080.
- Prakshale, R. D., Bangale, S. V., Kamble, M. M., & Sonawale, S. B. (2023). Synthesis and Characterization of ZnO. 5CoO. 5Fe2O4 Nanoparticles for Gas Sensing Applications. *ECS Journal of Solid State Science and Technology*, 12(8), 087003.
- Shankar, P., & Rayappan, J. B. B. (2015). Gas sensing mechanism of metal oxides: The role of ambient atmosphere, type of semiconductor and gases-A review. *Sci. Lett. J*, 4(4), 126.
- Shinde, V. R., Gujar, T. P., & Lokhande, C. D. (2007). LPG sensing properties of ZnO films prepared by spray pyrolysis method: effect of molarity of precursor solution. *Sensors and actuators B: Chemical*, 120(2), 551-559.
- Shkir, M. (2023). Development of highly sensitive Al, Ga, and In-doped ZnO films by the drop-casting method for NH₃ gas sensing. *New Journal of Chemistry*, 47(10), 4880-4887.
- Singh, A., & Yadav, B. C. (2023). Green synthesized ZnO/NiO heterostructures based quick responsive LPG sensor for the detection of below LEL with DFT calculations. *Results in Surfaces and Interfaces*, 11, 100103.
- Singh, P. K., Singh, N., Singh, S. K., Singh, M., & Tandon, P. (2023). Co-doped ZnO nanostructures for liquefied petroleum gas sensing at room temperature. *Journal of Materials Science: Materials in Electronics*, 34(10), 915.
- Sowmya, B., John, A., & Panda, P. K. (2021). A review on metal-oxide based pn and nn heterostructured nano-materials for gas sensing applications. *Sensors International*, 2, 100085.

Gas Sensing Applications of Binary Metal Oxides: A Brief Review

Devendra Bhikaji Sonawane

Department of Physics, MGV's M.S.G. Arts, Science and Commerce College, Malegaon, Dist.- Nashik,
Affiliated to SPPU, Pune, and Maharashtra, India.

Corresponding author: swamidb1@gmail.com

Abstract

One of the challenges in metal oxide gas sensors is to achieve high sensitivity and selectivity towards specific gases of interest while minimizing cross-sensitivity to other gases present in the environment. This requires careful design and engineering of the sensor materials and operating parameters. Gas sensing applications of binary metal oxides have been an area of significant interest due to their high sensitivity, low cost, and stability. Binary metal oxides have shown promising results in detecting various reducing and oxidising gases, such as LPG, NH₄, CO, NO_x, H₂S, and VOCs. These metal oxides exhibit semiconducting properties, and their conductance changes when exposed to different gases, enabling their use in gas sensing applications. The future prospects for gas sensing applications of binary metal oxides are promising, with ongoing research focused on enhancing their selectivity, sensitivity, response time, and stability. Integration with advanced technologies such as nanomaterials, nanocomposites, and functionalization with noble metals or other catalytic materials is expected to further improve the performance of binary metal oxide gas sensors. Additionally, the development of miniaturised and portable gas sensors for environmental monitoring, industrial safety, and healthcare applications is a growing area of interest. This review points out the shortcomings of the existing work on binary metal oxides. The main aim of the current review article is to provide brief information on applications and methods of preparation of binary metal oxides.

Keywords: binary metal oxides, noble metals, gas sensing, nanomaterials, environmental monitoring.

1. Introduction

Air pollution poses significant threats to both human health and the environment [1]. It results from the release of various pollutants, such as particulate matter, carbon monoxide, sulfur dioxide, and nitrogen dioxide, into the atmosphere. These pollutants can cause respiratory issues, heart diseases, and even premature death in humans [1, 2]. Moreover, air pollution contributes to climate change, acid rain, and the depletion of the ozone layer, which in turn affects ecosystems, agriculture, and wildlife. To mitigate these impacts, it is crucial to implement stricter emission standards, promote clean energy, and encourage responsible practices in industries and households [3, 4]. Gas sensors play a crucial role in addressing several vital needs across various sectors, driven by the growing emphasis on safety, environmental monitoring, and industrial processes [5, 6]. In industrial area, gas sensors are essential for monitoring and detecting hazardous gases, such as hydrogen sulfide, carbon monoxide, ammonia, and volatile organic compounds. Early detection and alarm systems based on gas sensors are critical for ensuring the safety of workers and preventing potential gas-related accidents. Gas sensors are employed for environmental monitoring in both indoor and outdoor environments. They are used to detect and measure levels of pollutants, including carbon dioxide, nitrogen oxides, sulfur dioxide, and volatile organic compounds, to assess air quality and ensure compliance with environmental regulations [7, 8]. The need for gas sensors is evident in protecting human health, ensuring workplace safety, meeting environmental regulations, and enhancing the efficiency of industrial processes [8, 9].

Metal oxide gas sensors have garnered significant attention for their diverse applications in gas detection and environmental monitoring [10]. These sensors utilize the semiconducting properties of metal oxides to detect and quantify the presence of specific gases. Metal oxides are utilized in gas sensing

applications for detecting harmful gases such as carbon monoxide, nitrogen oxides, and volatile organic compounds. Their semiconducting properties enable the development of gas sensors for environmental monitoring, industrial safety, and automotive applications [10, 11]. Metal oxide gas sensors operate based on the principle of changes in electrical conductivity when exposed to target gases. Adsorption of gas molecules on the surface of the metal oxide alters its conductivity, leading to a measurable change in resistance. This change is then correlated to the concentration of the target gas [11].

Binary metal oxide (BMO) gas sensors refer to a specific type of gas sensor that utilizes a combination of two different metal oxide materials as the sensing element [12]. These sensors are primarily used for detecting and analyzing various gases in the environment. In a binary metal oxide gas sensor, the two metal oxides are mixed together, creating a heterogeneous mixture. This combination aims to improve the overall performance of the sensor by exploiting the synergistic effects between the two metal oxides [12, 13]. These effects can lead to enhanced selectivity, sensitivity, and stability in detecting specific target gases. The combination of these materials can result in improved gas sensing capabilities, making binary metal oxide gas sensors a valuable tool in various industries, such as environmental monitoring, industrial safety, and air quality control [13, 14]. The inadequacies of the previous research on binary metal oxides are highlighted in this study. The primary goal of this present article is to give a quick overview of the uses and preparation techniques for binary metal oxides.

2. Synthesis methods for Binary Metal Oxide gas sensors

The binary metal oxides are synthesised using various methods such as physical, chemical and biological [15-17]. Many methods are reported for the preparation or synthesis of binary metal oxide gas sensors. Fig. 1 reveals the methods adopted for synthesis of binary metal oxides for application of gas sensors.

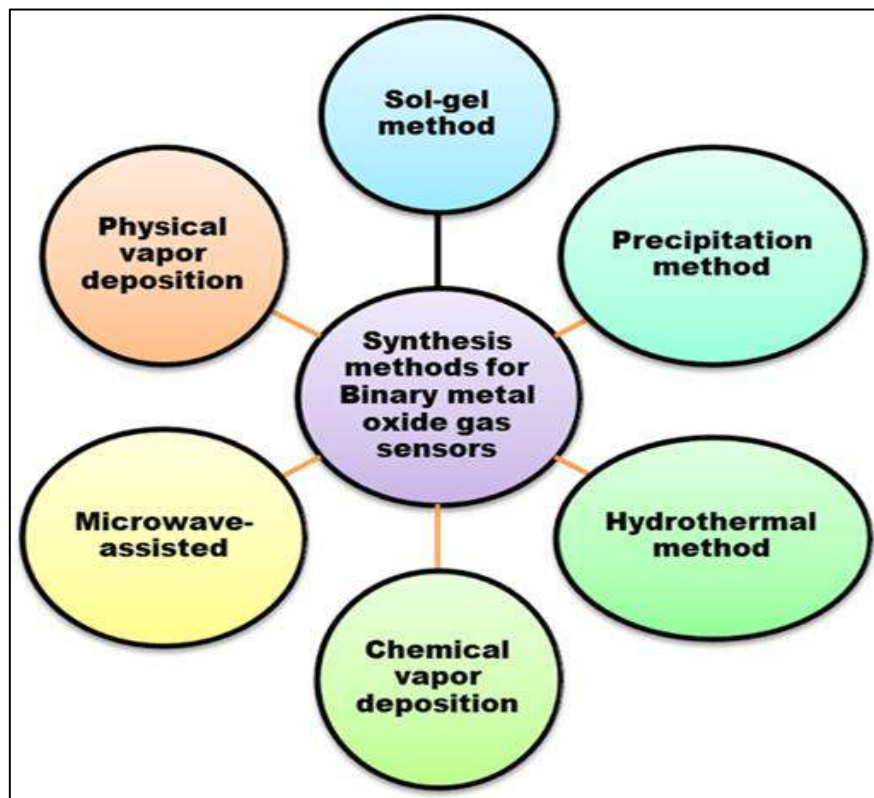


Figure 1: Synthesis methods of binary metal oxide gas sensors

2.1 Sol-gel method: This technique involves the formation of a sol (a colloidal suspension) by mixing metal alkoxides or metal salts with a solvent. The sol is then transformed into a gel through a hydrolysis and condensation process. The gel is dried and calcined at high temperatures to obtain the desired binary metal oxide. The sol-gel method allows for precise control over the composition, morphology, and particle size of the final product [18, 19].

2.2 Co-precipitation method: In this method, metal salts are dissolved in a solution containing a precipitating agent, such as ammonia or sodium hydroxide. The reaction between the metal ions and the precipitating agent leads to the formation of a binary metal oxide precipitate. The precipitate is then washed, dried, and calcined to obtain the final product. This method is suitable for producing binary metal oxides with a wide range of compositions [19, 20].

2.3 Hydrothermal and solvothermal synthesis: These methods involve the reaction of metal precursors in a high-temperature, high-pressure aqueous or non-aqueous solution, respectively. The reaction takes place in a closed, temperature-controlled autoclave. The binary metal oxide product forms as a result of the controlled crystallization process. Hydrothermal and solvothermal synthesis can produce binary metal oxides with well-defined structures and controlled particle sizes [21, 22].

2.4 Chemical vapor deposition (CVD): These techniques involve the deposition of binary metal oxide thin films on a substrate by introducing metal precursors in the gas phase. CVD uses chemical reactions between the precursors and the substrate [21].

2.5 Physical vapor deposition (PVD): PVD relies on physical processes like sputtering or evaporation. These methods are suitable for producing thin-film binary metal oxide gas sensors with controlled thickness and composition [22].

2.6 Microwave-assisted synthesis: In this method, binary metal oxide materials are synthesized using microwave radiation as the heat source. Microwave-assisted synthesis can lead to rapid and uniform heating of the reaction mixture, resulting in shorter synthesis times and improved control over the final product's properties [22, 23].

3. Factors affecting the gas sensing performance of the binary metal oxide gas sensors

Several factors influence the gas sensing performance of binary metal oxide gas sensors. These factors can affect the sensitivity, selectivity, response time, and stability of the sensors [24]. Some key factors are shown in Fig. 2.

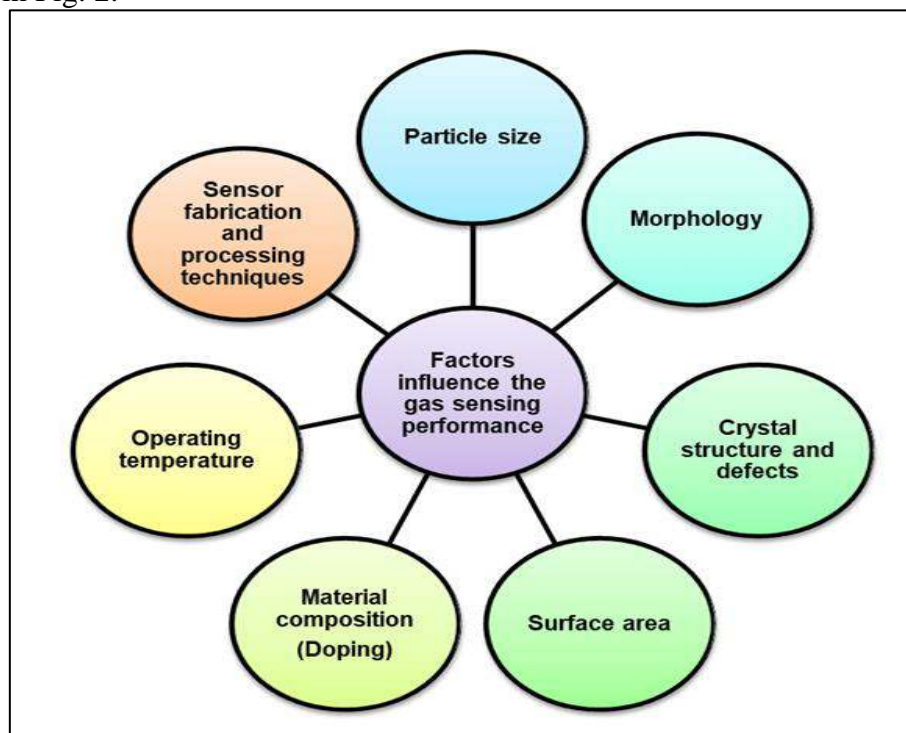


Figure 2: Factors influence the gas sensing performance of binary metal oxide gas sensors

3.1 Material composition: The choice of metal oxides and their proportions in the binary mixture play a significant role in determining the gas sensing properties. The combination of two metal oxides can lead to synergistic effects, which can improve the overall performance of the sensor.

3.2 Particle size and morphology: The size and shape of the binary metal oxide particles can impact the sensor's response to target gases. Smaller particles typically exhibit higher surface area, leading to increased

sensitivity. Additionally, the morphology of the particles can affect the gas diffusion and adsorption process, which in turn influences the sensor's performance.

3.3 Surface area: A higher surface area allows for more active sites on the sensor's surface, resulting in improved sensitivity to target gases. The surface area can be influenced by factors such as particle size, porosity, and agglomeration.

3.4 Crystal structure and defects: The crystal structure and the presence of defects within the binary metal oxide material can impact the gas sensing properties. Defects can act as active sites for gas adsorption and interaction, which can enhance the sensor's sensitivity and selectivity.

3.5 Operating temperature: The temperature at which the sensor operates can significantly affect its performance. Higher temperatures generally lead to increased sensitivity and response speed, but they can also cause sensor degradation over time. Optimizing the operating temperature is crucial for achieving the best gas sensing performance.

3.6 Sensor fabrication and processing techniques: The methods used for synthesizing and processing the binary metal oxide material can influence the gas sensing properties. Factors such as the presence of impurities, grain size, and the uniformity of the film or particle distribution can impact the sensor's performance.

3.7 Gas concentration and humidity: The concentration of the target gas and the presence of humidity in the environment can affect the sensor's response. Some binary metal oxide sensors may be more sensitive to humidity, leading to potential cross-sensitivity and interference in the gas detection process.

3.8 Sensor design and integration: The design of the sensor, including the choice of transducer and the integration of the binary metal oxide layer, can also impact its gas sensing performance. Proper design and integration can help optimize the sensor's sensitivity, selectivity, response time, and stability.

4. Literature Survey:

In 1953, Brattain and Bardeen conducted the first research of the semiconductor material group on germanium (Ge). Heiland's research report on metal oxides' gas sensitivities was published in 1954. Seiyama's work from 1962 demonstrated that ZnO structures were susceptible to airborne reactive gases [24]. 1968 saw the introduction of Taguchi-type sensors to the marketplace and the industrialization of tin oxide gas sensors. Presently, real-time gas sensors that use chemiresistive metal oxide semiconductors have become increasingly important in both science and industry because of their high sensitivity to chemical environments, affordability, ease of implantation, safety, and durability at high temperatures and high pressures all of which indicate compelling conditions [25, 26]. One major issue with metal oxide gas sensors is gas selectivity. In recent investigations, it has been suggested to adopt a heating mode of a gas-sensing floor with continuous temperature modification to boost the selectivity of metal oxide sensors. Researchers stated that, by choosing the metal oxide material to have specific surface properties that enhance selectivity to the target gas [28, 29]. This can involve modifying the metal oxide composition or doping it with other elements. Also modifying the surface of the metal oxide with functional groups or coatings that selectively interact with the target gas [29, 30]. This can enhance the sensitivity and selectivity of the sensor. Adjusting the operating conditions such as temperature, humidity, and gas flow rate can improve the selectivity of the sensor to specific gases. Implementing these strategies can help mitigate the gas selectivity problem in metal oxide semiconductor gas sensors, improving their accuracy and reliability in gas detection applications [30, 31]. Hence now a days researchers are focused on the work on binary metal oxides sensors because binary metal oxides exhibit tunable properties based on the composition ratio of the two metals. This allows for fine-tuning of the sensor's response to specific gases, improving selectivity. The combination of two different metal oxides can result in synergistic effects, where the properties of the binary oxide are different from the individual components [32, 33]. This can lead to improved sensitivity and selectivity. It offer a promising avenue for enhancing the sensitivity and selectivity of gas sensors, making them valuable for various industrial, environmental, and healthcare applications.

5. Conclusion and future scope

Binary metal oxides, are compounds composed of two different metal cations bonded to oxygen, have garnered significant interest due to their diverse properties and potential applications. Drawing conclusions about these materials involves considering their current applications, ongoing research trends,

and potential future directions. BMO hold great promise for a wide range of applications, and ongoing research efforts aimed at understanding their properties and behavior will likely lead to further advancements and practical implementations in various fields. Efforts to integrate BMO into practical devices, such as batteries, sensors, and catalytic reactors, will drive their commercialization and real-world impact.

References:

1. Kampa, M. and Castanas, E., 2008. Human health effects of air pollution. *Environmental pollution*, 151(2), pp.362-367.
2. Manisalidis, I., Stavropoulou, E., Stavropoulos, A. and Bezirtzoglou, E., 2020. Environmental and health impacts of air pollution: a review. *Frontiers in public health*, 8, p.14.
3. Kenessary, D., Kenessary, A., Adilgireiuly, Z., Akzholova, N., Erzhanova, A., Dosmukhametov, A., Syzdykov, D., Masoud, A.R. and Saliev, T., 2019. Air pollution in Kazakhstan and its health risk assessment. *Annals of global health*, 85(1).
4. Bruce, N., Perez-Padilla, R. and Albalak, R., 2000. Indoor air pollution in developing countries: a major environmental and public health challenge. *Bulletin of the World Health organization*, 78(9), pp.1078-1092.
5. Azad, A.M., Akbar, S.A., Mhaisalkar, S.G., Birkefeld, L.D. and Goto, K.S., 1992. Solid-state gas sensors: A review. *Journal of the Electrochemical Society*, 139(12), p.3690.
6. Wang, Y. and Yeow, J.T., 2009. A review of carbon nanotubes-based gas sensors. *Journal of sensors*, 2009.
7. Dai, J., Ogbeide, O., Macadam, N., Sun, Q., Yu, W., Li, Y., Su, B.L., Hasan, T., Huang, X. and Huang, W., 2020. Printed gas sensors. *Chemical Society Reviews*, 49(6), pp.1756-1789.
8. Liu, X., Cheng, S., Liu, H., Hu, S., Zhang, D. and Ning, H., 2012. A survey on gas sensing technology. *Sensors*, 12(7), pp.9635-9665.
9. Stetter, J.R. and Li, J., 2008. Amperometric gas sensors a review. *Chemical reviews*, 108(2), pp.352-366.
10. Dhall, S., Mehta, B.R., Tyagi, A.K. and Sood, K., 2021. A review on environmental gas sensors: Materials and technologies. *Sensors International*, 2, p.100116.
11. Jimenez-Cadena, G., Riu, J. and Rius, F.X., 2007. Gas sensors based on nanostructured materials. *Analyst*, 132(11), pp.1083-1099.
12. Nikolic, M.V., Milovanovic, V., Vasiljevic, Z.Z. and Stamenkovic, Z., 2020. Semiconductor gas sensors: Materials, technology, design, and application. *Sensors*, 20(22), p.6694.
13. Dey, A., 2018. Semiconductor metal oxide gas sensors: A review. *Materials science and Engineering: B*, 229, pp.206-217.
14. Capone, S., Forleo, A., Francioso, L., Rella, R., Siciliano, P., Spadavecchia, J., Presicce, D.S. and Taurino, A.M., 2003. Solid state gas sensors: state of the art and future activities. *Journal of Optoelectronics and Advanced Materials*, 5(5), pp.1335-1348.
15. Morrison, S.R., 1987. Selectivity in semiconductor gas sensors. *Sensors and actuators*, 12(4), pp.425-440.
16. Endres, H.E., Jander, H.D. and Göttler, W., 1995. A test system for gas sensors. *Sensors and Actuators B: Chemical*, 23(2-3), pp.163-172.
17. Sivaperuman, K., Thomas, A., Thangavel, R., Thirumalaisamy, L., Palanivel, S., Pitchaimuthu, S., Ahsan, N. and Okada, Y., 2023. Binary and ternary metal oxide semiconductor thin films for effective gas sensing applications: A comprehensive review and future prospects. *Progress in Materials Science*, p.101222.
18. Chen, D.H. and He, X.R., 2001. Synthesis of nickel ferrite nanoparticles by sol-gel method. *Materials research bulletin*, 36(7-8), pp.1369-1377.
19. Kandpal, N.D., Sah, N., Loshali, R., Joshi, R. and Prasad, J., 2014. Co-precipitation method of synthesis and characterization of iron oxide nanoparticles.
20. Lateef, A. and Nazir, R., 2017. Metal nanocomposites: synthesis, characterization and their applications. *Sci. Appl. Tailored Nanostructures*, pp.239-256.

21. Ikim, M.I., Yu Spiridonova, E., Belysheva, T.V., Gromov, V.F., Gerasimov, G.N. and Trakhtenberg, L.I., 2016. Structural properties of metal oxide nanocomposites: Effect of preparation method. *Russian Journal of Physical Chemistry B*, 10, pp.543-546.
22. Nandagudi, A., Nagarajarao, S.H., Santosh, M.S., Basavaraja, B.M., Malode, S.J., Mascarenhas, R.J. and Shetti, N.P., 2022. Hydrothermal synthesis of transition metal oxides, transition metal oxide/carbonaceous material nanocomposites for supercapacitor applications. *Materials Today Sustainability*, 19, p.100214.
23. Jamjoum, H.A.A., Umar, K., Adnan, R., Razali, M.R. and Mohamad Ibrahim, M.N., 2021. Synthesis, characterization, and photocatalytic activities of graphene oxide/metal oxides nanocomposites: A review. *Frontiers in Chemistry*, 9, p.752276.
24. Sarf, F., 2020. Metal oxide gas sensors by nanostructures. *Gas Sensors*, 1.
25. Liu X, Cheng S, Liu H, Hu S, Zhang D, Ning HA. Survey on gas sensing technology: Review. *Sensors*. 2012;12:9635-9665. DOI: 10.3390/s120709635
26. Nandy T, Coutu RA Jr, Ababei C. Carbon monoxide sensing technologies for next-generation cyber-physical systems: Review. *Sensors*. 2018;18:3443-3478. DOI: 10.3390/s18103443
27. Gardner DE et al. *Acute Exposure Guideline Levels for Selected Airborne Chemicals*. Vol. 6. 2007. ISBN: 0-309-11214-1, 318 pages, 6 x 9. Available from: <http://www.nap.edu/catalog/12018.html>
28. Shankar P, Rayappan JBB. Gas sensing mechanism of metal oxides: The role of ambient atmosphere, type of semiconductor and gases—A review. *Science Letters Journal*. 2015;4:126-133
29. Dilonardo E, Penza M, Alvisi M, Di Franco C, Palmisano F, Torsi L, et al. Evaluation of gas-sensing properties of ZnO nanostructures electrochemically doped with Au nanophases. *Beilstein Journal of Nanotechnology*. 2016;7:22-31. DOI: 10.3762/bjnano.7.3
30. Varpula A, Novikov S, Haarahiltunen A, Kuivalainen P. Transient characterization techniques for resistive metal-oxide gas sensors. *Sensors and Actuators B*. 2011;159:12-26. DOI: 10.1016/j.snb.2011.05.059
31. Gangu KK, Maddila S, Jonnalagadda SB. A review on novel composites of MWCNTs mediated semiconducting materials as photocatalysts in water treatment. *The Science of the Total Environment*. 2019;646:1398-1412. DOI: 10.1016/j.scitotenv. 2018.07.375
32. Gao C, Guo Z, Liu J, Huang X. The new age of carbon nanotubes: An updated review of functionalized carbon nanotubes in electrochemical sensors. *Nanoscale*. 2012;4:1948. DOI: 10.1039/c2nr11757f
33. Nguyen LQ, Phan PQ, Duong HN, Nguyen CD, Nguyen LH. Enhancement of NH₃ gas sensitivity at room temperature by carbon nanotube-based sensor coated with Co nanoparticles. *Sensors*. 2013;13:1754-1762. DOI: 10.3390/s130201754

Study of Electrical and Gas Sensing Properties of Cadmium Sulfide Thick Films

Devendra Bhikaji Sonawane

Department of Physics, MGV's M.S.G. Arts, Science and Commerce College, Malegaon, Dist. - Nashik,
Affiliated to SPPU, Pune, and Maharashtra, India.

Corresponding author: swamidb1@gmail.com

Abstract

The study of electrical and gas-sensing properties of Cadmium Sulfide (CdS) thick films is crucial for understanding their potential applications in gas sensing technologies. CdS is a wide bandgap semiconductor material that exhibits a unique property called photo-conductivity, which means its electrical conductivity changes in response to light or gas exposure. This property makes CdS a promising candidate for gas sensing applications. In the present research work author investigated the electrical and gas sensing properties of CdS thick films developed by screen printing method. The electrical and gas sensing properties were investigated using static electric and gas sensing system. The resistivity of the films was studied using half bridge method. The resistivity, TCR and activation energy of films were found to be $509575 \Omega.m$, $-0.00233 / ^\circ C$ and $0.1067 eV$ respectively. A film shows maximum gas response to the NO_2 gas at operating temperature $120 ^\circ C$. The maximum sensitivity was found to be 73.68% . The films exhibit quick response and recovery time.

Keywords: Thick films, Cadmium Sulfide, gas sensors, air pollution, photoconductive.

1. Introduction:

Air pollution refers to the presence of contaminants and excessive amounts of certain substances in the Earth's atmosphere. These contaminants can originate from both natural sources, such as volcanic eruptions and wildfires, and human activities, including industrial processes, transportation, and energy production [1, 2]. Air pollution can have severe consequences on public health, climate change, and ecosystems. Some major components of air pollution include particulate matter (PM), ground-level ozone, nitrogen oxides (NO_x), sulfur dioxide (SO_2), carbon monoxide (CO), and volatile organic compounds (VOCs). These pollutants can lead to respiratory and cardiovascular diseases, premature death, and other health issues when inhaled by humans [1-3]. Nitrogen dioxide (NO_2) is a significant air pollutant and a major component of photochemical smog. It is primarily produced by combustion processes, such as those occurring in vehicles, power plants, and industrial facilities. The presence of NO_2 in the atmosphere can have various detrimental effects on human health, the environment, and materials [4, 5]. Prolonged exposure to NO_2 is lead to respiratory problems, aggravate existing respiratory and cardiovascular diseases, and cause premature death. It can irritate the airways, lungs, and eyes, leading to symptoms like coughing, wheezing, and shortness of breath. Children, the elderly, and people with pre-existing health conditions are particularly vulnerable to the effects of NO_2 [5, 6].

Metal sulfides, being a class of semiconductor materials, have been extensively researched and utilized in the development of gas sensors [7]. These sensors function based on the interaction between the metal sulfide material and the target gas molecules. When gas molecules adsorb onto the metal sulfide surface, it causes a change in the material's electrical properties, such as resistance or capacitance. This

change can then be measured and translated into a detectable signal, allowing for the identification and quantification of the gas present. Metal sulfide-based gas sensors have been applied to detect various gases, including oxidizing and reducing gases, offering potential for use in air quality monitoring, industrial safety, and environmental applications [7, 8]. Cadmium Sulfide (CdS) is a chemical compound commonly used in various applications due to its unique properties. It is a semiconductor material with a wide bandgap, which makes it suitable for photoconductive and photovoltaic devices [9]. Additionally, CdS has been employed in the production of red light-emitting diodes (LEDs) and as a pigment in the past, although its use as a pigment has been largely replaced by safer alternatives due to health and environmental concerns [9- 11].

Screen printing is a widely used technique for depositing thick films on various substrates, including those employed in gas sensor fabrication [12]. This method offers several advantages, such as cost-effectiveness, high throughput, and the ability to produce complex patterns. When it comes to creating thick films for gas sensors, screen printing can be particularly useful for depositing conductive inks or pastes that respond to specific gas concentrations [13, 14]. The major aim of the current research work is to study the electrical and gas sensing properties of CdS thick films developed by screen printing method.

2. Materials and methods

The commercially available CdS nanopowder purchased from sigma enterprises, Nashik was used for the development of thick films. The films were developed on glass substrate by screen printing method. The inorganic and organic materials 70:30% ratio was used to develop pure CdS thick films [15]. The inorganic material consists of CdS nanopowder while organic materials including butyl carbitol acetate and ethyl cellulose. Fig. 1 reveals the schematic diagram of development of thick films using screen printing method.

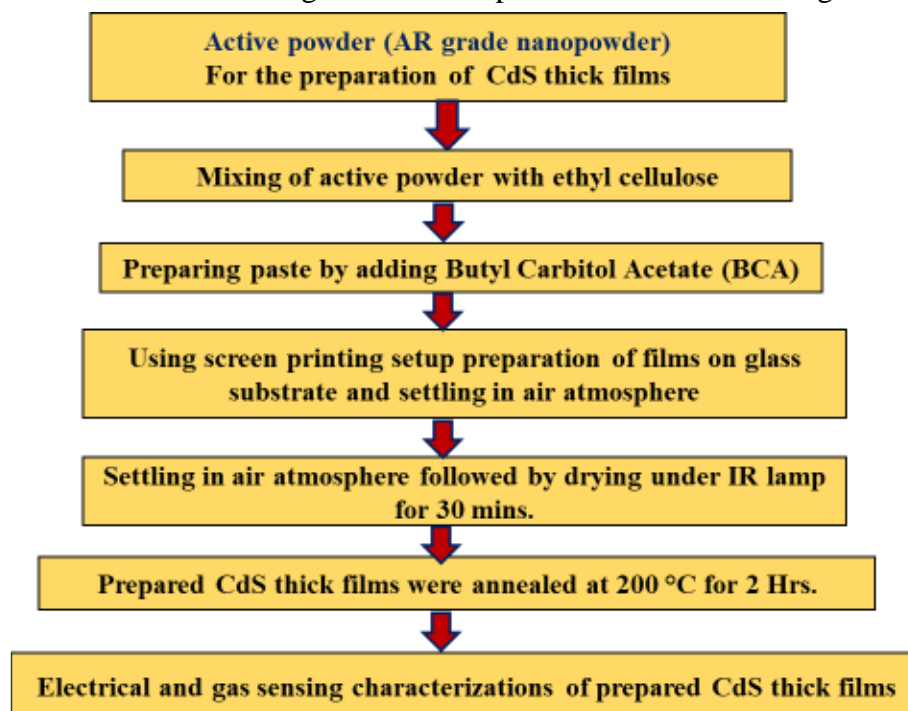


Figure 1: Steps of development of CdS thick films using screen printing method

3. Result and discussion

The half-bridge circuit configuration is a widely used method for electrical characterization, particularly for measuring resistance, inductance, and capacitance in various electronic components and circuits. It offers several advantages, such as simplicity, high accuracy, and the ability to handle high voltages and currents. The schematic diagram of half-bridge circuit configuration is shown in Fig. 2 [15, 16]. Resistivity of thick films refers to the measure of a material's resistance to the flow of electric current

when formed into a film with a significant thickness. The resistivity of thick films is an essential parameter for various applications, such as conductive inks, coatings, and printed electronic devices, including gas sensors, flexible displays, and RFID tags. Resistivity (ρ) is a fundamental property of a material and is defined as the resistance (R) per unit length (L) of a conductor with a uniform cross-sectional area (A). The relationship between these parameters can be expressed by the formula (Eq. 1).

$$\rho = R \times A / L \tag{1}$$

Where, ρ = Resistivity, R = resistance at room temperature, L = length and A = area of film

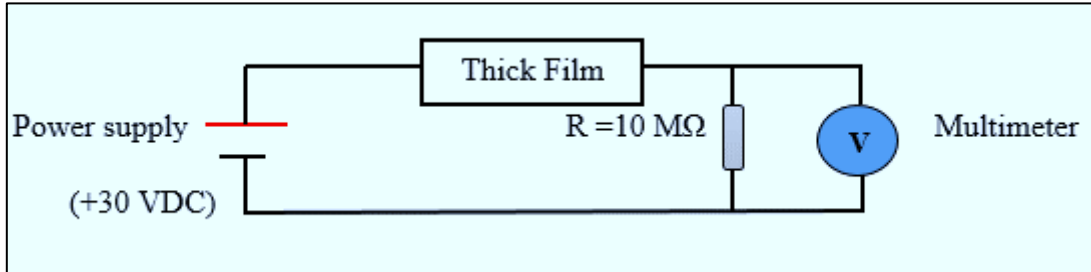


Figure 2: Schematic of a half-bridge circuit

Fig. 3 shows the resistance versus temperature plot of CdS thick films. It has been observed that from Fig. 3 the resistance of the films is decline as ambient temperature is increased [17, 18]. This type of nature of graph indicating semiconducting nature of the film. The resistance of the film decreased due to increase the mobility of carrier concentration as heat increases.

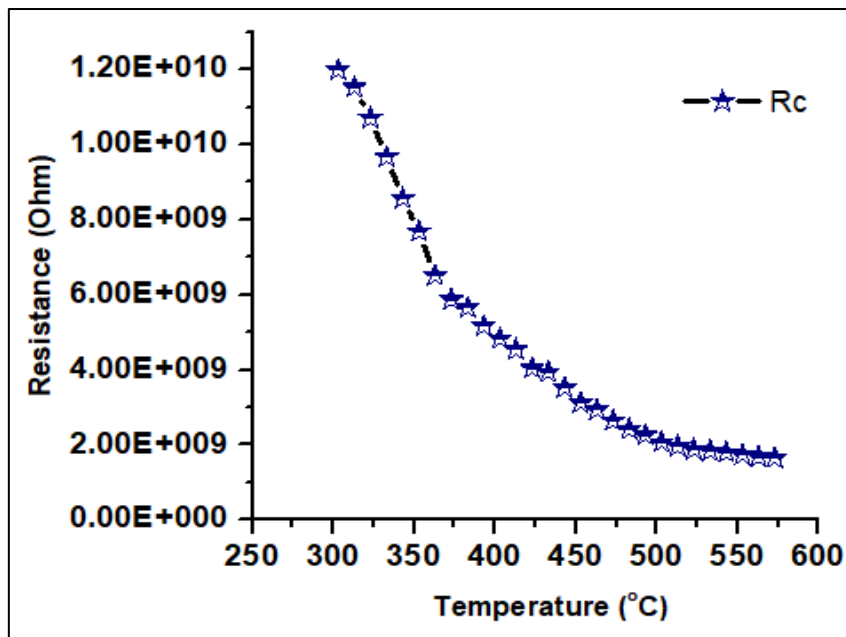


Figure 3: Resistance versus temperature plot of CdS thick films

Activation energy of thick films is a crucial parameter in gas sensing applications, as it significantly affects the performance and reliability of the sensors [18, 19]. The activation energy refers to the minimum amount of energy required for a chemical reaction to occur. In the context of gas sensing, it is crucial for understanding the interaction between the thick film and the target gas molecules. It is crucial for gas sensing applications, as it influences the sensitivity, selectivity, response time, stability, temperature dependence, and data interpretation of the gas sensor [20, 21]. By optimizing the activation energy and understanding its impact on the gas sensing process, one can enhance the overall effectiveness of gas sensors. The Arrhenius equation is a mathematical model that relates the rate of a reaction to the temperature at which it occurs. The activation energy is calculated by measuring the rate constant (k) at

different temperatures (T) and using the known pre-exponential factor (A) for a specific reaction. The Arrhenius equation is presented in Eq. 2.

$$\Delta E = \frac{\log R}{\log R_0} \times KT$$

(2)

Where, ΔE = Activation energy, R = Resistance at elevated temperature, R₀ = Resistance at room temperature. Fig. 4 reveals the plot of log Rc vs. 1/T of CdS thick films. By employing Arrhenius equation (Eq.2) the activation energy was estimated. The activation energy for CdS thick films was found to be 0.14580 eV and 0.10679 eV at higher and lower temperature regions respectively.

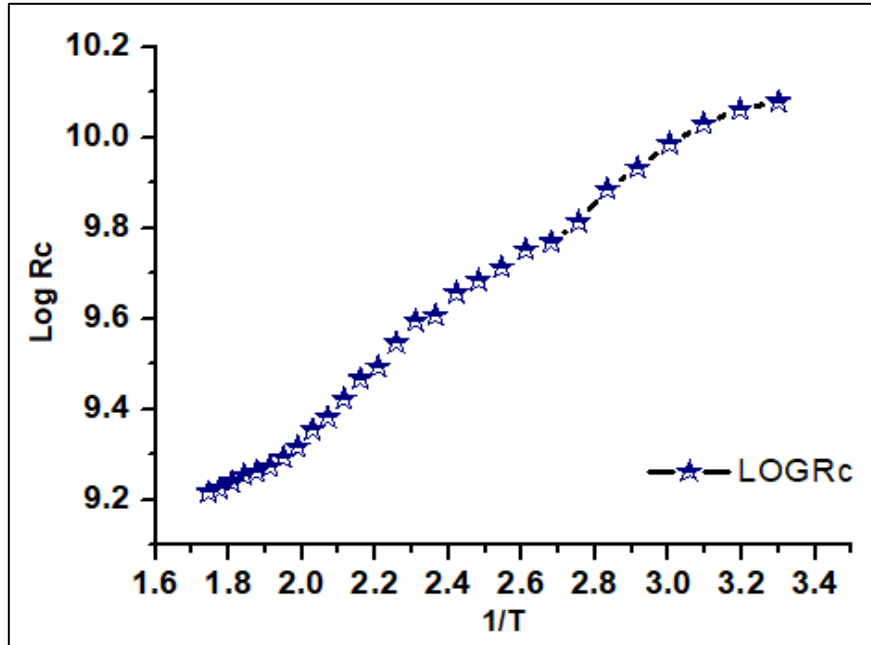


Figure 4: Arrhenius plot of log Rc vs. 1/T of CdS thick films

The Temperature Coefficient of Resistance (TCR) of thick films is indeed important for gas sensing applications. TCR is a measure of how much a material's electrical resistance changes with a change in temperature [15, 21]. In the context of gas sensing, it plays a significant role in determining the performance and reliability of the gas sensor. The TCR of the thick film material influences the sensitivity of the gas sensor. As the temperature of the thick film changes, its resistance also varies, which in turn affects the electrical signal generated by the sensor. A higher TCR can lead to a more significant change in resistance with temperature, potentially increasing the sensitivity of the gas sensor towards the target gas. The TCR of films was estimated using Eq. 3 and it was found to be -0.00233 /°C.

$$TCR = \frac{1}{R_0} \left(\frac{\Delta R}{\Delta T} \right) / ^\circ C \tag{3}$$

Where, ΔR = change in resistance, ΔT = temperature difference between T₁ and T₂ and R₀ = Resistance of the film sample at room temperature.

Gas sensor sensitivity refers to the ability of a gas sensor to detect and respond to changes in the concentration of a particular gas. It is affected by factors such as relative humidity, temperature, response time, and time of exposure to the gas. The sensitivity of the films was estimated using Eq. 4. sensitivity (S%) is defined as ratio of change in resistance in air to the change in resistance in presence of gas for reducing gases and for oxidizing ratio of change in resistance in air to the change in resistance in presence of gas [15, 16].

$$\text{Sensitivity (\%)} = Ra/Rg \text{ or } Rg/Ra \times 100 \tag{4}$$

Where, Ra stands for the resistance of gas sensors in the reference gas (usually the air) and Rg stands for the resistance in the reference gas containing target gases.

Gas sensors can have different levels of sensitivity depending on the type of sensor and the gas being detected [19]. Fig. 5 reveals the sensitivity versus temperature plot of CdS thick films. From Fig. 5, the CdS thick films shows more sensitivity to NO₂ gas compare to other selected. The maximum sensitivity was found to be 73.68% at operating temperature 120 °C and the gas concentration was 1000 ppm. The CdS thick film sensors work by detecting the presence and concentration of various gases in the air using physical or chemical reactions to convert the concentration of gases into electrical signals [18, 21]. The gas molecules react with the sensing material in the sensor, causing a change in its electrical conductivity or potential, which is then measured and converted into a signal [19, 20].

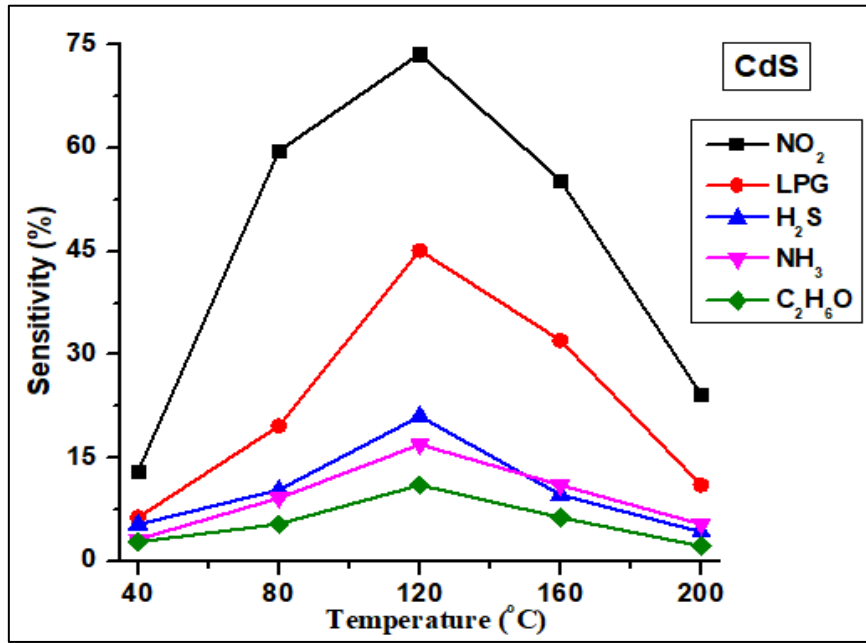


Figure 5: Sensitivity versus temperature plot of CdS thick films

Selectivity in gas sensors refers to the ability of a sensor to specifically recognize and respond to a single target gas species without significant responses to other interfering substances present in the environment [21, 21]. Enhancing selectivity is essential for accurate measurements and reliable operation of gas sensors, especially in complex atmospheres containing multiple gases. Fig. 6 shows the selectivity plot of CdS thick films to selected gases.

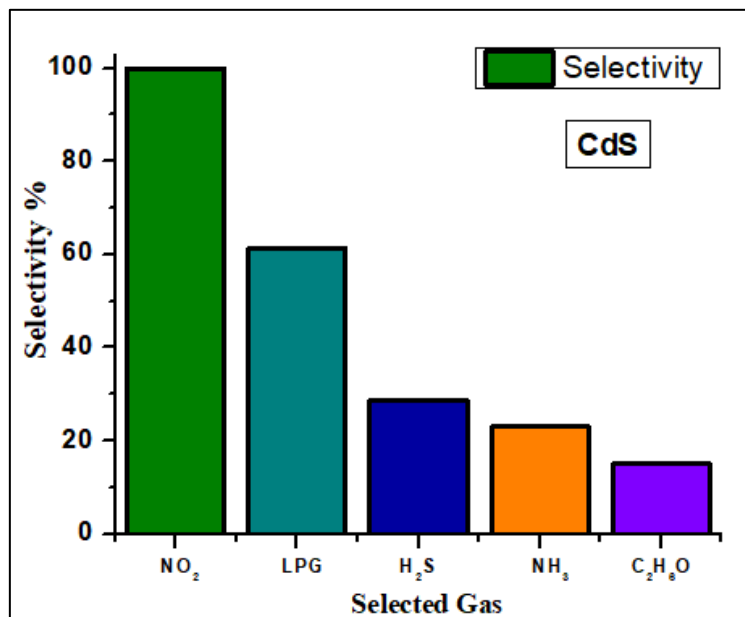


Figure 6: Selectivity graph of CdS thick films

The response time of a gas sensor is the time it takes for the sensor to register a change in the presence of a gas, typically from 10% to 90% of the overall signal change. It is an important parameter as it determines how quickly the sensor can detect the presence of a gas. The recovery time, on the other hand, is the time it takes for the sensor to return to its initial state after being exposed to a gas. This is crucial for ensuring that the sensor is ready to detect a new gas concentration [19, 20]. Both response and recovery times are essential for the effective operation of gas sensors, with faster times being generally more desirable. The response and recovery times can be influenced by various factors such as the sensor material, temperature, and experimental setup [20, 21]. Fig. 7 display the response and recovery time plot of CdS thick films to NO₂ gas. The response and recovery time was found to be 12 and 65 seconds respectively to the CdS films.

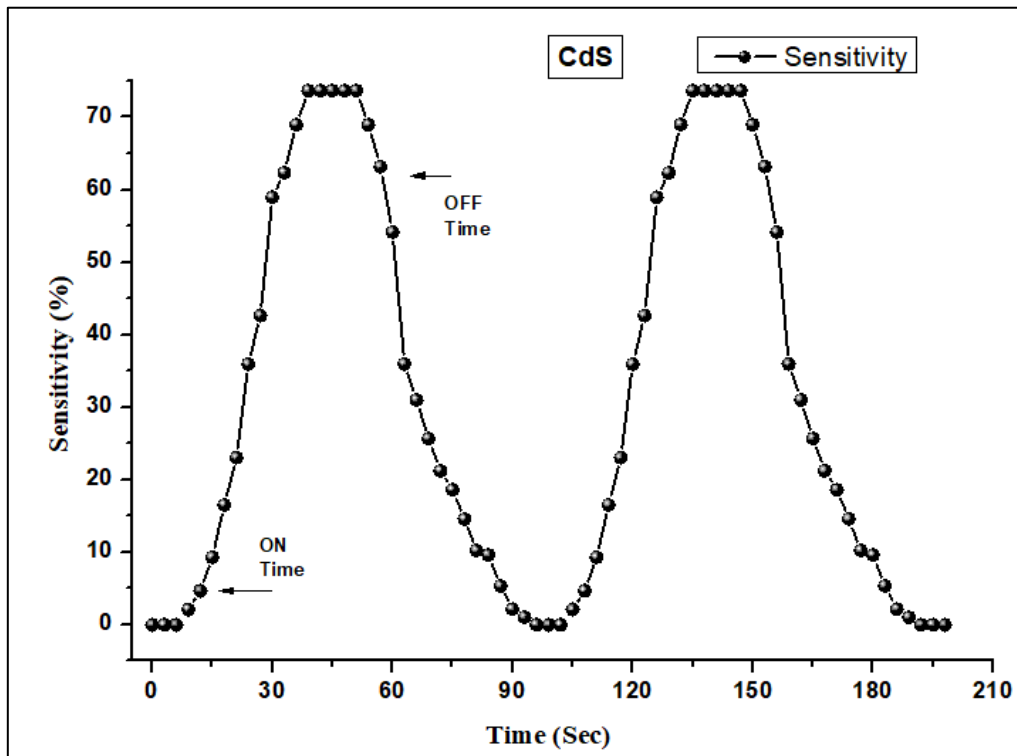


Figure 7: Response and recovery time plot of CdS thick films to NO₂ gas

The Gas sensing mechanism of CdS thick films to NO₂ gas involved chemosensor principle [21]. When NO₂ molecules adsorb onto the CdS surface, capturing free electrons from the conduction band (CB). As NO₂ adsorbs onto the CdS surface, the number of free electrons in the CB decreases, leading to an increase in resistance and change in resistance is recorded as sensitivity or gas response of the film [22, 23].

Conclusions and future scope:

The thick film gas sensing applications span across various industries and sectors, playing a vital role in maintaining environmental quality, ensuring industrial and domestic safety, optimizing processes, and improving overall efficiency. The versatility and cost-effectiveness of thick film gas sensors make them an indispensable tool for gas detection and monitoring. The CdS thick films were successfully prepared on glass substrate by using screen-printing technique. Prepared films shows semiconducting nature with negative TCR. Films shows maximum sensitivity to NO₂ gas at operating temperature 120 °C. Prepared films could be used of the fabrication of NO₂ gas sensor.

Acknowledgment

Author thanks to the Principal of M. G. V's M. S. G. Arts, Science and Commerce College, Malegaon, Malegaon camp, Dist- Nashik, India, for providing necessary support for the present research work.

References

1. Glencross DA, Ho TR, Camina N, Hawrylowicz CM, Pfeffer PE. Air pollution and its effects on the immune system. *Free Radical Biology and Medicine*. 2020 May 1;151:56-68.
2. Bernstein JA, Alexis N, Barnes C, Bernstein IL, Nel A, Peden D, Diaz-Sanchez D, Tarlo SM, Williams PB. Health effects of air pollution. *Journal of allergy and clinical immunology*. 2004 Nov 1;114(5):1116-23.
3. Kampa M, Castanas E. Human health effects of air pollution. *Environmental pollution*. 2008 Jan 1;151(2):362-7.
4. Hesterberg TW, Bunn WB, McClellan RO, Hamade AK, Long CM, Valberg PA. Critical review of the human data on short-term nitrogen dioxide (NO₂) exposures: evidence for NO₂ no-effect levels. *Critical reviews in toxicology*. 2009 Oct 1;39(9):743-81.
5. Chen TM, Kuschner WG, Gokhale J, Shofer S. Outdoor air pollution: nitrogen dioxide, sulfur dioxide, and carbon monoxide health effects. *The American journal of the medical sciences*. 2007 Apr 1;333(4):249-56.
6. Bosson JA, Mudway IS, Sandström T. Traffic-related air pollution, health, and allergy: the role of nitrogen dioxide. *American Journal of Respiratory and Critical Care Medicine*. 2019 Sep 1;200(5):523-4.
7. Tang H, Sacco LN, Vollebregt S, Ye H, Fan X, Zhang G. Recent advances in 2D/nanostructured metal sulfide-based gas sensors: mechanisms, applications, and perspectives. *Journal of Materials Chemistry A*. 2020;8(47):24943-76.
8. Chatterjee B, Bandyopadhyay A. Review on the synthesis of metal sulfides gas sensors and their performances at room temperature. *Materials Science and Engineering: B*. 2023 Nov 1;297:116781.
9. An BG, Kim HR, Chang YW, Park JG, Pyun JC. Photosensors-based on cadmium sulfide (CdS) nanostructures: a review. *Journal of the Korean Ceramic Society*. 2021 Nov 1:1-4.
10. Mir FA, Chattarjee I, Dar AA, Asokan K, Bhat GM. Preparation and characterizations of cadmium sulfide nanoparticles. *Optik*. 2015 Jun 1;126(11-12):1240-4.
11. Al-Jawad SM, Rafic SN, Muhsen MM. Preparation and characterization of polyaniline–cadmium sulfide nanocomposite for gas sensor application. *Modern Physics Letters B*. 2017 Sep 20;31(26):1750234.
12. Pan J, Tonkay GL, Quintero A. Screen printing process design of experiments for fine line printing of thick film ceramic substrates. *Journal of Electronics Manufacturing*. 1999 Sep;9(03):203-13.
13. Ménil F, Debéda H, Lucat C. Screen-printed thick-films: from materials to functional devices. *Journal of the European ceramic society*. 2005 Jan 1;25(12):2105-13.
14. Burnside S, Winkel S, Brooks K, Shklover V, Graetz M, Hinsch A, Kinderman R, Bradbury C, Hagfeldt A, Pettersson H. Deposition and characterization of screen-printed porous multi-layer thick film structures from semiconducting and conducting nanomaterials for use in photovoltaic devices. *Journal of Materials Science: Materials in Electronics*. 2000 Jun;11:355-62.
15. Tupe UJ, Zambare MS, Patil AV, Koli PB. The binary oxide NiO-CuO nanocomposite based thick film sensor for the acute detection of Hydrogen Sulphide gas vapours. *Material Science Research India*. 2020 Dec 10;17(3):260-9.
16. Koli PB, Kapadnis KH, Deshpande UG, Tupe UJ, Shinde SG, Ingale RS. Fabrication of thin film sensors by spin coating using sol-gel LaCrO₃ Perovskite material modified with transition metals for

- sensing environmental pollutants, greenhouse gases and relative humidity. *Environmental Challenges*. 2021 Apr 1;3:100043.
17. Wagh SL, Tupe UJ, Patil AB, Patil AV. Influence of Annealing Temperature on Structural and Electrical Properties of Screen Printed Lanthanum Oxide Thick Films. *Iranian Journal of Materials Science & Engineering*. 2022 Dec 1;19(4).
 18. Lad UD, Kokode NS, Deore MB, Tupe UJ. MgO incorporated ZnO nanostructured binary oxide thin film ethanol gas sensor. *IJSDR*. 2021;6(1):135-42.
 19. Patil A, Tupe UJ, Patil A. Reduced graphene oxide screen printed thick film as NO₂ gas sensor at low temperature. *Advanced Materials Research*. 2021 Dec 9;1167:43-55.
 20. D'Arsié L, Alijani V, Brunelli SS, Rigoni F, Di Santo G, Caputo M, Panighel M, Freddi S, Sangaletti L, Goldoni A. Improved recovery time and sensitivity to H₂ and NH₃ at room temperature with SnO_x vertical nanopillars on ITO. *Scientific reports*. 2018 Jul 3;8(1):10028.
 21. Ponzoni A. A Statistical Analysis of Response and Recovery Times: The Case of Ethanol Chemiresistors Based on Pure SnO₂. *Sensors*. 2022 Aug 23;22(17):6346.
 22. Yadava L, Verma R, Dwivedi R. Sensing properties of CdS-doped tin oxide thick film gas sensor. *Sensors and Actuators B: Chemical*. 2010 Jan 29;144(1):37-42.
 23. Li P, Jin H, Yu J, Chen W, Zhao R, Cao C, Song W. NO₂ sensing with CdS nanowires at room temperature under green light illumination. *Materials Futures*. 2022 Jun 27;1(2):025303.

Ansari Mohammed Saeed Mohammed Ishaque

Assistant professor, Dept. of Statistics

M. S. G. Arts, Science & Commerce College, Malegaon – Camp

Abstract

Education has a key and decisive role in this scenario of contingencies. The National Education Policy 2020 (here on referred to as the NEP) has therefore been transformed into the framework of this reform, which could help to build a new education system in the country. The purpose of the National Education Policy is to develop students' in critical thinking skills, scientific temper, and imagination, along with instilling values like empathy, courage, and resilience. This paper endeavors to introduce you to the key aspects of the National Education Policy, discuss its pros and cons, and offer solutions and recommendations to potential problems observed.

Recommendations are made for the design and implementation of NEPs at national and HEIs (Higher Education levels).

Keywords: National Education Policy, GDP, Teacher training, Indian Education, HEIs

1. Introduction

As the education system dealt with a huge blow due to the Covid-19 pandemic, a National Education Policy was introduced by the government in an attempt to soften the blow and revise the current, long-standing, under-productive, over-expensive education system. Offline schooling was shifted online, and new teaching routines and pedagogy were set in motion to optimize learning. It was also essential that India transforms its education system by inculcating multidisciplinary, innovation, and flexibility to adapt to the current times and compete with the standards of education of the western countries.

Difference Between NEP 2020 And Previous Policies Introduced

The previous policies concentrated a lot more on increasing the access to education. The Right of Children to Free and Compulsory Education Act 2009 makes certain that every child has a right to receive a quality education from age 6-14(class 8), irrespective of their social and economic background. The National Education Policy 1986 (modified in 1992) is a solid foundation to the NEP 2020. The NEP 2020 focuses on the relatively newer concepts and strategies to promote a multidisciplinary and holistic approach towards education.

Statistics And Figures Related to the Indian Education Sector

In 2020-2021 Budget, the education sector was allotted Rs 93,224 crore for 2021, with Rs 54,873 crore for school education and literacy and Rs 38,350 crore for the higher education sector. As per the latest 'World Talent ranking report' by IMD, although total public expenditure on education as a percentage of GDP ranks at 35th, expenditure per student - as well as both measures of the quality of education (pupil-teacher ratio in primary and secondary school) - rank at 62nd in the list of 104 countries.

The study has pegged the overall literacy rate in the country at about 77.7 percent. In rural areas, the literacy rate is 73.5 percent compared to 87.7 percent in urban areas of the country. At the all-India level, the male literacy rate is higher at 84.7 percent compared to 70.3 percent among women. Kerala tops the national literacy survey at 96.2%

Index

Sr.No	Title of the Paper	Author's Name	Pg.No
1	National Education Policy : An Opportunity to fill the Global Skill Gap	Prof (Dr) R.V.Tribhuvan	05
2	NEP 2020 and English in Multilingual Education Framework	Dr. Anil Krishna Aher	07
3	Multidisciplinary Education: The Master Key of NEP 2020 for Quality Transformation in Higher Education	Prof. Sunetra Meshramkar	10
4	'Significant Attributes of New Education Policy (NEP) 2020 In Higher Education'	Dr. Kamalakar B. Gaikwad	15
5	Senior College Teachers and Students Attitude Towards NEP 2020	Dr. Nikam Ramesh Namdeo	20
6	National Education Policy-2020 and its Magnitudes	Dr. Sahebrao. P. Kamble	24
7	NEP-2020: Role of IQAC in the Implementation in Higher Educational Institutes in India.	Dr. Devram G. Jadhav	27
8	New Education Policy 2020: Strengths and Weaknesses	Dr. Gautam Kolte	31
9	The National Education Policy 2020: A step to reform the existing education system	Dr. Premal R. Deore	33
10	National Education Policy 2020	Mr. Udhav Kalu Kudase	35
11	New Education Policy 2020 of India: A Statistical Analysis	Ansari Mohammed Saeed Mohammed Ishaque	38
12	Role of ICT in NEP 2020	Prof.Shubham U. Patil	43
13	National Education Policy 2020 and Skill Development	Mr. Ajay Ahir	47
14	New Education Policy: An Overview	Mr. Subhash Laxman Ahire	52
15	राष्ट्रीय शिक्षा नीति 2020 और भाषाएं	श्रीमती उषा देवी	55
16	राष्ट्रीय शिक्षा नीति 2020 और भारतीय भाषा-साहित्य: एक दृष्टिकोण	डॉ. कमलिनी पशीने	58
17	नई शिक्षा नीति का महत्व	प्रा हर्षल गोरख बच्छाव	63
18	राष्ट्रीय शिक्षण धोरण 2020 : वास्तवता व आव्हाने	डॉ. बाबासाहेब विबक मोताळे	66
19	नवे शैक्षणिक धोरण : एक चिंतन	प्रा. निलेश विठ्ठलराज नागरे	71
20	राष्ट्रीय शैक्षणिक धोरण 2023	अशोक वाघचौरे	75
21	राष्ट्रीय शैक्षणिक धोरण 2020 आणि बहुविद्याशाखीय शिक्षण	डॉ. मनीष सोनवणे	79
22	राष्ट्रीय शैक्षणिक धोरण : 2020	डॉ. चंद्रसिंग दगोसिंग राजपूत	82

ON UNIFORM STATISTICAL CONVERGENCE OF SERIES OF FUNCTIONS

KAILAS S. AHIRE AND SURYABHAN A. SANGALE

(Received: 20 August 2023, Revised: 13 June 2024)

ABSTRACT. A statistical convergence was introduced in connection with problems of series of functions. The concept of statistical convergence is directly connected to convergence of such statistical characteristics as the mean and standard deviation. In this paper we introduce a uniform statistical convergence for series of real valued functions. Also examine the validity of some theorems on Uniform convergence of series of real valued functions and uniform statistical convergence of series of real valued functions.

Keywords: Series of functions, Uniform Convergence, Statistical Convergence, Uniform Statistical Convergence.

1. INTRODUCTION

The idea of statistical convergence was given by [1], Fast [2] and Steinhaus [3] and also by Zygmund [4] in his monograph published in Warsaw in 1935. Later on, under the different names statistical convergence has been applied in the theory of Fourier analysis, ergodic theory, number theory [4], measure theory [5], trigonometric series [[4],[6]] and Banach space [7]. Tripathy [8] introduce a notation of convergence of series extended and statistically convergence series. Also in [9] the concept of a uniform statistical Cauchy sequence for functional sequences and proved that it is equivalent to uniform statistical convergence of sequence of functions. Ahire [10] discuss on statistical and uniform statistical convergence of sequences of functions. Salat [11] investigated sequence space point of view and linked with summability theory . Some results in Goldberg [12] helps to prove new results. [13] focused on integrability of functions and related summability. The statistical convergence of the partial sums of the series was introduced by [14]. Dindos and et. al. [15] noticed on infinite series in linear normed space. Cinar [16] studied on uniform statistical convergence. In [17] Gokhan et.al. discussed equivalences of pointwise statistically convergent and statistically Cauchy of the sequence of functions on a set.

2020 *Mathematics Subject Classification.* 40A05, 40A25, 40A30, 40A99.
Corresponding Author. (Kailas S. Ahire).
Suryabhan A. Sangale.

2. PRELIMINARIES

In this section, we recall the definitions that will be needed in this paper.

2.1. Definition. A subset A of the ordered set N of natural numbers is said to have density $d(A)$. If $\lim_{n \rightarrow \infty} \frac{|A_n|}{n} = A$, where, $A(n) = k < n : k \in A$ and $|A|$ denotes the cardinality of the set $A \subset N$.

Clearly finite subset of N have zero density and $d(A') = 1 - d(A)$ where $d(A') = N - A$. If a property $P(k)$ holds for all $k \in A$ with $d(A) = 1$. We say that P holds for almost all k , i.e. a.a.k.

2.2. Definition. A sequence of functions $\{f_k\}$ is statistically convergent to f on a set M of real numbers. If for every $\varepsilon > 0$ $\lim_{n \rightarrow \infty} \frac{1}{n} [\{k \leq n : |f_k(x) - f(x)| \geq \varepsilon, \text{ for every } x \in M\}] = 0$,

$$\text{i.e. for all } x \in M, \quad |f_k(x) - f(x)| < \varepsilon, \text{ a.a.k.} \quad (2.1)$$

In this case, we write $st - \lim f_k(x) = f(x)$ uniformly on M . **Or**

$$f_k \xrightarrow{st} f.$$

2.3. Definition. If u_1, u_2, \dots are real valued functions on a set M of real numbers. The $\sum_{n=1}^{\infty} u_n$ statistically converges to f on M , if the sequence of functions $\{s_n\}_{n=1}^{\infty}$ statistically converges to f on M where $s_n = u_1 + u_2 + \dots + u_n$.

We write as $\sum_{n=1}^{\infty} u_n = f$ statistically, ($x \in M$).

Example 1: For $u_n(x) = x^n, (-1 < x < 1)$ then $\sum_{n=1}^{\infty} u_n(x) = \sum_{n=1}^{\infty} x^n$ statistically converges to $f(x) = \frac{1}{1-x}, (-1 < x < 1)$.

2.4. Definition. If u_1, u_2, \dots are real valued functions on a set M of real numbers. We say that $\sum_{n=1}^{\infty} u_n$ converges uniformly to f on M , if $\{s_n\}_{n=1}^{\infty}$ where $s_n = u_1 + u_2 + \dots + u_n$ converges uniformly to f on M .

In this case we write $\sum_{n=1}^{\infty} u_n = f$ uniformly, ($x \in M$).

2.5. Definition. If u_1, u_2, \dots are real valued functions on a set M of real numbers. We say that $\sum_{n=1}^{\infty} u_n$ uniform statistically convergent to f on M , if $\{s_n\}_{n=1}^{\infty}$ uniform statistically convergent to f on M , where $s_n = u_1 + u_2 + \dots + u_n$.

In this case we write $\sum_{n=1}^{\infty} u_n = f$ uniform statistically, ($x \in M$).

Lemma 2.1. (Theorem 3.1[10]) *Let $\{f_k\}$ be a sequence of real valued functions defined on a metric space M which is uniformly statistically convergent to function*

f on M . If each $f_k, (k \in I)$ is continuous at $a \in M$. Then f is also continuous at a .

Lemma 2.2. (Theorem 2.2[17]) Let $\{f_k\}$ be a sequence of functions defined on a set S . The following statements are equivalent.

- i) $\{f_k\}$ is a pointwise statistically convergent sequence on S .
- ii) $\{f_k\}$ is a statistically Cauchy sequence on S .

Lemma 2.3. (Theorem 3.2 [9]) Let $\{f_k\}$ be a sequence of functions defined on a set S . The following statements are equivalent.

- i) $\{f_k\}$ is a uniformly statistically convergent sequence on S .
- ii) $\{f_k\}$ is a uniformly statistically Cauchy sequence on S .

3. SOME RESULTS

Theorem 3.1. Let $\{f_k\}$ be a sequence of continuous real valued functions defined on a compact on a metric space M such that

$$f_1(x) \leq f_2(x) \leq \dots \leq f_k(x) \leq \dots, (x \in M). \tag{3.1}$$

If $\{f_k\}$ statistically converges to f on M to the continuous function f then $\{f_k\}$ uniformly statistically converges to f on M .

Proof: For each $n \in I$. Let $g_k = f - f_k$. Then from (2.1).

$$g_1(x) \geq g_2(x) \geq \dots \geq g_k(x) \geq \dots \geq 0., (x \in M). \tag{3.2}$$

Since $\{f_k\}$ statistically converges to f on M .

$$\therefore \lim_{k \rightarrow \infty} g_k(x) = 0, (x \in M). \tag{3.3}$$

Hence $\{g_k\}$ is statistically converges on M .

By lemma (2.2, 2.3) $\{g_k\}$ is uniformly statistical converges to 0 on M .

Hence $\{f_k\}$ uniformly statistically converges to f on M .

Theorem 3.2. Let u_1, u_2, \dots be real valued functions on a metric space M . If $\sum_{n=1}^{\infty} u_n$ uniformly statistical converges to f on M , and if each u_n is continuous at the point $a \in M$, then f is also continuous at a .

Proof: The $\sum_{n=1}^{\infty} u_n$ uniformly statistical converges to f on M , hence the sequence of functions $\{s_n\}_{n=1}^{\infty}$ uniformly statistical converges to f on M , where $s_n = u_1 + u_2 + \dots + u_n$. Now each u_k is continuous at a point $a \in M$, then each s_n is continuous at $a \in M$.

Hence $u_1 + u_2 + \dots$ is continuous at the point $a \in M$. Then by lemma (2.1), f is continuous at a .

Example 2: The series $\sum_{n=1}^{\infty} x(1-x)^n$ converges on $[0, 1]$ to the function f where $f(0) = 0$ and $f(x) = 1, (0 < x \leq 1)$.

If $0 < x < 1$, then $\sum_{n=1}^{\infty} x(1-x)^n = x \sum_{n=1}^{\infty} (1-x)^n x \left[\frac{1}{1-(1-x)} \right] = 1$.

Now, if $u_n(x) = x(1-x)^n$; ($0 \leq x \leq 1$) is continuous on $[0, 1]$.

Since f is not continuous on $[0, 1]$.

The $\sum_{n=1}^{\infty} x(1-x)^n$ does not uniformly statistically convergent on $[0, 1]$.

Theorem 3.3. Let $\sum_{k=1}^{\infty} u_k$ be a series of real-valued functions on a metric space M . If there exists positive numbers M_1, M_2, \dots , with $\sum_{k=1}^{\infty} M_k < \infty$ such that $\sum_{k=1}^{\infty} u_k(x) \ll \sum_{k=1}^{\infty} M_k(x)$, $x \in M$ then $\sum_{k=1}^{\infty} u_k$ uniformly statistically convergent on M .

Proof: Let, $s_n = \sum_{k=1}^n u_k$ and $t_n = \sum_{k=1}^n M_k$.

Since $\sum_{k=1}^{\infty} M_k < \infty$.

$\Rightarrow \lim_{n \rightarrow \infty} \frac{1}{n} [\{k \leq n : |t_k(x) - t(x)| \geq \varepsilon, \text{ for every } x \in M\}] = 0$.

Hence the sequence $\{t_n\}_{n=1}^{\infty}$ is statistically convergent on M .

Hence by lemma (2.2) $\{t_n\}_{n=1}^{\infty}$ is statistically Cauchy sequence.

Thus for given $\varepsilon > 0$ there exists $N \geq N_1$ such that

$\lim_{n \rightarrow \infty} \frac{1}{n} [\{k \leq n : |t_m(x) - t_n(x)| \geq \varepsilon, \text{ for every } x \in M, m, n \geq N\}] = 0$.

Now

$$\begin{aligned} |s_m(x) - s_n(x)| &= \left| \sum_{k=n+1}^m u_k(x) \right| \leq \sum_{k=n+1}^m |u_k(x)| \leq \sum_{k=n+1}^m M_k \\ &= t_m - t_n, (x \in M). \end{aligned} \quad (3.4)$$

Then by (3.4) $\lim_{n \rightarrow \infty} \frac{1}{n} [\{k \leq n : |s_m(x) - s_n(x)| \geq \varepsilon, \text{ for every } x \in M, m, n \geq N\}] = 0$.

i.e. sequence $\{s_n\}_{n=1}^{\infty}$ is uniformly statistically convergent on M .

By lemma (2.3) $\{s_n\}_{n=1}^{\infty}$ is uniformly statistically Cauchy sequence on M .

Hence $\{s_n\}_{n=1}^{\infty}$ is uniformly statistically convergent sequence on M .

This means that $\sum_{k=1}^{\infty} u_k$ is uniformly statistically convergent on M .

Example 3: For a real number x the series $\sum_{k=1}^{\infty} \frac{\sin nx}{n^3} \ll \sum_{k=1}^{\infty} \frac{1}{n^3}$.

But $\sum_{k=1}^{\infty} \frac{1}{n^3}$ is uniformly statistically convergent.

Hence $\sum_{k=1}^{\infty} \frac{\sin nx}{n^3}$ is uniformly statistically convergent.

Theorem 3.4.

If the power series $\sum_{k=1}^{\infty} a_k x^k$ statistically converges for $x = x_0$

$$(3.5)$$

then $\sum_{k=1}^{\infty} a_k x^k$ uniformly statistically convergent on $[-x_1, x_1]$ where x_1 is any number such that $0 < x_1 < |x_0|$.

Proof: The $\sum_{k=1}^{\infty} a_k x^k$ statistically convergent for $x = x_0$ then $|\sum_{k=1}^{\infty} a_k x^k|$ statistically convergent for any x with $|x| < x_0$.

In particular, if $0 < x_1 < |x_0|$ then $|\sum_{k=1}^{\infty} a_k x^k|$ statistically convergent for $x = x_1$,

i.e. $|\sum_{k=1}^{\infty} a_k x_1^k| < \infty$.

Since $\sum_{k=1}^{\infty} a_k x^k \ll \sum_{k=0}^{\infty} |a_k| x_1^k$; ($|x| \leq x_1$).

By theorem (3.3) the series (3.5) uniformly statistically convergent for $|x| \leq x_1$.

Example 4: The series $\sum_{k=1}^{\infty} \frac{x^k}{k}$ statistically converges for $-1 \leq x \leq 1$.

By theorem (3.4) $\sum_{k=1}^{\infty} \frac{x^k}{k}$ uniform statistically converges for $-a \leq x \leq a$,

where any number a such that $0 < a < 1$.

But series $\sum_{k=0}^{\infty} \frac{x^{k-1}}{(k-1)!}$ does not uniform statistically converges on $(-\infty, \infty)$.

Theorem 3.5. Let $\sum_{k=1}^{\infty} u_k$ be a series of continuous nonnegative real valued functions on a compact metric space M . If $\sum_{k=1}^{\infty} u_k$ statistically converges on M to the continuous function f then $\sum_{k=1}^{\infty} u_k$ uniformly statistically converges to f on M .

Proof: For $n \in I$. $s_n = u_1 + u_2 + \dots + u_n$. Since each $u_k(x) \geq 0$ for all $x \in M$.

We have $s_1(x) \leq s_2(x) \leq s_3(x) \leq \dots \leq s_n(x) \leq \dots, x \in M$.

By theorem (3.1) $\lim_{n \rightarrow \infty} s_n = f(x), x \in M$.

Hence the sequence $\{s_n\}$ uniformly statistically converges to f on M .

Therefore $\sum_{k=1}^{\infty} u_k$ uniformly statistically converges to f on M .

Example 5: The series $\sum_{n=1}^{\infty} \frac{n^2 x}{1 + n^4 + x^2}$ is non uniformly statistical convergent in $[0, 1]$.

$$\text{Let, } u_n = \frac{n^2 x}{1 + n^4 + x^2} \quad x \in [0, 1].$$

$$\lim_{n \rightarrow \infty} u_n(x) = u(x) = 0, \quad x \in [0, 1].$$

$$\therefore |u_n(x) - u(x)| = \frac{n^2 |x|}{1 + n^4 + x^2} < \varepsilon. \quad (3.6)$$

If $x = \frac{1}{n}$, put $\varepsilon = \frac{1}{n}$ then equation (3.6) does not holds.

Hence the series $\sum_{n=1}^{\infty} \frac{n^2 x}{1 + n^4 + x^2}$ is non uniformly statistical convergent in $[0, 1]$.

REFERENCES

1. Buck, R.C., (1946) The measure Theoretic Approach to density, *AM.J. Maths*, **68**, 560-580.
2. Fast, H., (1951) Sur la Convergence Statistique, *Coll. Maths*, **2**, 241-244.
3. Steinhaus, H., (1951) Sur la Convergence Ordinaire et al Convegence Asymptotique , *Coll. Maths*, **2**, 73-74.
4. Zygmund, A., (1979) Trigonometric Series, *Cambridge Uni. Press, Cambridge*.
5. Erdos, P., Tenenbaum, G., (1989) Sur les densites de certaines suites dentiers, *Pro. London Maths. Soc.*, **59(3)**, 417-438.
6. Miller, H.I., (1995) A measure theoretical subsequence characterization of statistical convergence, *Trans. Am. Maths. Soc.*, **347(5)**, 1811-1819.
7. Connor, J., Ganichev, M., Kadets, V., (2000) A characterization of Banach spaces with separable duals via weak statistical convergence, *J. Math. Anal. Appl.*, **244(1)**, 251-261.
8. Tripathy, B.C., (1999) On Statistically Convergence Series, *Punjab University, J. Maths.*, **XXXII**, 1-8.
9. Gungor, M., Gokhan, A., (2005) On Uniform Statistical Convergence, *Int.J. Pure. Appl. Maths*, **19(1)**, 17-24.
10. Ahire, K.S., (2020) Statistical and Uniform Statistical Convergence Of Sequences of Functions and Applications, *J.Emerging Tech. Inno. Res.*, **7 (12)**, 74-77.
11. Salat, T., (1980) On Statistically Convergent Sequences of Real Numbers, *Math. Slovaca.*, **30(2)**, 139-150.
12. Goldberg, R. R., (1970), *Methods of Real Analysis*, Oxford and IBH Publishing Co.PVT. Ltd, New Delhi.
13. Schoenberg, I.J., (1959) The Integrability of Certain Functions and Related Summability Methods, *Am. J. Maths.*, **66**, 361-375.
14. Dindos, M., Salat, T., Tomba, V., Bratislava., (2003) Statistical Convergence of Infinite Series, *Czechoslovak Math.J.*, **53(128)**, 989-1000.
15. Dindos, M., Martissovits, I., Salat, T., (2000) Remarks On Infinite Series In Linear Normed Space, *Tatra Mt. Math. Publ.*, **19**, 31-46.

16. Cinar, M., Karakas, M., Et, M., (2013) On Pointwise and Uniform Statistical Convergence of Order α for Sequence of Functions, *Fixed Point Theory, Appl.*, Article Id **33**.
17. Gokhan, A., Gungor, M., (2002) On Pointwise Statistical Convergence, *Indian J. Pure. Appl. Math.*, **33(9)**, 1379-1384.

M. S. G. COLLEGE, MALEGAON CAMP. INDIA,(M.S.), PIN- 423 105.

Email address: ksahire111@gmail.com

M. S. G. COLLEGE, MALEGAON CAMP. INDIA,(M.S.), PIN- 423 105.

Email address: sangalesa@gmail.com

Dr. Devram G. Jadhav

Assistant Professor, PG Dept. of Botany,

MGV's, Maharaja Sayajirao Gaikwad College, Malegaon Camp, Dist. Nashik, (M.S.) India

Abstract:

In India, the National Education Policy 2020 (NEP 2020) was unveiled in July 2021. The Indian education system has not seen such big changes in the previous 34 years. As a result, it's a historic moment for all of India and has the potential to spark a much-needed reformation movement. Numerous modifications have been suggested for the primary, secondary, college, and university education systems at all levels. The NAAC is crucial in the evaluation and accreditation of institutions of higher learning. It also directs IQACs towards advancement. IQACs work at the institutional level to ensure that policy is implemented correctly. This article explores how IQAC might positively contribute to the effective implementation of NEP 2020 in Indian HEIs.

Key words: IQAC, HEI's, Implementation, NEP 2020.**Introduction:**

The National Assessment and Accreditation Council (NAAC), an organisation created in 1994 by the Government of India by an Act of Parliament to ensure quality in the nation's higher education sector, the idea of an internal quality assurance cell (IQAC) was introduced. The primary goal of IQAC in higher education institutions is to guarantee excellence and quality for all stake holders involved in Assessment and Accreditation process. It is a required cell that serves as a conduit between HEI management and stakeholders involved in accordance with the NAAC's guidelines, it aims to make quality the defining element of higher education in India through a combination of self and external quality evaluation, promotion, and sustenance initiatives.

Presently IQAC is mandatory for every Higher Education Institution (HEI) after the first cycle of assessment and accreditation as set by the NAAC and UGC. It is a fact that without NAAC assessment and accreditation no HEI is funded by the Government of India. HEIs are being funded by the Rashtriya Uchchhatar Shiksha Abhiyaan (RUSA) of the Government on the basis of the NAAC accreditation. The introduction of NEP 2020 by the government of India in July 2021 has brought hopes of new changes in the field of education system particularly in the field of higher education. The role of IQAC is very significant in implementation of NEP 2020 in HEIs in India. The present article focuses an understanding of the essence of NEP 2020 and the role of IQACs in the HEIs of India

NEP 2020:

The NEP 2020 is the result of many conversations, debates, and feedback from several stakeholders from all over the nation. NEP aims to transform India into Bharat, a departure from Macaulay. Bharat-centered education would seek solutions to the current issues in the educational system. It focuses on holistic, practical education that combines modernism with our ancient Indian knowledge system. The fusion of heritage and modernity is flawless. India has three national education policies, nevertheless. The government of Mrs. Indira Gandhi created the first National Education Policy in 1968. The second, adopted in 1986 when Mr. Rajiv Gandhi was the country's prime minister. In 1992, the administration of Prime Minister Narasimha Rao changed the same. The most recent education policy was developed by the Sri Narendra Modi's administration and approved by the parliament on July 29, 2020.



Consequently, it became known as NEP 2020. It is the India-centered education system that directly helps to changing our country sustainably into an equitable and thriving knowledge society, by offering high quality education to all. NEP 2020 seeks to foster independent individuals. As a result, life skills are taught starting at the primary level. With the national skill curriculum framework starting at IX standard education, several adjustments are suggested for secondary education.

The key points of higher education that will bring it up to line with international standards are as follows.

NAAC Accreditation and Assessment System:

Using the seven major fields of higher education as a foundation, the National Assessment and Accreditation Council has created a unique evaluation methodology. In addition to gathering quantitative data about the institution, there are seven other criteria. Although the general testing is the same, templates for colleges and institutions change as well. It is the responsibility of IQAC in HEI to provide the data and keep the records required for evaluation. These are the seven criteria: Criterion 1. Curricular Aspects, Criterion 2. Teaching, Learning and Evaluation, Criterion 3. Research, Innovations and Extension, Criterion 4. Infrastructure and Learning Resources, Criterion 5. Student Support and Progression, Criterion 6. Governance, Leadership and Management and Criterion 7. Institutional Values and Best Practices. NAAC has developed standard system of assessment of HEIs in India, the education system was not fully compatible with parameters required for assessment and accreditation. It was difficult for IQAC to answer the questions which are not practiced in the institutions. But NEP 2020 has given opportunities to introduce required courses and planning to make the institution student friendly.

Following points empower IQACs to bring about qualitative changes in the HEIs with the support of NEP 2020 policy. By implementing this policy in all over the India, what kind of inputs comes out are discussed in this article.

Curricular Aspects.

NEP 2020 permits HEIs to offer a broad-based, comprehensive curriculum. It broadly discusses education that is focused on need of locality. The policy places a strong emphasis on Indian Knowledge System. Four-year honours degrees in traditional fields of study including B.A., B.Com., B.Sc., B.B.A., B.V.A. etc. have been reinstated. For those who choose to abandon the course in the middle, there will be a variety of access and departure points. The Academic Bank of Credits will transfer their credits. This policy responds to the NAAC issues regarding horizontal and vertical mobility. Students are free to switch between fields and resume studies they had previously stopped. Universities now have the authority to modify rules to conform to NEP 2020 requirements. A mechanism called Academic Bank Credits (ABC) is successfully launched. The student has the option of taking both online and traditional courses, and they can combine their qualified credits with other types of programmes.

Teaching, Learning and Evaluation:

NEP 2020 mentions cutting-edge instructional methods. Life learning and the use of contemporary technology have been emphasised. Through NEP 2020, experiential learning is encouraged. For implementation of NEP 2020, Apps, online courses and modules, satellite TV channels, online publications, ICT-equipped libraries and Adult Education Centres will be developed. The system of formative and summative evaluation has been modified. Technology use has been encouraged at all educational levels by NEP 2020. Education planning, instruction, evaluation, teacher, school, and student training will all include technology. Regional language e-content will be made available, starting with 8 major ones. IQAC can make it easier to use resources that are available in various languages.



Research, Innovation and Extension:

NEP 2020 placed a strong emphasis on the necessity for research at all levels of education. Both student and teacher research are encouraged by developing R&D research and development centres. For the first time, the policy places a strong emphasis on student research. The fourth-year courses for the four-year honours programmes include research components. Dissertations and research technique have been introduced. Under this programme, students who have completed their dissertation in the fourth year are eligible to apply for admission to the Ph.D. course. This will promote college-level research. College-level research centres can be strengthened through IQAC. College professors are being given the responsibility of guiding Ph.D. students. Extension activities are naturally encouraged due to Skill Enhancement Courses and Internships. At the collegiate level, IQAC can have a significant impact on how these new rules are put into practise.

Infrastructure and Learning Resources:

The institution's infrastructure is crucial to the implementation of any policy. Multidisciplinary courses call for extra classrooms and laboratories, which NEP 2020 strategy supports. Even those studying the arts can choose an open elective in a scientific or engineering field. There is a significant influx of students from many streams. Institutions must establish physical infrastructure to handle new changes. IQAC play significant role in developing the infrastructure needed for the college's teaching, learning, and research activities. The issue for institutions is to update the libraries with fresh learning resources, in particular. The institution must be assisted by IQAC in modernising the required facilities and instructional materials.

Student Support and Progression:

The tools offered to enhance their study and career preparation are part of the student support and advancement in HEIs. NEP 2020 offers education that is skill-based. For improved education, it is essential to incorporate all the necessary abilities. Sports, cultural, NSS, NCC, yoga, YRC, and other extracurricular activities are taken into account for credit under the new system. It is the duty of IQAC to raise awareness and see that the courses are implemented correctly.

Governance, Leadership, and Management:

According to the draught paper, there will be significant changes to the governance, leadership, and management structure. The emphasis has been on institutional autonomy to improve quality and excellence. In the phase-wise time, all HEIs will be self-sufficient. Since universities from around the world can compete with Indian universities, there would be a lot of competition. It is possible for foreign universities to establish the campuses in India. The idea is for CET to be used for HEI admissions. The National Testing Agency (NTA) will conduct the universal entrance exam for all higher education institutions. For some programmes, the exam will, however, be optional. The NEP 2020 plan places a strong emphasis on providing high-quality higher education that is inclusive and equitable and fosters traits like goodness, creativity, and humanity. The worldviews and values of both the traditional and modern eras must be taken into account. Large multidisciplinary colleges and universities are being established, and there is a focus on multidisciplinary education.

Institutional Values and Best Practices:

One of the criteria used to determine the level of a HEI's quality is its institutional values and best practises. It examines institutional ideals related to inclusivity and gender fairness. Programmes and practises that are friendly to the environment are taken into account. The ideal procedure must be distinct and helpful to the community. Many of these chances for practise are provided by NEP 2020 policy, and IQAC has a bigger role to play in identifying the finest best practises.

Conclusion:

When all the stake holders related to HEI's are actively involved and contribute positively, the policy is successfully executed. The creation of policies is done with the best of intentions. NEP offers numerous such ground-breaking adjustments to the higher education sector. When all HEIs fully comprehend the policy, it will be more effectively applied at the local level. IQAC is the best coordinating cell in any HEI for improving policy understanding. As a result, the IQAC's contribution to the implementation of NEP 2020 at higher education institutions is very much crucial.

References:

1. NEP 2020 draft guidelines: Draft_NEP_2019_EN_Revised.pdf (education.gov.in)
2. NAAC IQAC guidelines : <http://naac.gov.in/index.php/en/2-uncategorised/68-guidelines>
3. Dr Guranath K Badiger and Dr. Uma B Pujar, "Role of IQAC in Implementation of NEP 2020 in HEIs in India", International Journal of Creative Research Thoughts (IJCRT), Volume 11, Issue 1, 2023. b 989-993.
4. S.C. Sharma and Shyam Singh Inda, "Assessment and Accreditation of Indian Higher Education Institutions in Light of New Education Policy 2020", Policy Paper, Vol. XIV, No.1, 2021, pp 125-129.
5. Dr. Nisha Jain, Dr. Renu Jain and Dr. Prativindhya Saini, "Analysis of NEP 2020 in the Light of NAAC Accreditation: An Analytical Study of Academicians Opinion", International Journal for Research in Applied Science & Engineering Technology (IJRASET), Volume 10, Issue XII, 2022, pp 799-802.



Study of Medicinal Plants of family Asteraceae of Nasik District (M.S.) India.

Dilip Ahire

P. G. Department of Botany, M.S.G. College Malegaon Camp, Nasik.

ABSTRACT

Present paper deals with report 22 medicinal plants collected from different localities of Nasik district. A portion of them have gained naturalization and are now a part of our native plants. Since ancient times, Vaidyas and tribal people have prepared primitive medications using various plant parts. The current study aims to list the medicinal plants that tribal people employ and their respective medical applications.

Key words: Medicinal plants, family Asteraceae, Nashik

INTRODUCTION

The Nasik district of Maharashtra is located between latitudes 19°35' and 20°50' and longitude 73°55' and extended an over an area of 15.582 sq. km. It is finite on the north-west by the Dang and Surat district of Gujarat, on the north by Dhulia district, and on the east by Jalgaon district and towards the south-west the Thane district.

Medicinal plants found in Nasik region of Maharashtra are naturalized in some parts of forest along roadsides, dams, canals, under, on hedges of fields and they are dominating to the native vegetation. During exploration tour in forest found that the tribal communities and villagers are regularly using some plants for the purpose of medicine and so we have collected medicinal plants. A large part of population is dominated by the social group inhabitants like Varlis, Mahadev Kolis, Konkans, Bhila, Mali etc. The tribal and local communities cure their ailments by easy remedies. Ethnobotanical work of this region is carried out by Jain (1991), Ghate (1998), Ghate and Vartak (1996), Jain S.K (1981) and Bhattacharjee (2008).

MATERIAL AND METHODS

Present studies was carried out in Nasik district in the year 2011-2012.for the study of medicinal plants of Nasik region. The ethnobotanical data was collected through interviews, discussions with them collected the data on medicinal uses also the literature available on same plants. The medicinal plants identified by using flora like, Flora of (Almeida 1990), Naik (1999), Lakshminarsimhan & Sharma (1991), Shah (1978),Sharma et al (1996). All these plants are enumerated (22 plants) in the following ways.

***Ageratum conyzoides* L.**

Local Name : 'Boradu'.

Herbs, erect, annual hairy, 30 cm high. Leaves ovate, less or more hairy on both sides, apex subacute. Heads small white or pale blue, in dense terminal, corymbs, pappus paleaceous awned or aristate little longer than achenes, pappus scales 5, aristate. Achenes sharply 5-angled, black, sparsely spiculate on agnles.

Fl. & Fr.: July-February.

Medicinal uses :

Leaves are antiseptic, used for wounds, cuts. Cancer, leprosy, boils, burns and skin diseases. Roots are used for the treatment of kidney stones. Entire plant is used for uterine disorders, piles, ring-worm, tumwes, diarrhoea, scabies, sores, tumour, colic, head-ache and muscular pains. Plant is used for snake poison.

***Blumea lacera* (Burm. f.) DC.**

Local Name : 'Borandu'.

Herbs, 25-80 cm high, erect, aromatic, stem grooved, glandular pubescent. Leaves obovate-oblong, incised or some time lyratly lobed. Achenes oblong, sparsely hairy.

Fl. & Fr.: October-May.

Medicinal uses :

Leaf juice is anthelmintic, used for thread-worms. Leaf paste is applied on burns, wounds, cuts, piles and urine complaints. Root juice is used as astringent and febrifuge. Root juice is used for diarrhoea.

***Blumea malcolmii* Hook.f.**

Local Name : 'Tantani'.

Herbs 1 m high, decumbent strongly aromatic. Leaves obovate, sessile. Achene dark brown sparsely pubescent.

Fl. & Fr.: October-January.

Medicinal uses :

Leaf juice is used for eye disease.

***Chrysanthemum indicum* Linn.**

Local Name : 'Sevanti'.

Herbs ,perennial, stem erect. Head yellow.

Fl. & Fr.: August- October.

Medicinal uses :

The decoction of whole plant used for bronchitis, whooping cough, boils, swelling and rheumatism.

Cichorium intybus L.

Local Name : 'Kasai'.

Herbs, erect, appressed hairy with thick taproot. Lower leaves short petioled, lyrate-pinnatifid, oblong, acute at apex, upper ones sagittate with rounded dentate margins. Head solitary or clustered, florets blue or pink corollas. Achenes 5-angular. Pappus scales short.

Fl. & Fr.: October- March

Medicinal uses :

Leaf paste is applied to treat wounds and cuts. Root decoction is used for stomach pain, rheumatic, gout problem and jaundice .

, **Echinops echinatus** Roxb.

Local Name : 'Udkata' 'Utkatkar'.

Annual, herbs, 30-90 cm high. Leaves sessile, oblong, deeply pinnatifid, glabrous or minutely pubescent. Heads white, Pappus short, yellow, forming short cylindrical brush above achenes. Achenes obconic.

Fl. & Fr.: September-January.

Medicinal uses :

Entire plant is considered as bitter tonic and diuretic. Plant is used to treat malaria and fever. Roots are used for bone-ache, skin diseases and chewed on urinal complaints.

Eclipta prostrata L.

Local Name : 'Maka'.

Herbs, annual, prostrate or erect. Leaves sessile, oblong-lanceolate or oblong-elliptic, sparsely strigose on both surfaces. Heads solitary or 2 together on unequal axillary peduncles yellow. Achenes oblong-obovate tubercled all over, trigonous, brown to black.

Fl. & Fr.: July-February.

Medicinal uses :

Leaf juice is used for tonic, juice is considered as antiseptic, used on carbuncle, fever, malaria, gastric complaint, cure skin diseases, promotes hair growth, sores and swelling of ears. Root decoction is used as emetic and purgative. Root paste is applied to treat ulcers and wounds. Entire plant is used for bronchitis, asthma, jaundice, liver complaint, leucoderma, toothache, hepatic diseases, ulcers and wounds.

Elephantopus scabra L.

Local Name :

Annual, herbs, 20-30 cm high, erect, softly pubescent. Leaves mostly radical, obovate-oblong, few cauline. Heads arranged in terminal dichotomous cymes, flowers bluish. Pappus 5, paleaceous, scaly produced in to a fine aristae. Achenes oblong, ribbed, tapering at base, hairy in between ribs.

Fl. & Fr.: August-January.

Medicinal uses :

Leaf juice is applied to wounds and heal fresh cuts. Leaves are also eczema and ulcers. Decoction of root is used for dysentery, vomiting and stomach. Root paste is also used for painful urination.

Emilia sonchifolia (L.) DC.

Local Name : 'Dhamapan'.

Herbs, erect. Leaves variable, lower with petioles, lyrate-pinnatifid, cauline. Heads in terminal lax corymbose panicles, with purplish flowers. Pappus copious white. Achenes narrow 5-ribbed, brown, scabrid on ribs.

Fl. & Fr.: August-December.

Medicinal uses :

Leaf juice is used on sore eye, night blindness and ears. Leaves are used for boils, bruises. Roots are used for diarrhoea, cuts and wounds.

Guizotia abyssinica (L.f.) Cass.

Local Name : 'Khursani'

Herbs, stout, erect 30 -100 cm high. Leaves lanceolate, apex acute, base cordate sparsely hairy on both sides.

Heads solitary on axillary peduncles. Achenes black 4 -angled oblong.

Fl. & Fr.: September- October

Medicinal uses:

Seeds are used in the treatment of rheumatism, cough and burn.

Helianthus annuus Linn.

Local Name : 'Suryaphool'.

Erect, woody annuals, 1-3 m high, stem hispid, branched. Lower leaves opposite, upper alternate ovate, acute apex. Heads solitary, terminal on short peduncles. Involucral bracts strongly ciliate, florets with ligulate yellow corollas, central florets with tubular 5-fid, brownish-purple corollas. Achene black. Pappus of 2 scale like awns.

Fl. & Fr.: September-December.

Medicinal uses:

Leaves are used for malarial fever. Roots are used for diarrhoea, dysentery and dysentery.

Lagascea mollis Cav.

Local Name : 'Phulari'.

Herbs, annual, slender laxly branched, villous. Leaves ovate, apex acute, upper surface coarsely hairy, lower surface densely silky. Heads clustered at the end of branches on long peduncles. Pappus as a short fimbriate tuft. Achenes cuneate, enclosed within involucre.

Fl. & Fr.: July- October

Medicinal uses:

Leaf paste applied on cuts and wounds. Extract of flower heads is applied around eyes for conjunctivitis.

Parthenium hysterophous Linn.

Local Name : 'Congress grass'.

Herbs, 30-60 cm high. Leaves appressed hairy. Heads 0.2 cm in diameter, peduncled, in panicles. Flowers white. Achenes compressed, triquetrous.

Fl. & Fr.: September-November

Medicinal uses:

The flowers and seeds are used for leucoderma. It is also useful to dysentery, malaria, diarrhoea and rheumatic pain.

***Sonchus oleraceus* L.**

Local Name : 'Mhatara'.

Fl. & Fr.: December-February

Herbs, annual, 90 cm high, erect. leaves sessile, oblong or obovate. Heads yellow in terminal umbellate cymes. Achenes ovoid.

Fl. & Fr.: September-may.

Medicinal uses :

Leaves are used for cuts and injuries. Roots and leaves are used in indigestion and as febrifuge. Stem are prescribed as sedative as tonic. An ointment made from decoction of root is used for wounds and ulcers.

***Sphaeranthus indicus* L.**

Local Name : 'Gorakhmun', 'Mudi'.

Herbs, highly branched spreading. Leaves obovate-oblong, glandular-hairy narrow at base. Heads on solitary glandular peduncles. Achenes stalked.

Fl. & Fr.: November-may.

Medicinal uses :

Leaf paste is given to treat elephantiasis. Leaf decoction is used for leucorrhoea. Plant juice is used for treat gastric problems and liver. Whole plant paste is used for the small pox infected areas. Root decoction is used for chest pain, bowel complaints and cough.

***Spilanthus calva* DC**

Local Name : 'Akkalkara'.

Herbs, suberect. Leaves opposite ovate apex acute. Heads solitary, yellow brownish ovoid. Achenes compressed.

Fl. & Fr.: October-January.

Medicinal uses :

Leaves are used as anaesthetic, used in tooth-ache and scabies. Root is used as purgative. Roots are used for diarrhoea, cough and cold. Decoction of plant is given as diuretic, and employed as a bath for rheumatism. Flowers are chewed to relieve tooth-ache, throat and gums and paralysis of tongue. Entire plant is used in dysentery.

***Tagetes erecta* Linn.**

Local Name : 'Zendu'.

Herbs 0.5-1.2 m high erect annual. Leaves opposite or upper alternate, pinnately divided into lanceolate. Heads solitary. Marginal florets with yellow ligules, central florets with yellow, tubular corollas. Achenes linear-oblong. Pappus scale united.

Fl. & Fr.: Throughout year.

Medicinal uses :

Leaf juice is useful on ear-ache and leaves are also used on urine complaints, cuts and wounds. Flowers are used on ulcers.

***Tridax procumbens* L.**

Local Name : 'Dagadipala'.

Annual, herb, erect, branched at base. Leaves opposite, ovate-lanceolate, margins serrate to coarsely incised dentate or trilobed. Heads heterogamous, produced on erect, retrorsely hirsute and glandular peduncles, rayflorets yellow or white, disc floret bright yellow. Pappus of numerous aristate bristles. Achenes oblong, densely pilose, black.

Fl. & Fr.: Throughout the year.

Medicinal uses :

Leaves are antiseptic, used on boils, blisters, eczema, dysentery, diarrhoea, eye diseases, leprosy. Bronchitis, skin diseases sores, stomach-ache, tooth-ache, cuts and wounds. Roots are used for fever. Stem and leaf combination used for stone in urinary bladder.

***Vicoa indica* DC.**

Local Name : 'Bhangser'.

Herbs, perennial, erect, 90 cm high. Leaves sessile, linear-lanceolate. Heads yellow slender peduncles. Pappus of disc florets scanty.. Achene brown, sparsely hairy.

Fl. & Fr.: December-February

Medicinal uses :

Leaves and roots together are used on head-ache and stomach complaints.

***Vernonia cinerea* (L.) Less.**

Local Name : 'Sahadevi'.

Herbs, 30-50 cm high, erect. Leaves petaloid, broadly elliptic or lanceolate, pubescent on both surfaces, obtuse or acute at apex. Heads terminal or axillary corymbose cyme pink. Outer pappus small, connate at base inner longer than achenes, plumose. Achenes oblong terete.

Fl. & Fr.: July-February.

Medicinal uses :

Leaf juice is used to treat elephantiasis. Leaf paste is applied to treat ring worm diseased on skin, eczema, herpes and to stop bleeding from cuts. Flowers are used for rheumatism and fever Root is used as anthelmintic and its decoction is used as to treat diarrhoea and stomachic.

***Wedelia chinensis* (Osbeck) Merr.**

Local Name : 'Bhanra.'

Herbs, procumbent. Leaves oblanceolate, shortly appressed hispid on both surfaces, acute at apex. Heads yellow, solitary on terminal peduncles. Achenes rugulose, dark brown, achenes of ray florets triquetrous, disc florets compressed.

Fl. & Fr.: Throughout the year.

Medicinal uses :

Leaf juice to given to treat jaundice, skin diseases, bile and liver problem. Decoction of plant is given to treat menorrhagia and hemorrhage.

Xanthium indicum L

Local Name : 'Shankeshvar'.

Annual, herbs, stem rough, short hairs. Leaves broadly ovate, triangular appressed hairy. Heads green in terminal and axillary spikes. Fruits ellipsoid or oblong, pale yellow or dark brown. Achenes black.

Fl. & Fr.: January-May.

Medicinal uses :

Leaves are used on malaria, herpes, against ring worm. Roots are used for boils, abscesses and ulcers. Roots are bitter tonic and used for cancer and scrofula. Decoction of herbs is used in leucorrhoea, urinary diseases and chronic malaria. Seed oil is used for rheumatism. Seeds are also used for cancer and eye diseases.

RESULTS AND DISCUSSION

Many of the rural and tribal people are using herbal medicine for their primary health cure. The information collected indicates that in all 22 plants are traditionally utilized for treatment of various kinds of diseases such as piles rheumatism dysentery etc. So the tribals can be used the traditional medicine and they are benefited. Therefore there is an urgent need for ethnobotanist to direct their efforts immediately to gather information regarding medicine plants.

REFERENCES

- Almeida, S.M. (1990). The Flora of Savanantwadi, Scientific Publ.Jodhpur.
- Bhattacharjee, S.K. (2008) Handbook of Medicinal Plants(5th Rev .Edn.).Pinter Publisher,Jaipur.
- Ghate, V. S. (1998). Plants in patra-pooja: Notes on their identity and utilization. Ethnobotany 10: 6-15.
- Ghate, Vinaya S. and V.D. Vartak (1996). Socio-economic and domestic utilization of forest tree resources by tribal communities in western Maharashtra. In: Ethnobiology in Human Welfare (Ed.S.K.Jain): 329-330. Deep Publication, New Delhi, India.
- Jain S.K. (1981). Contribution to Ethnobotany of India, Scientific Publication Jodhpur.
- Jain S.K. (1991).Dictionary of Indian Folk Medicine and Ethnobotany, Deep Publication, New Delhi.
- Lakshimnarsimhan P. & Sharma B.D. (1991).The Flora of Nasik District BSI Calcutta.
- Naik, V.N (1999). The Flora of Marathawada, AmurtPrakashan, Station road, Aurangabad.
- Shah, G.L.(1978). Flora of Gujarat. Vols. I-II, S.P.Vallabh Vidyanagar.
- Sharma, B. D.,Karthikeyan S. and Singh N.P. (1996). Flora of Maharashtra State.BSI

Maturity index of of Pimpalner Forest of Dhule District, Maharashtra (India)

¹ Nikita Shivaji Deore, ² J.T. Jadhav
Department of Botany, M.S.G College,
Malegaon Camp, 423203, Nashik (Maharashtra)
Email - drjtjadhav@gmail.com

Abstract: In this present work 3 stands of about 33 quadrates randomly sampled to collect varied species from Shendvad forest. Maturity index provides the information about the maturity of the forest community and species dominant within the community. From the study it can be observed that the degree of maturity is less or high in forest.

Key Words: Maturity Index, Pimpalner forest, Dhule, Maharashtra

1. INTRODUCTION:

Phytosociological studies deal with qualitative study of the structure of the vegetation with an emphasis on quantitative relationship of few species which are to be dominant on the belief that these largely control the community and there by occurrence of a large number of a rare species. As author aware, their detailed account on the phytosociology of Chotadeupur forests, (Shah, Yadav and Parabia, 1979): Pachamahalas (Shah and Bhatt, 1980) Dangs forests (Yadav, 1979): From Maharashtra Talegaon (Jadhav 2016), Sapgaon (Jadhav 2018) Trymbakeshwar (Jadhav, 2018) Saptashringi Forest (Jadhav 2020) similar investigation is carried out in 3 stands of Shendvad forest with view to study the maturity of the forest community, Species dominant within the community and the degree of maturity is less or highest in forest.

2. MATURITY INDEX: As suggested by Pichi-Sermoli (1948), an index for the establishment of the maturity in plant communities based on the frequency percent of all species in the stands of a community. The principle is the long-accepted notion that higher the frequency percent of each species and smaller the number of sporadic species, the more mature is the community. The index of maturity of each stand is compared with each other stands to establish the general maturity of the community.

3. AREA OF STUDY: Pimpalner is a Village in Sakri Taluka in Dhule District of Maharashtra State, India. It belongs to Khandesh and Northern Maharashtra region. It belongs to Nashik Division. It is located 80 KM towards west from District headquarters Dhule. 13 KM from Sakri. Pimpalner Latitude is 20.92928 and Longitude is 73.99107. The vegetation is dry deciduous or mixed type, sometime scrub forest is also observed. The vegetation is rich in the localities like Saltek, Kalgaon , Sayane, Pimpalner, Kondaibari etc.

4. METHODOLOGY: Three stands' area located randomly throughout the study area in the Shendvad forest. Quadrates of 10 x 10 m were laid down in different directions in forest. So that quadrates represented almost all species in the area. All together 33 plots (3300 Sq m.) are laid down. Frequency (%) was calculated by the formula given by Raunkiaer (1934). Maturity index is based on the frequency percentage of all species in the stands of community. it is obtained by number of species in the stand (Pichi- Sermoli, 1948).

5. OBSERVATION: Maturity index provides information about the maturity of the forest community. It also impresses up on the dominance of specie within the community. From Table I, it can be seen that the stand No-3 showing maximum maturity index where as other stands are within much less maturity index. This can be attributed due to the factors operating upon the vegetation on some patches and stands which are showing highest maturity index are under the control of forest department.

From fig. 1: showing the histogram of Maturity Index. It can be seen that highly matured vegetation is in the stands of 2 and 3. The average Maturity Index (57.37) is higher.

6. DISCUSSION AND CONCLUSION: The Maturity Index value at Shendvad forests shows that as a whole these are of two types.

1. Still under the process of succession: At stand No.3 maturity values are 51.11 respectively.
2. Moderately mature: Stand No 3 shows the maturity index values is 60.5

Table 1. Showing the three (3) stands and Their Maturity Index with Average maturity Index of a whole forest.

Localities	Sr. No	Maturity Index (M.I.)
Stand 1	1	51.11
Stand 2	2	56
Stand 3	3	60.5
Total		172.11
Average M. I		57.37

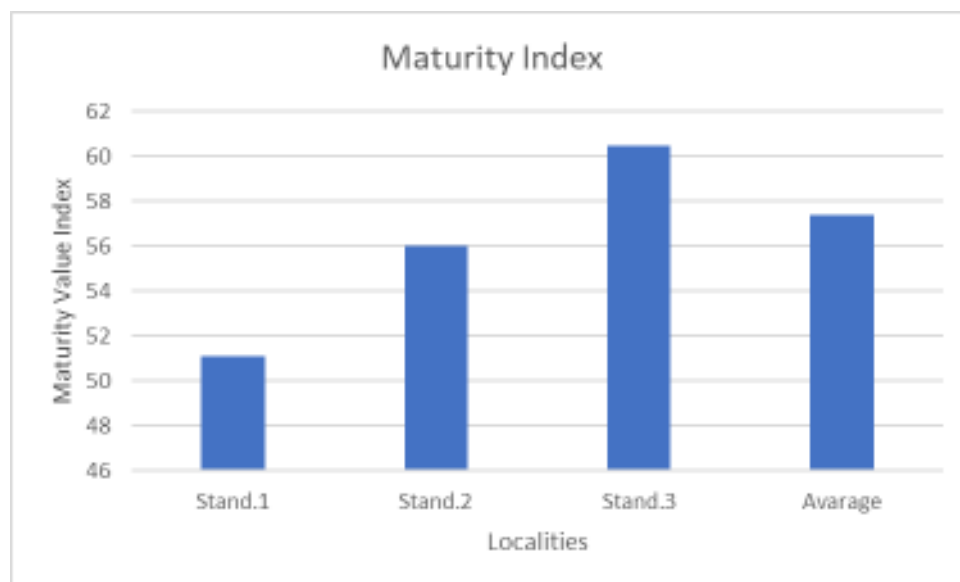


Figure 1.

REFERENCES:

1. Jadhav, J.T. (2004): Phytosociological studies on the vegetation of Triambakeshwar, Vani and Saptashringi forest of Nashik District, Maharashtra, Maturity Index. Col. Env. & Cons. Enviromedia. Vol.10 (1): 87-90.
2. Pichi-Sermolli (1948): An index for establishing the degree of maturity in plant communities. J.Ecol.36: 85-90.
3. Raunchier, C. (1934): The life forms of plants and Statistical plant Geography. The Clarendon press Oxford: 632.
4. Shah, G.L.and R.G. Bhatt 1980, Phytosociological studies of the forests of Panchmahals district in Eastern Gujrat, Indian j. For 3(I):47-53.
5. 5. Shah, G.L. Yadav, S.S. and Parabia, M.H. (1979): Phytosociological studies on the vegetation of Chotaudepur forest division, Eastern Gujarat. J. Indian Forestry. 1: 312 – 318
6. Yadav, S.S. 1979. A contribution to the floristic and Phytosociology of some parts of South Gujarat. Ph.D. Thesis. Part-II. Sardar Patel University, Vallabh Vidyanagar.

Maturity index of of Pimpalner Forest of Dhule District, Maharashtra (India)

¹ Nikita Shivaji Deore, ² J.T. Jadhav
Department of Botany, M.S.G College,
Malegaon Camp, 423203, Nashik (Maharashtra)
Email - drjtjadhav@gmail.com

Abstract: In this present work 3 stands of about 33 quadrates randomly sampled to collect varied species from Shendvad forest. Maturity index provides the information about the maturity of the forest community and species dominant within the community. From the study it can be observed that the degree of maturity is less or high in forest.

Key Words: Maturity Index, Pimpalner forest, Dhule, Maharashtra

1. INTRODUCTION:

Phytosociological studies deal with qualitative study of the structure of the vegetation with an emphasis on quantitative relationship of few species which are to be dominant on the belief that these largely control the community and there by occurrence of a large number of a rare species. As author aware, their detailed account on the phytosociology of Chotadeupur forests, (Shah, Yadav and Parabia, 1979): Pachamahalas (Shah and Bhatt, 1980) Dangs forests (Yadav, 1979): From Maharashtra Talegaon (Jadhav 2016), Sapgaon (Jadhav 2018) Trymbakeshwar (Jadhav, 2018) Saptashringi Forest (Jadhav 2020) similar investigation is carried out in 3 stands of Shendvad forest with view to study the maturity of the forest community, Species dominant within the community and the degree of maturity is less or highest in forest.

2. MATURITY INDEX: As suggested by Pichi-Sermoli (1948), an index for the establishment of the maturity in plant communities based on the frequency percent of all species in the stands of a community. The principle is the long-accepted notion that higher the frequency percent of each species and smaller the number of sporadic species, the more mature is the community. The index of maturity of each stand is compared with each other stands to establish the general maturity of the community.

3. AREA OF STUDY: Pimpalner is a Village in Sakri Taluka in Dhule District of Maharashtra State, India. It belongs to Khandesh and Northern Maharashtra region. It belongs to Nashik Division. It is located 80 KM towards west from District headquarters Dhule. 13 KM from Sakri. Pimpalner Latitude is 20.92928 and Longitude is 73.99107. The vegetation is dry deciduous or mixed type, sometime scrub forest is also observed. The vegetation is rich in the localities like Saltek, Kalgaon , Sayane, Pimpalner, Kondaibari etc.

4. METHODOLOGY: Three stands' area located randomly throughout the study area in the Shendvad forest. Quadrates of 10 x 10 m were laid down in different directions in forest. So that quadrates represented almost all species in the area. All together 33 plots (3300 Sq m.) are laid down. Frequency (%) was calculated by the formula given by Raunkiaer (1934). Maturity index is based on the frequency percentage of all species in the stands of community. it is obtained by number of species in the stand (Pichi- Sermoli, 1948).

5. OBSERVATION: Maturity index provides information about the maturity of the forest community. It also impresses up on the dominance of specie within the community. From Table I, it can be seen that the stand No-3 showing maximum maturity index where as other stands are within much less maturity index. This can be attributed due to the factors operating upon the vegetation on some patches and stands which are showing highest maturity index are under the control of forest department.

From fig. 1: showing the histogram of Maturity Index. It can be seen that highly matured vegetation is in the stands of 2 and 3. The average Maturity Index (57.37) is higher.

6. DISCUSSION AND CONCLUSION: The Maturity Index value at Shendvad forests shows that as a whole these are of two types.

1. Still under the process of succession: At stand No.3 maturity values are 51.11 respectively.
2. Moderately mature: Stand No 3 shows the maturity index values is 60.5

Table 1. Showing the three (3) stands and Their Maturity Index with Average maturity Index of a whole forest.

Localities	Sr. No	Maturity Index (M.I.)
Stand 1	1	51.11
Stand 2	2	56
Stand 3	3	60.5
Total		172.11
Average M. I		57.37

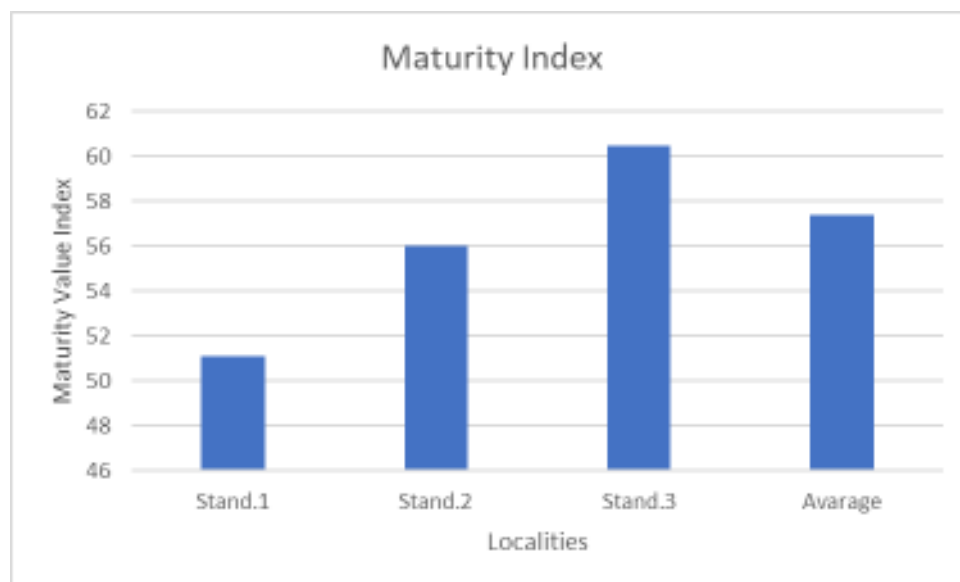


Figure 1.

REFERENCES:

1. Jadhav, J.T. (2004): Phytosociological studies on the vegetation of Triambakeshwar, Vani and Saptashringi forest of Nashik District, Maharashtra, Maturity Index. Col. Env. & Cons. Enviromedia. Vol.10 (1): 87-90.
2. Pichi-Sermolli (1948): An index for establishing the degree of maturity in plant communities. J.Ecol.36: 85-90.
3. Raunchier, C. (1934): The life forms of plants and Statistical plant Geography. The Clarendon press Oxford: 632.
4. Shah, G.L.and R.G. Bhatt 1980, Phytosociological studies of the forests of Panchmahals district in Eastern Gujrat, Indian j. For 3(I):47-53.
5. 5. Shah, G.L. Yadav, S.S. and Parabia, M.H. (1979): Phytosociological studies on the vegetation of Chotaudepur forest division, Eastern Gujarat. J. Indian Forestry. 1: 312 – 318
6. Yadav, S.S. 1979. A contribution to the floristic and Phytosociology of some parts of South Gujarat. Ph.D. Thesis. Part-II. Sardar Patel University, Vallabh Vidyanagar.

Occurrence and Conservation Status of *Ceropegia anjanerica* Malpure *et al.*, in Nasik District

Nikam P. Dinkar¹, Shinde H. Prabhakar^{2*}, Pawar R. Prabhakar³ and Waghmode A. Vitthal⁴

DOI: 10.18811/ijpen.v9i01.13

ABSTRACT

The present review article deals with the distribution, morphology, habitat, ecology, threat, and conservation status of *Ceropegia anjanerica* Malpure *et al.*, in and around Nasik district. The genus *Ceropegia* L. belongs to the subfamily Asclepiadoideae (milk weeds) within the family Apocynaceae. A total of 6 species and 2 varieties of this genus have been recorded in Nasik district viz., *C. anjanerica* Malpure; Kamble and Yadav, *C. bulbosa* Roxb. var. *bulbosa*, *C. bulbosa* Roxb. var. *lushii* (Graham) Hook.f., *C. hirsuta* Wight and Arn., *C. lawii* Hook.f., *C. mahabalei* Hemadri and Ansari, *C. media* (H. Huber) Ansari and *C. vincifolia* Hook. Of these species, *C. anjanerica* is the 'endangered' plant species endemic to Anjaneri hills of Nasik district part of the northern western Ghats. The plant body is erect herbaceous with tuberous rootstock, tubers are generally 2-5 cm in diameter, globose or discoid with fibrous roots. Recent investigations show that this species has been recorded from hill tops, plateaus, and adjacent village areas.

Keywords: *Ceropegia anjanerica*, occurrence, conservation, Anjaneri Plateau, Nasik.

International Journal of Plant and Environment (2023);

ISSN: 2454-1117 (Print), 2455-202X (Online)

INTRODUCTION

Ceropegia L. is the genus consists of 244 species that have been distributed in Africa and Madagascar which extends from the east to Arabia, India and China, northern part of Australia up to Canary Islands (Mabberley, 1997; Bruyns, 2014). Studies revealed three genera viz. *Ceropegia*, *Brachystelma* and *Riocreuxia* has a generic complex that leads to many interesting taxonomic problems at the generic and specific levels. (*Botanical Survey of India*; 2002).

Ceropegia is one of the genera belonging from subfamily Asclepiadoideae (milkweeds) within family Apocynaceae. This genus represents about 260 taxa worldwide (*The plant list*, 2013) distributed around the Canary Islands, India, Madagascar, New Guinea, northern Australia, South East Asia, tropical Arabica, and Africa (Meve, 2002; 2017). In India, this genus represents 62 species of which 26 are found in Maharashtra (Karthikeyan *et al.*, 2009; Kambale and Yadav, 2019; Murugesan *et al.*, 2019).

In IUCN red data book this species has been assigned in the endangered category under the criteria B1ab(iii)+2ab(iii) ver. 3.1. (Pethe and Watve, 2021). There are 6 species with 2 varieties of *Ceropegia* recorded in Nashik district viz., *Ceropegia bulbosa* Roxb. var. *bulbosa*, *C. hirsuta* Wight and Arn., *C. lawii* Hook.f., *C. bulbosa* Roxb. var. *lushii* (Graham) Hook.f., *C. mahabalei* Hemadri and Ansari, *C. media* (H. Huber) Ansari, *C. anjanerica* Malpure *et al.*, and *C. vincifolia* Hook (Lakshminarasimhan and Sharma, 1991). Out of which *C. anjanerica* is the species that is endemic to Northern-Western Ghat. Records on adjacent villages and hill tops of Anjaneri plateau revealed the occurrence of this species in 'Navardevi', 'Kushegaon' and Igatpuri tehsil of Nashik district (Auti *et al.*, 2019).

With the geographical location (19°55'11.14" N and 73°34'18.0"E), Anjaneri plateau is the basalt rocky, flat-topped hill with the steep and cliff edges which is actually the group of 5 hills collectively known as "Tryambak range" from the Northern-Western Ghats. *C. anjanerica* generally grows rocky areas at an altitude of 700-1,100 meters (IUCN Assessment 2021, Pethe and Watve, 2015). It has been reported little above the middle

^{1,3}Research Center in Botany, L.V.H. Arts, Science and Commerce College, Panchavati, Nasik, Maharashtra, India

²Department of Botany, K.V.N. Naik, College, Nasik, Maharashtra, India

⁴Department of Botany, Sadguru Gadge Maharaj College, Karad, Satara, Maharashtra, India

*Corresponding author: Shinde H. Prabhakar, Department of Botany, K.V.N. Naik, College, Nasik, Maharashtra, India, Email: shindehemant79@gmail.com

How to cite this article: Dinkar, N.P., Prabhakar, S.H., Prabhakar, P.R. and Vitthal, W.A. (2023). Occurrence and Conservation Status of *Ceropegia anjanerica* Malpure *et al.*, in Nasik District. *International Journal of Plant and Environment*. 9(1), 81-84.

Conflict of interest: None

Submitted: 16/01/2023 **Accepted:** 20/02/2023 **Published:** 30/03/2023

portion of Anjaneri plateau. (Auti *et al.*, 2020). All species from the series *Attenuatae* have a restricted distribution in Konkan ranges, while *C. anjanerica* is the only species that grows at a high altitude. Major threats to the species include degradation of habitat, over-exploitation of tubers and various human interferences. Apart from the unavailability of pollinators, less seed formation and associated reproductive biological barriers lead to the continuous decrease in the species' natural population. (Chavan *et al.*, 2018).

Systematic enumeration

Kingdom: Plantae
Phylum: Tracheophyta
Class: Magnoliopsida
Order: Gentianales
Family: Apocynaceae

Scientific Name: *Ceropegia anjanerica* Malpure, Kamble and Yadav, 2006.

Common name: Anjaneri wax fountain (English); Lahani Kharpudi (Marathi).

Utility Of The Species

The species' Tubers have traditionally eaten by tribals (IUCN Assessment 2021, Pethe and Watve;2015). Many *Ceropegia* species contain starch, sugars, gum, albuminoids, fats, crude fibres. Species like *C. bulbosa*, *C. hirsuta* have been recognized as edible tuberous plants. (Deshmukh and Rathod, 2013). Few species have been described for their utility as food plant for insects like butterflies. (Almeida; 1996). These valuable constituents are important in many Ayurvedic formulations that are effective against the diseases like diarrhea and dysentery. The major pharmacological importance of *Ceropegia* is due to the presence of "Ceropegine" which is pyridine alkaloid (Sukumar *et al.*, 1995), that is an analgesic drug can be used against ulcers and inflammations (Adibatti *et al.*, 1991; Khare, 2007).

Morphology And Phenology

Ceropegia anjanerica also called as flytrap flower (Auti *et al.*, 2019) is a perennial erect herbaceous plant species and has a few floral morphological similarities with *attenuate*; however, it's distinguishing features includes it's shorter, obovate, flat corolla lobes that make obovate head (IUCN Assessment 2021, Pethe, and Watve;2015).

The plant attains vegetative growth in monsoon season (July to August) before flowering in August and continues until October. September to October is the peak flowering period with moist, misty and sunny climates. Fruits mature in October-November and then seed dispersal which occurs in the month of November. In December month, the plant withers and all mature tubers become dormant and undergo perennation. The rootstock is tuberous and the size of the tubers varies from 2–5 cm which are discoidal or globose in shape with fibrous roots. (IUCN Assessment 2015, Pethe and Watve;2015). Flowering and fruiting season have been recorded from September to October and the chromosome number of the species is 22 (2n) (Gosavi *et al.*, 2012).

Habitat And Ecology

C. anjanerica is an erect tuberous herbaceous with about 20 cm in height. The species generally grows in well-aerated, shallow and gravel soil. Sometimes found along with grasses and other small herbaceous plant species. *C. anjanerica* is generally found growing well in lateritic soils with high elevated mountains as compare to its other counterparts (Kambale and Yadav; 2019).

According to some reports this species is found growing in soils with 2-12 cm depth along with some medicinal herbs like *Celosia argentea*, *Justicia betonica*, *Lepidagathis sp.* and *Senecio dalzellii* (IUCN Assessment 2021, Pethe and Watve,2015). Also, the species have been found growing at an altitude of 1300 meters in well-drained soils with plant species viz. *Cyanotis fasciculata* (B. Heyne ex Roth) Schult. f., *Justicia procumbens* L., *Senecio bombayensis* Balakr. and *Swertia minor* (Maity *et al.*, 2021). Some recent reports and field explorations revealed the appearance of *C. anjanerica* in localities viz. Bramhagiri and Bramha hills, Vatwad hills, Harihar fort, etc. (Fig. 1). (Maity *et al.*, 2021).

Threat And Conservation Status

IUCN assigned *C. anjanerica* in Red data book as Critically Endangered (CR B1ab (iii,v)+B2ab(iii)) (Pethe *et al.*, 2015). The species was reported from the Anjaneri hills of Nasik district and



Fig. 1: Distribution of *C. anjanerica* Malpure *et al.*: 1-Vatwad Hill | 2-Bhaskargad | 3-Harihar fort | 4-Bramha Hill | 5-Bramhagiri Hill | 6-Anjaneri Hill (Type locality) | 7-Kushegaon. (Maity *et al.* 2021).

about 100 individuals of species were reported in September 2005. Initially, this species was assigned threatened in Red data book with threat status as "Critically endangered" and endemic to Maharashtra (Mishra and Singh, 2001; Yadav *et al.*, 2006; Yadav and Kamble, 2008). The species has not been reported elsewhere in Western Ghats since. The species was newly described that's why there were very less or no reports have been found on its occurrence after an extensive field exploration. The area of occupancy was found to be below 10 sq. km. and hence the species has been assigned Critically endangered [CR: B2 a, b (i, ii, iii)] (Kambale and Yadav; 2019).

However; very less or no supporting data like Population trends, Extent of Occurrence (EOO) or Area of Occupancy (AOO) is available and this fact depicts the need of review and reassessment of the current status of this species according to IUCN guidelines. According to some earlier studies by some workers, anthropogenic operations like over-exploitation of tubers, tourism, habitat degradation, etc., are the major threats to this species. Along with this poor pollination, less seed formation are some other important factors responsible for the reduction in the population of species. (Chavan *et al.*, 2018).

Earlier assessment of *anjanerica* Malpure *et al.*, by IUCN placed it under the assessment category Endangered B1ab (iii)+2ab(iii) ver 3.1. The current population trend was found to be decreasing. It was in the critically endangered category (IUCN; 2013) and was therefore facing an increased risk of extinction. Many of anthropogenic activities are operative in this area leading to the continued depletion of this species (Pethe and Watve, 2021).

Anjaneri hill area is visited by many pilgrims, amateur tourists, trekkers, mountaineering groups and nature photographers. The habitat is subjected to degradation caused by anthropogenic pressures such as free grazing of cattle and fires. As a part of



Fig. 2: Red List Assessment category *C. anjanerica* Malpure *et al.*

developmental initiatives taken up by local government and forest department, a permanent road has been proposed to the plateau top for developing tourism that imposes a threatening pressure on population of *C. anjanerica* on the top of plateau. Apart from Anjaneri hill; the other three locations are under threat due to the enhanced tourism and its impacts in terms of trampling and infrastructure development. (IUCN Assessment; Pethe and Watve; 2021).

C. anjanerica has been assessed as “critically endangered” under the criteria “CR B1ab (iii,v) + B2 ab (iii)” by Pethe *et al.*, (2015) and subsequently as “Endangered” under the criteria “B1ab(iii)+2ab(iii)” by Pethe and Watve (2021) of the IUCN Red List. (Fig. 2). Though the type locality, i.e., Anjaneri hills, Nasik, is declared as an ‘Anjaneri Conservation Reserve’ and due care has been taken by Maharashtra state forest department for its conservation. Other than Anjaneri Conservation Reserve, all the localities are tourist places; therefore, frequent tourist visits generally destroy the habitats. (Table 1). Controlled tourism and awareness among tourists will help in reducing the threat to some extent. Unnecessary uprooting of the tuber just for growing this endemic species in captivity should be avoided as it will not survive outside its habitat for more than a year or so, if appropriate care is not taken. Surveys undertaken to Bhaskargad, Harihar fort, Bramha Hill and Bramhagiri Hill resulted in the collection of *C. anjanerica*. This study highlights the need for designated surveys to locate such endemic species reported from their type localities only. Moreover, earlier workers emphasize the need for research to monitor life history and distribution trends, ecological threats, and conservation planning. (Table 2). This will help in prioritizing the conservation of threatened species (Fig. 2). (Maity *et al.*, 2021).

With potential pharmacological, ornamental and medicinal use this species has least reproductive success, so attempts for *in-vitro* propagation of *C. anjanerica* have been done by many workers. Well-grown plantlets hardened, acclimatized and

established in the greenhouse which exhibited 78% survival. (Nalawade *et al.*, 2014). Likewise, *in-vitro* propagation attempts have been done for many *Ceropegia* species such as *C. bulbosa* (Shete; 2014), *C. woodii* (Barakat; 2021). Molecular phylogenetic analysis of 81 *Ceropegias* aligned them in many clades (Surveswaran *et al.*, 2009). The methanol extract of *C. juncea* are medicinally valuable and possess various pharmaceutical applications (Visveshwari *et al.*, 2017).

CONCLUSION

C. anjanerica Malpure *et al.*, has been reported to have the least reproductive success and it has potential in the medicinal field. It can be concluded that insufficient study has been done so far on *C. anjanerica*, As the species has ornamental and medicinal potential, conservational actions should be undertaken. Also, there is a need to undertake reproductive biological studies along with phytochemical and pharmacological examinations so as to asses and evaluate the reproductive barriers.

ACKNOWLEDGEMENT

Authors acknowledge the support provided by Research Center in Botany, L.V.H. College, Panchavati, Nasik for providing all research requirements. Department of Botany, K.V.N. Naik College, Nasik for support and guidance. Also, the authors acknowledge and appreciate the great work on this plant species by Jui Pethe and Aparna Watve and all other research workers for their valuable suggestions, which have improved the quality of this overall work to a better level.

AUTHOR CONTRIBUTIONS

Shinde H.P has conceptualized the review article; Nikam P.D did the methodology and draft preparation. The formal analysis was conducted by Pawar, R.P. and Software technical assistance was contributed by Waghmode A.V.

Table 1: Threats to the Species (IUCN Red List Assessment 2021, Pethe and Watve, 2021).

Threat	Timing	Scope	Severity	Impact Score
2. Agriculture & aquaculture -> 2.3. Livestock farming & ranching -> 2.3.2. Small-holder grazing, ranching or farming	Ongoing	Whole (>90%)	Unknown	Unknown
Stresses: 1. Ecosystem stresses -> 1.2. Ecosystem degradation				
4. Transportation & service corridors -> 4.1. Roads & railroads	Future	Whole (>90%)	Very rapid (medium)	Medium Impact: 7
Stresses: 1. Ecosystem stresses -> 1.2. Ecosystem degradation				
6. Human intrusions & disturbance -> 6.1. Recreational activities	Ongoing	Majority (50-90%)	Slow, significant (medium)	Medium Impact: 8
Stresses: 1. Ecosystem stresses -> 1.2. Ecosystem degradation 2. Species Stress -> 2.2. Species disturbance				

Table 2: Research Needed (IUCN Red List Assessment 2021, Pethe and Watve, 2021).

1. Research -> 1.2. Population size, distribution & trends
1. Research -> 1.3. Life history & ecology
1. Research -> 1.5. Threats
2. Conservation Planning -> 2.1. Species Action/Recovery Plan
2. Conservation Planning -> 2.2. Area-based Management Plan
3. Monitoring -> 3.1. Population trends
3. Monitoring -> 3.4. Habitat trends

REFERENCES

Adebatti, N. A., Tirugnanasambantham P., Kulothugan C., Viswanathan S., Kameswaran L., Balkrishna K., Sukumar E. (1991). A pyridine alkaloid from *Ceropegia juncea*. *Phytochemistry* 30(7):2449–2450. ISSN 0031-9422, [https://doi.org/10.1016/0031-9422\(91\)83683-C](https://doi.org/10.1016/0031-9422(91)83683-C).

Almeida, M.R. (1996). *Flora of Maharashtra—Vol. 2*. St. Xeviers College, Mumbai, 194pp.

Auti, S. G., Gosavi, K. V. C., Golait, S., & Kambale, S. S. (2019). Notes on *Ceropegia anjanerica* (Family: Apocynaceae): A Critically Endangered and Endemic Fly Trap Flower of Northern Western Ghats. *Journal of the Bombay Natural History Society (JBNHS)* 116: 181-182.

Auti, S. G., Kambale, S. S., Gosavi, K. V. C., and Chandore, A. N. (2020). Floristic diversity of Anjaneri Hills, Maharashtra, India. *Journal of Threatened Taxa* 12(10): 16295-16313. DOI: 10.11609/jott.3959.12.10.16295-16313.

Botanical Survey of India (2002). *Studies on rare and endangered species*. <http://www.envfor.nic.in/bsi/research.html>.

Bruyns, P.V. (2014). The Apocynaceae of Namibia. *Strelitzia* 34. *South African National Biodiversity Institute*, Pretoria. <http://pza.sanbi.org/references/bruyns-pv-2014-apocynaceae-namibia-strelitzia-34-south-african-national-biodiversity>.

Chavan J. J., Gaikwad N. B., Dixit G. B., Yadav S. R., Bapat V. A. (2018). Biotechnological interventions for propagation, conservation and improvement of ‘Lantern Flowers’ (*Ceropegia* spp.). *S. Afr. J. Bot.* 114, 192–216. <https://doi.org/10.1016/j.sajb.2017.10.021>.

- Deshmukh S. and Rathod, V. (2013). Nutritional evaluation of some wild edible tuberous plants. *Asian J. Pharm. Clin. Res.* 6, 58–60.
- IUCN (2013). The IUCN Red List of Threatened Species. Version 2013.1. <www.iucnredlist.org>.
- IUCN. (2021). The IUCN Red List of Threatened Species. Version 2021-2. Available at: <www.iucnredlist.org>.
- Kambale, S. S., and Yadav, S. R. (2019). Taxonomic revision of *Ceropegia* (Apocynaceae: Ceropegieae) in India. *Rheeda* 29(1),11-15. <http://dx.doi.org/10.22244/rheede.2019.29.1.01>.
- Karthikeyan S, Sanjappa M, Moorthy S. (2009). Flowering plants of India, Dicotyledons (Acanthaceae-Avicenniaceae). (*Botanical Survey of India, Calcutta*). 1:160-164.
- Khare C. P. (2007). Indian Medicinal Plants Library of Congress Control Number: 2007922446 ISBN: 978-0-387-70367-5. DOI:10.1007/978-0-387-70638-2.
- Lakshminarasimhan, P. and Sharma B. D. (1991). Flora of Nashik District. Botanical Survey of India, Calcutta, 644pp.
- Mabberley, D. J. (1997) The Plant Book. Cambridge University Press, Cambridge, ISBN 9780521820714, pp 114–115.
- Maity, S.S., A.N. Gangurde, S.S. Kambale, A.R. Gholave, A.A. Adsul, G.B. Pawar & K.V.C. Gosavl (2021). Additional distribution records of *Ceropegia anjanerica*, an endemic and 'endangered' lantern flower of the northern Western Ghats, India. *Journal of Threatened Taxa* 13(12): 19874–19877. <https://doi.org/10.11609/jott.6879.13.12.19874-19877>.
- Malpure, N., M. Kamble and S.R. Yadav (2006). A new species of *Ceropegia* L. (Asclepiadaceae) from the Western Ghats of India with a note on series *Attenuatae* Huber. *Current Science* 91(9): 1140–1142.
- Meve, U. (2002). *Ceropegia*, pp. 63–106. In: Albers, F. & U. Meve (eds). *Illustrated Handbook of Succulent Plants: Asclepiadaceae*. Springer, Berlin.
- Meve U., Heiduk A., Liede-schumann, S. (2017). Origin and early evolution of *Ceropegieae* (Apocynaceae-Asclepiadoideae). *Syst. Biodivers.* 15, 143–155.
- Mishra, D.K. and Singh, N.P. (2001). Endemic and Threatened Flowering Plants of Maharashtra. Botanical Survey of India, Calcutta, 196–197.
- Murugesan, M., A.A. Mao, L.R. Meitei and S.S. Kambale (2019). *Ceropegia khasiana* (Apocynaceae: Ceropegieae), a new species from Meghalaya, Northeast India. *Gardens' Bulletin Singapore* 71(2): 519–525. doi: 10.26492/gbs71(2).2019-17.
- Nalawade, A. S., Desai M. T., Gaikwad N. B., Gurav R. V., Dixit G. B., Yadav S. R. (2014). In Vitro Propagation of *Ceropegia anjanerica* Malpure et al.: A rare endemic plant from Maharashtra. *Springer*, <http://dx.doi.org/10.1007/s40011-014-0420-x>.
- Pethe J., Tillu A. and A.Watve. (2015). Threat status assessment of *Ceropegia anjanerica* Malpure et al. (Magnoliopsida: Gentianales: Apocynaceae) from Anjaneri Hills, Nashik district, Maharashtra, India. *Journal of Threatened Taxa* 7(3): 6965–6971. <https://doi.org/10.11609/JoTT.03772.6965-71>.
- Pethe, J. & Watve, A. (2021). *Ceropegia anjanerica* Malpure, M.Y.Kamble & S.R.Yadav. The IUCN Red List of Threatened Species 2021: <https://doi.org/10.2305/IUCN.UK.2021-2.RLTS.T177964188A177969117.en>.
- Shete, R. U. (2014). In-vitro multiplication of *Ceropegia bulbosa* Var *bulbosa* Roxb. *International Journal of Science and Technology* 11(3):383-385 ISSN: 2277- 2812.
- Sukumar, E., Gopal, R.H., Rao, R.B., Viswanathan, S., Thirugnanasambantham P. and Vijayasekaran, V. (1995). Pharmacological actions of ceropegin, a novel pyridine alkaloid from *Ceropegia juncea*. *Fitoterapia* 66(5):403–406
- Surveswaran, S., Kamble, M.Y., Yadav, S.R. and Sun, M. (2009). Molecular phylogeny of *Ceropegia* (Asclepiadaceae, Apocyanaceae) from Indian Western Ghats. *Plant Syst. Evol.* 281:51-63. <http://dx.doi.org/10.1007/s00606-009-0182-8>.
- The Plant List (2013). Version 1.1. Published on the Internet; <http://www.theplantlist.org/tpl/record/kew-2603917> (accessed 20 March 2015).
- Visveshwari M., Subbaiyan B., Thangapandian V. (2017). Phytochemical analysis antibacterial activity FTIR and GCMS analysis of *Ceropegia juncea* Roxb. *International Journal of Pharmacognosy and Phytochemical Research* 9(7): 914-920. <https://doi.org/10.25258/phyto.v9i07.11155>.
- Yadav, S. R., Kamble M. R., Malpure, N. V. (2006). A new species of *Ceropegia* L. (Asclepiadaceae) from the Western Ghats of India with a note on series *Attenuatae* Huber. *Current Science*. 91(9):1140-1142
- Yadav, S.R. and M.Y. Kamble (2008). Threatened *Ceropegias* of the Western Ghats and Strategies for Their Conservation, pp 123–134. In: Rawat, G.S. (ed.). *Special Habitats and Threatened Plants of India*. ENVIS Bulletin: Wildlife and Protected Areas, Vol. 11(1). Wildlife Institute of India, Dehradun, India.

Pharmacological and ecological aspects of *Chlorophytum borivilianum* Sant. and Fern.: a review.

Aspectos farmacológicos y ecológicos de *Chlorophytum borivilianum* Sant. y Fern.: una revisión.

Pawar, Rahul P.¹, Nikam, Pravin D.² Waghmode, A.V.³ and Shinde, Hemendra P.^{4*}

^{1,2}Research Center in Botany, L.V.H. Arts, Science & Commerce College, Panchavati, Nasik.

³Sadguru Gadage Maharaj College, Karad, Maharashtra, India.

⁴Department of Botany, K.V.N. Naik, College, Nasik, Maharashtra, India.

^{4*}Corresponding Author: shindehemant79@gmail.com

ABSTRACT

Chlorophytum borivilianum; Sant. and Fern. is one of the important medicinal herb belonging to family Liliaceae. Traditionally known as 'Safed Musali' in the Indian drug market. An efficacy of its tuberous roots has been assessed for the treatment of few sexual disorders in males. Also, phytochemical evaluation revealed the richness of alkaloids, saponins, carbohydrates, steroids, vitamins, proteins etc. Apart from the aphrodisiac properties mostly confined to the roots; the efficacy of this important medicinal herb needs to be investigated for other attributes especially on human model. In India as well as across the world; from the pharmacological point of view; this plant serves as valuable medicinal herb with a great potential to cure many diseases. However; this plant has been categorized as critically endangered plant according to IUCN red data list. Due to overexploitation, authentic identification and standardization as well as lack of ecological and conservation perspective; the species number of genus *Chlorophytum* is found to be decreasing consistently. Also, documentation of such ethnobotanicals and knowledge of traditional medicines can be significant contribution towards sustainable utilization of indigenous therapeutic plants.

Keywords: *Chlorophytum borivilianum*, ecological, pharmacological.

RESUMEN

Chlorophytum borivilianum; Sant. y helecho. Es una de las hierbas medicinales importantes que pertenece a la familia Liliaceae. Conocido tradicionalmente como "Safed Musali" en el mercado de drogas de la India. Se ha evaluado la eficacia de sus raíces tuberosas para el tratamiento de algunos trastornos sexuales en los machos. Además, la evaluación fitoquímica reveló la riqueza de alcaloides, saponinas, carbohidratos, esteroides, vitaminas, proteínas, etc. Además de las propiedades afrodisíacas que se limitan principalmente a las raíces; Es necesario investigar la eficacia de esta importante hierba medicinal para determinar otros atributos, especialmente en el modelo humano. Tanto en la India como en todo el mundo; desde el punto de vista farmacológico; esta planta sirve como una valiosa hierba medicinal con un gran potencial para curar muchas enfermedades. Sin embargo; esta planta

ha sido clasificada como planta en peligro crítico según la lista roja de datos de la UICN. Debido a la sobreexplotación, la identificación y estandarización auténticas, así como la falta de una perspectiva ecológica y de conservación; Se ha descubierto que el número de especies del género *Chlorophytum* disminuye constantemente. Además, la documentación de dichos elementos etnobotánicos y el conocimiento de las medicinas tradicionales pueden ser una contribución significativa hacia la utilización sostenible de plantas terapéuticas autóctonas.

Palabras clave: *Chlorophytum borivillianum*, ecológico, farmacológico.

INTRODUCTION

Traditional and herbal medicines have been utilized since ancient times and accounts for about 70-80% of population on a global basis. According to the World Health Organization; about 80-95% of population of developing as well as developed countries; uses herbal and traditional medicines or crude plant extracts; as a home remedies for their routine ailments. (Khan and Ahmad, 2019; Siddaramu *et al.*, 2022). India shows diverse topographic and climatic conditions that supports unique habitat for variety of medicinally important plant species. (Naveen *et al.*, 2022). Today; the demand for many natural crude therapeutic drugs are increasing all over the world. Recently; ethno-ecological survey of medicinal herbs is being carried out by different states. (Tandon and Shukla, 1995). The center of origin of *C. borivillianum* is tropical and subtropical Asia. (Chakraborty and Aeri, 2009). Earlier, it has been reported that, about 300 species of *Chlorophytum* are distributed across the world; especially tropical and subtropical regions of Africa which are most probably; the centers of origin of genus *Chlorophytum*. (Geetha and Maiti, 2002; Bansal, 2018). Currently; 23 species of genus *Chlorophytum* reported across the different regions of India. (Chandore and Yadav, 2019). Also, *C. borivillianum* is categorized as critically endangered status according to IUCN Red data list. (Bhat *et al.*, 2018; Gowthami *et al.*, 2021).

C. borivillianum is herbaceous plant belonging to the family Liliaceae, commonly known as 'Safed musali' is highly valuable medicinal plant in India and Indian system of Ayurveda. It is a multipurpose herb useful in maintaining better human health and gynecological disorders. (Nalawade *et al.*, 2022). Also, its commercial utilization is found to be rapidly expanding due to the presence of high medicinal properties in its different parts especially tuberous roots. During the last couple of decades; many endangered medicinal plant species; due to the lack of authentic identification and standardization; are being used as alternative resource which creates scarcity and eventually leads in adulteration. In this context; comparative morpho-anatomical and phytochemical evaluation of *Chlorophytum* species is essential. (Parveen and Singh, 2018).

Pharmacological Perspective:

Traditionally; tubers are also being used in the treatment of few other ailments like rheumatism. Also, leaves can be used in various culinary preparations. However; tubers have been most commonly used for its aphrodisiac properties lack of libido, male impotency, oligospermia. (Meena and Rao, 2005). The major biochemical constituent of *Chlorophytum borivillianum* are carbohydrate (42%), Protein (10%), fibers (20% to 30%) Saponins (2% to 17%) and alkaloids (15% to 25%). Also, primary saponin and alkaloids have been found to be the rich source of over 25 alkaloids,

vitamins,steroids, potassium, calcium, magnesium, phenol, resin, mucilage and polysaccharides. High quality of simple sugars mainly sucrose, glucose, fructose, xylose, mannose, and galactose and more recently; Stigmasterol, furostanol, chlorophytoside as well as polysaccharide fraction etc. have been be isolated. (Thakur *et al.*,2011; Rungtung *et. al* 2013). Arsenic induced toxicity in *C. borivilianum* and its impact on reproductive system has been studied by Sharma *et al.*, 2012. The presence of various vital bioactive compounds and medicinally important secondary metabolites like alkaloids, glycosides, steroids etc. have been confirmed in many earlier phytochemical studies as well as by chromatographic and spectrophotometric analyses. (Vyas *et al.*, 2020).

C. borivilianum; recognized worldwide as ‘herbal viagra’, and ‘Indian ginseng’ in India; found significant in curing stress induced weakness and other such ailments. (Sharma and Muzumdar; Singh *et. al.*, 2012, Giribhau *et. al.*, 2014; Thakur and Dixit, 2016). Similarly; the root extract of *C. borivilianum* have found to be helpful in prevention of sperm count and impairment in sperm characteristic and morphology. (Kothari; Thakur *et al.*, 2004). Traditionally; it is used as health promoting tonic along with anti-oxidant, anti-pyretic, anti-viral, anti-mutagenic, anti-tumors, antifungal activity. (Bhat *et al.*, 2008, Deore and Khadabaddi, 2007; 2008; 2010; Akki and Patil 2006; Singh *et al.*, 2012). Few researchers have reported that the human disorders such as renal and pulmonary cancer can be better managed by herbal drugs like ‘Safed Musali.’ Singh *et al.*, Saxena *et al.*, 2012).

Pharmacological evaluation has been attempted by many workers which revealed few inherent medicinal properties such as aphrodisiac, immunomodulatory activity and anti-aging properties. (Kothari, 2004; Singh *et al.*, 2008; Chakraborty, 2012). Traditionally; the tuberous rootsof *C. borivilianum* are being used in the manufacturing of crude herbal drugs. It has been shown to work very well in curing impotency. (Sharma and Muzumdar, 2012; Desale, 2013; Giribhau *et al.*, 2014; Bhat *et al.*, 2018). Many ethnic communities across the different states of India like Rajasthan (“Meena”), Mizoram (“Mizo”), Maharashtra (“Thakur”), Madhya Pradesh (“Korku” and “Bharia”) have been found to be enjoying the health, vitality and longevity by using ‘Safed musali’ in their health caresystem. (Patil, 2010; Jagtap *et al.*, 2009; Meena and Rao, 2010; Deshwal and Trivendio, 2011). Indigenous people in the states like Maharashtra have found to be utilizing the root tubers of *C. borivilianum* for the variety of medicinal purposes and have initiated its cultivation; which indicates its socio-economic importance. (Patil, and Patil, 2000; 2001).

In earlier research; it was reported that *C. borivilianum* is medicinally significant especially in rejuvenation. (Miraj *et al.*, 2020, Verma *et al.*, 2020). Also, studies have indicated that the root extraction is better equip testicular cell against the different oxidative stresses. (Vyas *et al.*, 2022). *C. borivilianum* consist of many useful secondary metabolites helping in sexual problems mostly stigmasterol (Pratiwi *et. al.*, 2021), Saponin (Khan *et al.*, 2022). Recent studies have identified nine compounds including 5-methylhex-2-y, pentadecyl ester (23.69).9, 10- anthracenedione (19.02). (Vyas *et al.*, 2020).

Most of the pharmacological investigations and studies conducted previously lack critical assessment and substantial scientific evidences. Also, all the studies merely highlighted the toxicity, quality and the commercial utilization of *Chlorophytum borivilianum*; which is insufficient to gather comprehensive information so as to focus on the existing lacunae and future research. (Khanam *et al.*, Ashraf *et al.*,2013).

Tubers and other body parts like leaf and stem of *C. borivilianum*; are rich in alkaloids, glycosides, tannins, and saponin enriched fraction etc. These have been assessed for nutritional as well as cytotoxic, hemolytic properties. (Somanath,2008; Singh *et al.*, 2022). Few works have focused antidiabetic, anti-oxidant, anti-stress, anti-helminthic and anti-larvicidal property of *C. borivilianum*. (Sharma *et al.*, 2017). Recently; the use of *C. borivilianum* as a dietary supplementation is found effective as heat stress ameliorator in dairy cows. Similarly; in rat model; this vital herb has been shown to possess antimicrobial, antimutagenic, antioxidant, antiulcer, properties. (Devi *et al.*, 2021). Different plant parts of *C. borivilianum* have been used to evaluate the medicinal properties, pharmacological and physiological response in various experiments conducted on animals mostly rats, cows as well as human beings. (Table 1).

Characterization of enzymes responsible for Saponin biosynthesis has been attempted by few researchers (Karla *et al.*, 2013). The seeds of *C. borivilianum* are quite dormant and their viability is low, which necessitates its *in vitro* regeneration and its large scale cultivation for agricultural and commercial purposes. Also, the presence of secondary metabolites irrespective of topographical and climatic conditions; can be enhanced through micropropagation and *in vitro* culture techniques which can be considered as novel approach in bioprospecting of phytopharmaceuticals. (Purohit *et al.*, 1994; Jha and Bansal, 2018; Kaushal *et al.*,2021).

ECOLOGICAL PERSPECTIVE

The genus *Chlorophytum* is originated from the tropical and subtropical Africa and about 300 species are distributed predominantly in tropical and subtropical forests up to 1500 m altitude (Nayar and Sastry, 1988; Oudhia, 2001; Raghavendra *et al.*, 2005).

It is evident that, the plant species in which reproductive parts (fruit, flower, and seed) as well as vegetative parts (leaves, roots, rhizome etc.) are harvested for commercial purposes; are more endangered in comparison; than any other plant species. Commercially; it is one of the important crop with high level of ethno-medicinal properties, low risk, and high returns can be fetched within a short period of one year. (Manjunatha *et al.*, 2008).

The decline in the number of species and extinction of some species of genus *Chlorophytum*, is largely due to the ecological disturbances, cultivation/harvesting practices by unskilled labor leading to poor natural regeneration, over exploitation for commercial purposes etc. (Mishra, 2011). Naturally, seed setting in most of the flowering plant species occurs by adopting variety of pollination mechanisms. Likewise; there are different insect pollinators which play an important role in pollination biology. (Shivanna *et al.*, 2001). The pollinators of *C. borivilianum* include diverse group of insect species that transfer pollen in flowering plant. Interaction between plants and pollinators is valued for increasing food production and maintaining ecosystem function to support biodiversity. (Gomez *et al.*, 2007; Ollerton,2017, Celep *et al.*, 2020).

C. borivilianum is small annual herbaceous plant which is grows wild as well as cultivated in different regions of India. Indigenous tribal people mostly collect its tubers for economic and medicinal purposes. It is one of the important ethno-medicinal herb utilized by tribal population in several districts of Maharashtra as well as different states in India. (Khairnar and Gadekar, 2019). Moreover; the studies evaluating the role of bioactive phyto-

constituents of *C. borivilianum* in nectar formation, pollinators and other fundamental ecological processes, global change etc. are being attempted by few workers. (Stevenson *et al.*, 2017; Spyros *et al.*, 2023). In India alone; different agro based field experiments have been conducted across the states so as to study the response shown by *C. borivilianum* such as increase in overall root yield, its effective conservation and management in natural habitats. (Table 2).

C. borivilianum has been categorized into critically endangered status according to the IUCN red data list. (Ved *et al.*, 2015). Due to the consistent rise in the popularity and consumption of *C. borivilianum*; and also, huge economic returns; national and international phytopharma market is expanding at rapid rate. Review of relevant literature revealed that the consistent research and developmental activities are needed especially at educational, pharmaceutical institutions and medicinal plant repositories so as to explore genetic diversity, phytopharmaceuticals/ nutraceuticals from *C. borivilianum*. (Tandon *et al.*, 2012). Moreover, countries like India; are providing subsidies for the promotion of cultivation, processing and marketing of *C. borivilianum*. (Gunjan *et al.*, 2015; Verma and Bisen *et al.*, 2020).

DISCUSSION

In India as well as across the world; from the pharmacological point of view; *C. borivilianum* serves as valuable medicinal herb with a great potential to cure many diseases. Plants like *C. borivilianum* possess great medicinal importance. Apart from their medicinal role *Chlorophytum* species have also been recognized as food source across different regions of the world. *C. borivilianum* is having great potential in treating sexual disorders like impotency and many other such ailments which could be treated in coming future. Apart from the aphrodisiac properties mostly confined to the roots; the efficacy of this important medicinal herb needs to be investigated for other attributes especially on human model.

Currently, *C. borivilianum* is categorized as critically endangered plant species by IUCN red data list. Also; due to overexploitation and lack of ecological as well as conservation perspective; the species number of *Chlorophytum borivilianum* is found to be decreasing consistently. This necessitates its study in detail; emphasizing its ecological conservation. Moreover; studies so as to understand novel gene, reproductive biology etc. are needed. Thus, more elaborative, innovative conservation approaches should be adopted to protect this plant from becoming endangered.

Table 1. Pharmacological and physiological response different organisms observed during various experiments.

Organism involved	Formulations/ Plant part used	Pharmacological/ Physiological response	Reference
Human	Root	Loss of vigour and sexual fatigue, for improving strength, Promoting the semen and sexual vigor.	Kumar <i>et al.</i> , 2004, Bansal, 2018; Khairnar and Gadekar, 2019.
	Root extract	Aphrodisiac and erectile dysfunction	Kumar and Gadhwal, 2020.
	Methanolic callus extract	pathogenic microbes and cytotoxicity against colon cancer cells.	Huang <i>et al.</i> , 2019.
Rat	Methanolic Seed extract	antioxidant and antimutagenic activity.	Rai <i>et al.</i> , 2022.
	Root extract	Maintaining normal blood glucose, insulin and lipid levels.	Giribabu <i>et al.</i> , 2014.
Cows	root powder	Stimulate lactation.	Deshwal <i>et al.</i> , 2011.
Crossbred Cows	Root extract	Antioxidant, improvement in immune response.	Devi <i>et al.</i> , 2021.
Earthworm (<i>Pheritima posthuma</i>)	Crude Spaoinin extract	Anthelmintic property against selected worms.	Sharma and Chandrul, 2017.
Fish (<i>Labeo rohita</i>)	Polysaccharide fraction	Improvement in immune response and disease resistance.	Giri <i>et al.</i> , 2015.
Yeast (<i>Saccharomyces cerevisiae</i>)	Polysaccharide fraction	Increase in the lifespan/longevity. Results to be used for studying the aging process.	Pannakal <i>et al.</i> , 2017.

Table 2. Effects of different parameters on growth and yield of *C. borivilianum*.

Region of Study	Parameters studied	Outcome of study	Reference
Karnataka, India.	Effect of bio formulations, organic and inorganic source of nutrients.	Growth in leaf area, Physiological Characters, Dry root yield.	Hiremath <i>et al.</i> , 2020.
Faizabad, Uttar Pradesh	The effect of organic manures	overall growth and root yield.	Ram <i>et al.</i> , 2014.
Bhopal, India	plant ecology, biology, collection and Use/trade parameters.	Ex situ conservation and management of plant in the natural forests.	Mishra, 2011.
Akola, Maharashtra.	Effect of inter cropping with pigeon pea (3:1).	Increase in the overall yield and economic return	Tapre <i>et al.</i> , 2021.

ACKNOWLEDGEMENT

Authors are thankful to P.G. Department of Botany, K.V. N. Naik Arts Commerce & Science College and Research Center of Botany L.V.H. College, Panchvati, Nasik, India for providing all the necessary requirements and administrative support.

AUTHOR CONTRIBUTIONS

Conceptualization, Shinde, H.P., referencing and draft preparation, Pawar, R. P. formal analysis, Nikam, P. D. technical assistance, Waghmode, A.V.

REFERENCES

- Acharya, D., Mitaine-Offer A.C., Kaushik, N. *et al.* (2009). Cytotoxic spirostane-type saponins from the roots of *Chlorophytum borivilianum*. *Journal of Natural Products*, 72(1):177-181.
- Akki, B.G. and Patil, S.H. (2006). Preliminary phytochemical investigation and *in-vitro* anti stress activity of safed musli- *Chlorophytum borivilianum*. *Indian Drugs*. 43 (11), 878-880.
- Ashraf Mehdi Farshad, Maheeran Abd Aziz, Johnson Stanslas, Ismanizan Ismail, Mihdzar Abdul Kadir (2013). Assessment of antioxidant and cytotoxicity activities of Saponin and crude extracts of *Chlorophytum borivilianum*, 10 (2), doi: 10.1155/2013/216894.
- Ashraf, M.F., Aziz, M.A., Kemat, N., Ismail, I. (2013). Effect of Cytokinin types, concentrations and their interactions on in vitro shoot regeneration of *Chlorophytum borivilianum* Sant. & Fernandez. *Electronic J. Biotechnol.* 17, 275-279.
- Bansal, Neetu (2018). Safed musli *Chlorophytum borivilianum* Review article. *MOJ Bioequivalence & Bioavailability*, 5(6):327-330.
- Bhat, M.H., Fayaz, M., Kumar, A., Jain, A.K. (2018). Phytochemical, pharmacological and nutritional profile of *Chlorophytum tuberosum* (Roxb.) Baker (Safed musli): A Review. *Int. J. Theor. Appl. Sci.* 10(1), 93-99.
- Chakraborty, G.S. and Aeri, V. (2009). Immunomodulatory activity of *Chlorophytum borivilianum*. *Pharmacology online*. 3: 54-57.
- Deore, S. L. and Khadabadi, S.S. (2007). *In vitro* antimicrobial studies of *Chlorophytum borivilianum* (Liliaceae) root extracts, *Asian J. Microbiol. Biotech. Env. Sci.* 9(4), 807-809.
- Deore, S. L. and Khadabadi, S.S. (2008a). Anti- Inflammatory and antioxidant activity of *Chlorophytum borivilianum* root extracts. *Asian J. Chem.* 20(2), 983-986.
- Deore, S. L. and Khadabadi, S.S. (2010). Isolation and characterization of phytoconstituents from *Chlorophytum borivilianum*. *Phcog Res.* 2:343-349.
- Desale, P. (2013). Safed Musli: Herbal Viagra for male impotence. *Journal of Medicinal Plants Studies*, 1(3), 91-97.
- Deshwal, R.K. and Trivedi, P. (2011). Effect of kinetin on enhancement of tuberous root production of *Chlorophytum borivilianum*. *International Journal of Innovations in Biological and Chemical Sciences*. 1:28-31.
- Devi, P., Singh, M., Somagond, Y. M., and Aggarwal, A. (2021). Alleviation of heat stress by *Chlorophytum borivilianum*: Impact on stress markers, antioxidant, and immune status in crossbred cows. *Trop. Anim. Health Prod.* 53, 351. doi:10.1007/s11250-021-02796-y.
- Geetha, K. and Maiti, S. (2002). Biodiversity of *Chlorophytum borivilianum*, Santapau & Fernandes. *International Plant Genetic Resource*. 129:52-53.

- Giri, S.S., Sen, S.S., Chi, C., Kim, H.J., Yun, S., Park, S.C., Sukumaran, V. (2015). *Chlorophytum borivilianum* Polysaccharide fraction provokes the immune function and disease resistance of *Labeo rohita* against *Aeromonas hydrophila*. *J Immunol Res.* 256510. doi: 10.1155/2015/256510.
- Giribabu, N., Kumar, K.E., Rekha, S.S., Sekaran, Muniandy, S. and Salleh, N. (2014). *Chlorophytum borivilianum* (Safed Musli) root extract prevents impairment in characteristics and elevation of oxidative stress in sperm of Streptozotocin-induced adult male diabetic Wistar rats. *BMC Compl.Alt. Med.* 14, 291.
- Gowthami, R., Sharma, N., Pandey, R., Agrawal, A. (2021). Status and consolidated list of threatened medicinal plants of India. *Genet Resour Crop Evol.* 68(6):2235-2263. doi: 10.1007/s10722-021-01199-0.
- Gunjan, M., Naing, T.W., Saini, R.S., Ahmad, A., Naidu, J.R. and Kumar, I. (2015). Marketing trends & future prospects of herbal medicine in the treatment of various disease. *World Journal of Pharmaceutical Research* 4(9): 132-155.
- Hiremath, Jagadish Chandra, Gangadharappa, P.M., Hegde, N.K., Kukanoor, L., Mastiholi. A.B. and Shiragur, Mukund, Mallikarjun Awati (2020). Role of bio-formulations in combination with inorganic and organic nutrient sources in enhancement of morpho-physiological characters and root yield in safed musli *Chlorophytum borivilianum* Sant. & Fernand. *International Journal of Ecology and Environmental Sciences* Online ISSN: 2664-7133; Print ISSN: 2664-7125.
- Huang, F., Long, Y., Liang, Q., Purushotham, B., Swamy, M.K., Duan, Y. (2019). Safed Musli *Chlorophytum borivilianum* callus-mediated biosynthesis of silver nanoparticles and evaluation of their antimicrobial activity and cytotoxicity against human colon cancer cells. *Journal of Nanomaterials.* 13;2019.
- Jha, A. and Bansal, Y.K. (2018). Estimation of some secondary metabolites from the in vitro cultures of *Chlorophytum borivilianum* Sant. et. Fern. *International Journal of Pharmacy and Pharmaceutical Sciences* ISSN- 0975-1491 Vol. 10 (1), Pp. 1-10.
- Kalra, S., Kumar, S., Lakhanpal, N., Kaur, J., Singh, K. (2013). Characterization of Squalene synthase gene from *Chlorophytum borivilianum* (Sant. and Fernand.). *Mol Biotechnol.* 54(3):944-53. doi: 10.1007/s12033-012-9645-1.
- Kaushal, N., Alok, A., Kajal, M. and Singh, K. (2021). Regeneration and genetic fidelity analysis of *Chlorophytum borivilianum* using flower stalk as explant source. *Advances in Bioscience and Biotechnology*, 12, 95-107. <https://doi.org/10.4236/abb.2021.124007>.
- Kenjale, R., Shah, R. and Sathaye, S. (2008). Effects of *Chlorophytum borivilianum* on sexual behavior and sperm count in male rats. *Phytotherapy Res.* 22(6), 796-801.
- Khairnar, Shrikant, Sanjayrao and Gadekar, Vipul Sanjay (2019). Studies on ethno botanical plants used by tribal community of Nashik district, Maharashtra, India. *Journal of Medicinal Plants Studies*; ISSN (E): 2320-3862 ISSN (P): 2394-0530 7(4): 200-202.
- Khan, M. S. A., & Ahmad, I. (2019). Herbal medicine: Current trends and future prospects. in *New Look to Phytomedicine Academic Press*,3-13.<https://doi.org/10.1016/B978-0-12-814619-4.00001X>.

- Khanam Zakia, Ompal Singh, Rampal Singh, Irshad Ul Haq Bhat (2013). Safed musli *Chlorophytum borivilianum*: a review of its botany, ethnopharmacology and phytochemistry. *J Ethnopharmacol.*,150(2):421-441. doi: 10.1016/j.jep.2013.08.064. Epub 2013.
- Kothari, S. K. and Sigh, K., (2003). Production technique for the cultivation of Safed Musli (*Chlorophytum borivilianum*). *J Hortic. Sci Biotech.* 8(2), 261-264.
- Kothari, S.K. (2004). Safed Musli (*Chlorophytum borivilianum*) revisited. *J. Med. Arom. Plant Sci.* 26, 60-63.
- Kumar, A. and Gadhwal, N. (2020). Traditional herbal medicines and their fertility potential: A Review. *Journal of Complementary and Alternative Medical Research.* 9, 24-32.
- Kumar, M., Gangwar, R., Sagar, S., Chaudhary, S., Kumar, Y., Kumar, V. (2018). Micropropagation of Safed musli (*Chlorophytum borivilianum*)- an endangered medicinal herb. *Technofame.* 7 (1), 26-31.
- Kumar, R., Suman, N.R. and Dash, S.S. (2004). Traditional uses of plants by tribals of Amarkantak region, Madhya Pradesh, Vol. 3 (4), Pp 383-390.
- Mishra, Manish (2011). Conservation of biodiversity in the natural forests of central India: A Case of Critically Endangered medicinal species safed musli in Bhopal forest (MP) India. *Bioscience Discovery*, 2(3):299-308, ISSN: 2229-3469 (Print).
- Miraj S.S. A Praveen, N., and Chaudhary, S.A. (2020).in back drop of overuse of synthetic drug ,can botanical be one of answer, a piolet study of medicinal use of Chlorophytum and curcuma by tribal in central india.ctm 6(1),75-85,doi;10.2174/2210838056661906121431220.
- Nalawade, Ajay Sarjerao Gurav, Rajaram Vithoba, Patil, Abhinandan Ravsaheb, Patwekar Mohsina, Patwekar, Faheem (2022). A comprehensive review on morphological, genetic and phytochemical diversity, breeding and bioprospecting studies of genus *Chlorophytum* Ker Gawl. from India. *Trends Phytochem. Res.* 6(1), 19-45.
- Naveen Chandra, Gajendra Singh, Shashank Lingwal, MPS Bisht, Lalit Mohan Tewari and Vinod Chandra Joshi (2022). Ecological status of Alpine medicinal and aromatic plants of Western Himalaya, *Journal of Herbs, Spices & Medicinal Plants*, 28:1, 73-88, DOI:10.1080/10496475.2021.1963903.
- Pannakal, S.T., Jäger, S., Durantón, A, Tewari, A,, Saha, S., Radhakrishnan, A., Roy, N,, Kuntz, J.F., Fermas, S., James, D., Mellor, J., Misra, N. and Breton, L. (2017). Longevity effect of a polysaccharide from *Chlorophytum borivilianum* on *Caenorhabditis elegans* and *Saccharomyces cerevisiae*. *PLoS One.* 12(7). doi:10.1371/journal.pone.0179813.
- Purohit S.D., Dave, A., Kukda, G. (1994). Micropropagation of safed musli *Chlorophytum borivilianum*, a rare Indian medicinal herb. *Plant Cell Tissue Organ Cult.* 39, 93-96.
- Rai, Jyoti, Rai, Dhananjay, Gupta, Amresh (2022). A Review on Safed musli *Chlorophytum borivilianum* Volume 9, Issue 7 (ISSN-2349-5162).
- Ram, D., Thenua, O.V.S. and Chandra, R. (2015). Effect of organic manures on plant growth and root yield of safed musli (*Chlorophytam borivilianum*) under agro-climatic condition of eastern Uttar Pradesh. *Ann. Agric. Res. New Series* Vol. 36 (1): 114-116.

- Rungsung, W., Dutta, S., Das, D., Hazra, J. (2013). A brief review on the botanical aspects and therapeutic potentials of important Indian medicinal plants. *International Journal of Herbal Medicine*. 1(3): 38-45.
- Santapau, H., and Fernandes, R. (1955). A new species of Chlorophytum from Salsette Island. *J. Bombay. Nat. Hist. Soc.* 52, 896-900.
- Sharma, G. and Kumar, M. (2012). Antioxidant and modulatory role of *Chlorophytum borivilianum* against Arsenic induced testicular impairment. *J Environ Sci (China)*. 24(12):2159-65. doi: 10.1016/s1001-0742(11)61019-x.
- Sharma, Payal and Chandrul, Kaushal K. (2017). *Chlorophytum borivilianum* (Safed musli): A vital herbal drug. *Int. J. Pharm. Med. Res.* ISSN: 2347-7008; 5(1):401-411.
- Siddaramu, Vidyashree, Uday, Kumar, Vishnu Halasahalli Venkataramaiah, Sowmyashree Krishnamurthy, Shruthi Gangur Rangaswamy, Harisha Ranganahali Puttahariyappa, Badenahally Chikkarangappa Nagaraja (2022). Herb diversity and their medicinal uses in Biodiversity conservation area of Jnanabharathi campus, Bangalore University, Karnataka. *Biological Diversity and Conservation*, 15 (1) ISSN 1308-8084 (O) 1308-5301 (P), Pp73-83.
- Singh, Rahul, Sharma, Rinku, Gorakh, Mal and Varshney, Rajat. (2022). A comparative analysis of saponin-enriched fraction from *Silene vulgaris* (Moench) Garcke, *Sapindus mukorossi* (Gaertn) and *Chlorophytum borivilianum* Santapau and Fernandes: an *in vitro* hemolytic and cytotoxicity evaluation, *Animal Biotechnology*, 33:1, 193-199, DOI:10.1080/10495398.2020.1775627.
- Spyros, Theodoridis, Evangelia, G. Drakou, Thomas, Hickler, Marco, Thines, David Nogues-Bravo (2023). Evaluating natural medicinal resources and their exposure to global change. *Lancet Planet Health* 7: e155-63.
- Stevenson, P.C., Nicolson, S.W., Wright, G.A. (2017). Plant secondary metabolites in nectar: impacts on pollinators and ecological functions. *Funct. Ecol.* 31: 65-75.
- Tandon, P., Kumaria, S., Das, M.C. (2012). Plant resources of India: potentials for future development. *Proc. Natl. Acad. Sci., India, Sect B Biol Sci*; 82(2): 283-9.
- Tapre, Varsha, Deshmukh, Swapnil, Muradi, Balkishor, Deshmukh, Amit, Pawar, Aditya and Rathod. Dhanraj. (2021). Performance of safed musli (*Chlorophytum borivilianum*) under different intercropping systems. *J Pharmacogn Phytochem* 10(1):787-789.
- Thakur, M., Connellan, P., Deseo, M.A., Morris, C., Dixit, V.K. (2011). Immunomodulatory Polysaccharide from *Chlorophytum borivilianum* roots. *Evid Based Complement Alternat Med.* 2011; 2011:598521. doi: 10.1093/ecam/neq012.
- Ved, D., Saha, D., Ravikumar, K. and Haridasan, K. (2015). *Chlorophytum borivilianum*. The IUCN Red list of threatened species 2015:e.T50126575A50131300. <http://dx.doi.org/10.2305/IUCN.UK.2015-2.RLTS.T50126575A50131300.en>.
- Verma, Ravindra, Misra, Vaibhav and Bisen, Prakash Singh. (2020). Nutritional and medicinal values of *Chlorophytum borivilianum*: Mini- review of current status and future possibilities. *Current Nutrition & Food Science*, 16, 1-8, Bentham Science Publishers.

Sustainability, Agri, Food and Environmental Research, (ISSN: 0719-3726), 11(X), 2023:
<http://dx.doi.org/10.7770/10.7770/safer-V12N1-art704>

Vyas, Ruchi, Garima, Sharma, Adya, Chaturvedi, Devki and Rashmi Sisodia (2020). GC-MS and HPLC analysis of *Chlorophytum Borivilianum* (Safed Musli), a plant from Ayurveda- herbal Viagra. *Glob J Reprod Med*. Vol. 7 (5) 5556723. DOI: 10.19080/GJORM.2020.07.5556723.

Received: 13th May 2023; Accepted: 23th September 2023; First distribution: 23th September 2023



Preliminary Phytochemical Analysis from the Bark of Plant *Boswellia Serrata* Roxb. Ex. Colebr.

Atul N. Wagh, Nandu B. Pawar, Akash K. Suryawanshi & Yahyakan A. Pathan

Department of Botany

L.V.H Arts, Science & Commerce College, Panchavati, Nashik &

J.A.T Arts, Science and Commerce College for Women, Malegaon

Email of corresponding author – atulwagh62@gmail.com

ABSTRACT:

Boswellia serrata Roxb. ex. Colebr. is one of the most primitive medicinal plant belongs to the family Burseraceae. The plant was undertaken to check phytochemical analysis based on ethnobotanical data collected from North East Region of Nashik District, Maharashtra. The bark of the plant has high medicinal value and used as anti-cancer and to cure joint pains, feet, spine, arthritis, swelling, sprains, bruises, back pain and as a stimulant for menstrual flow. The bark of the plant samples were collected from Malegaon taluka of Nashik District.

Key words – Phytochemical, Ethnobotany, *Boswellia serrata*, Medicinal

Introduction:

Phytochemical analysis of *Boswellia serrata* involves the study of the chemical components present in the plant species. *Boswellia serrata* also known as Indian frankincense, is a tree native to India, Pakistan, and the Arabian Peninsula. It has been used for centuries in traditional medicine due to its potential therapeutic properties. Phytochemical analysis aims to identify and quantify various bioactive compounds present in *Boswellia serrata*. These compounds include triterpenoids, essential oils, and flavonoids, among others. Triterpenoids, specifically boswellic acids, are considered the primary active constituents responsible for the plant's anti-inflammatory and anti-cancer properties. The analysis of *Boswellia serrata* involves extraction techniques to isolate the phytochemicals from the plant material. Different methods, such as cold extraction, hot extraction, solvent extraction or supercritical fluid extraction, may be employed to obtain the bioactive compounds. Once extracted, various analytical techniques are used to identify and quantify these compounds, including gas chromatography-mass spectrometry (GC-MS), high-performance liquid chromatography (HPLC), and nuclear magnetic resonance (NMR) spectroscopy.

The phytochemical analysis of *Boswellia serrata* helps in understanding the chemical composition of the plant and its potential bioactivity. It enables researchers to identify specific compounds responsible for the plant's medicinal properties and may aid in the development of therapeutic applications or standardized herbal preparations.

Material and Methodology

1. Extraction of powdered drugs

All the powdered drug samples were processed for the cold extraction by maceration with ultrasonication method. Five different solvents (water, methanol, ethanol, chloroform and petroleum ether) were used for the extraction. Cold extraction technique was intentionally used to restore the intactness of the phytoconstituents especially those are thermolabile in nature.

2. Experimental

For extraction, each powdered sample was weighed (20 gm) individually. These powdered samples were taken in stoppered conical flasks and 100 ml of specified solvents were added. The flasks were kept on orbital shaker for next 24 hrs with 5 min treatment of ultrasonication to each sample in between these shakings.





Sample No.	Drug quantity	Solvent used	Weight of crucible (gm)	Weight of crucible with extract (gm)	Weight of extract (gm)	Extraction yield (% w/w)
	20 gm	Water	66.13	67.53	1.4	7






Boswellia serrata	20 gm	Methanol	76.13	78.88	2.75	13.75
Roxb. ex Colebr.	20 gm	Ethanol	67.38	69.74	2.36	11.8
Roxb. ex Colebr.	20 gm	Chloroform	74.73	75.09	0.36	1.8
Roxb. ex Colebr.	20 gm	Pet. Ether	72.99	73.22	0.23	1.15



2. Preliminary Phytochemical Analysis

Above prepared extracts of each drug were used for preliminary phytochemical analysis. In this, chemical tests for the detection of some primary metabolites (carbohydrate, amino acid, protein, lipid and starch) and secondary metabolites (alkaloids, flavonoids, tannins, saponins, glycosides) were done.

Results for [Boswellia serrata Roxb. ex Colebr.](#)

Test for	Test	Observation	Inference	Pic of the test
Primary Metabolites -				
Carbohydrate	Molisch's test (General test) To 2-3 ml aqueous extract, add few drops of alpha-naphthol solution in alcohol, shake and add conc. H ₂ SO ₄ from side of the test tube.	Violet ring is formed at the junction of two liquids.	Present	
Amino Acid	Ninhydrin test (General test) Heat 3 ml T.S. and 3 drops 5% Ninhydrin solution in boiling water bath for 10 min.	Purple / bluish colour appears.	Present	
Protein	Biuret test (General test) To 3 ml T.S. add 4% NaOH and few drops of 1% CuSO ₄ solution.	Violet or pink colour not appeared.	Absent	
Lipid	Extract dropout on filter paper drought comes then lipids are present.	No permanent stain on filter paper	Absent	

Starch	Iodine test: Mix 3 ml test solution and few drops of dilute iodine solution. Blue colour appears, it disappears on boiling and reappears on cooling.	Blue colour does not appear	Absent	
Secondary Metabolites				
Alkaloids	Evaporated the aqueous, alcoholic and chloroform extracts separately. To residue, dilute HCl added. After shaking well and filtration, using filtrate, following test was performed.			
	Wagner's test 2-3 ml filtrate with few drops Wagner's reagent gives reddish brown ppt.	Reddish brown ppt	Present	
Flavonoids	Shinoda Test To dry powder or extract, add 5 ml 95% ethanol/t-butyl alcohol, few drops conc. HCl and 0.5 g magnesium turnings. Orange, pink, red to purple colour appears.	Orange red colour observed	Present	
Tannins	5% FeCl₃ solution	Deep blue-black colour	Present	
Saponins	Add water into sample and shake for 15 sec.	Foam is observed	Present	

Glycosides	Legal's test (Test for cardenoloids) To aqueous or alcoholic extract, add 1 ml pyridine and 1 ml sodium nitroprusside.	Pink to red colour appeared	Present	
	Test for deoxy sugar (Keller-Killiani test) To 2 ml extract, add glacial acetic acid, one drop 5% FeCl ₃ and conc. H ₂ SO ₄ . Reddish brown colour appears at junction of the two liquid layers and upper layer appears bluish green.	No reddish brown colour appears at junction of the two liquid layers.	Absent	

Result and Discussion

The specific phytochemical profile of *Boswellia serrata* can vary depending on factors such as geographical location, climate, and extraction methods used. Phytochemical analysis helps in determining the composition and concentration of these bioactive compounds, which in turn provides insights into the potential therapeutic applications.

The plant samples were tested to check the presence and absence of primary and secondary metabolites present in *Boswellia serrata*. The powdered drug sample was processed for cold extraction by maceration with ultrasonication method. Five different solvents (water, methanol, ethanol, chloroform and petroleum ether) were used for the extraction. Cold extraction technique was intentionally used to restore the intactness of the phytoconstituents especially those are thermolabile in nature. Carbohydrate, Amino Acid shows the presence, where Protein, Lipid and Starch is absent in bark of plant *Boswellia serrata*. Alkaloids, Flavonoids, Tannins, Saponins, Glycosides are present in Legal's test and absent in test for deoxy sugar (Keller-Killiani test).

References

- P. K. Mukherjee, Quality control of herbal drugs, Second reprint 2007, Business Horizons, New Delhi, 379-425
- K. R. Khandelwal, V. Sethi, Practical Pharmacognosy, 24th edition, Nirali Prakashan, Pune, 25.1-25.9.
- 2. Felter H, Lloyd J. I and II. Cincinnati: Ohio Valley Company, US; 1898. Kings American Dispensatory. [[Google Scholar](#)]
- 3. Howes FN. Age-old resins of the Mediterranean region and their uses. Econ Bot. 1950;4:307-16. [[Google Scholar](#)]
- 4. Krishnamurthy T, Shiva MP. Salai guggul (from *Boswellia serrata* Roxb.): Its exploitation and utilization. Indian Forest. 1977;103:466-74. [[Google Scholar](#)]
- 5. Verghese J. Olibanum in focus. Perfumer Flavorist. 1988;13:2-11. [[Google Scholar](#)]
- 6. Holmes P. Frankincense oil. Int J Arom. 1999;9:56-61. [[Google Scholar](#)]
- 7. Maupetit P. New constituents in olibanum resinoid and essential oils. Perfumer Flavorist. 1984;9:19-37. [[Google Scholar](#)]
- 8. Leung AY, Foster S. 2nd ed. New York: John Wiley and Sons; 1996. Encyclopedia of common natural ingredients used in food, drugs and cosmetics; pp. 389-91. [[Google Scholar](#)]
- 9. Wallis TE. 5th ed. London: J and A Churchill Limited; 1967. Textbook of Pharmacognosy; pp. 500-1. [[Google Scholar](#)]
- 10. Evans WC. 14th ed. London: WB Saunders Company Ltd; 1996. Trease and Evans Pharmacognosy; p. 289. [[Google Scholar](#)]
- 11. Chiavari G, Galletti GC, Piccaglia R, Mohamud MA. Differentiation between resins from *Boswellia carterii* and *Boswellia frereana* (Frankincense) of Somali region. J Essential Oil Res. 1991;3:185-6. [[Google Scholar](#)]
- 12. Sharma RA, Verma KC. Studies on gum obtained from *Boswellia serrata* Roxb. Indian Drugs. 1980;17:225. [[Google Scholar](#)]

-
- 13. Bhuchar VM, Agarwal AK, Sharma SK. Constituents of gum obtained from *Boswellia serrata* exudates. *Indian J Technol.* 1982;20:38. [[Google Scholar](#)]
 - 14. Gangwal ML, Vardhan DK. Carbohydrate contents of *Boswellia serrata*. *Asian J Chem.* 1995;7:677. [[Google Scholar](#)]
 - 15. Sharma S, Thawani V, Hingorani L. Pharmacokinetic study of 11-keto-beta-boswellic acid. *Phytomedicine.* 2004;11:255–60. [[PubMed](#)] [[Google Scholar](#)]

10.5958/0976-4755.2024.00124.4

BIOINFOLET 21 (3) : 412 - 416, 2024

CONVOLVULACEAE JUSS FROM SATMALA-CHANDWAD HILLS, NASHIK, MAHARASHTRA, INDIA.

Swapnil. D.Wagh, Atul. N. Wagh* and Manoj. T. Patil

KKHA Arts, SMGL Commerce & SPHJ Science College Chandwad, Dist. Nasik. India. 423101.

*MSG's Arts, Science & Commerce College, Malegaon Camp, Malegaon. Dist. Nasik. India. 423105

Email : swapnildwagh@gmail.com

ABSTRACT

Present paper gives an account of 15 taxa belonging to 07 genera of family *Convolvulaceae* Juss. *Ipomoea* L. is the largest genera with 08 taxa. Description of each taxon is provided with flowering-fruitlet, location, exsiccata, field note and photo.

Key words : Flora, Convolvulaceae, Satmala Hills.

Introduction:

Convolvulaceae Juss. is also known as Morning Glory Family. Its habit ranges from herb to woody vines, rarely tree. The family is represented by 2000 taxa and 58 genera all over the world (Staple and Yang, 1998). In India the family is represented by 158 taxa belonging to 20 genera (Oudhia, 2001). *Ipomoea* L. and *Convolvulus* L. are the major genera comprising third of the one total taxa (Conquist, 1988). In India taxa of the family distributed in the state of Bengal, Maharashtra, Gujarat, Goa, Karnataka, and Chhattisgarh (Undirwade et al, 2015). Lakshminarasimhan and Sharma (1991) documented 7 taxa in Flora of Nashik district. However, as sufficient literature is not available from Nashik district, present survey was undertaken in Chandwad-Satmala region to study the diversity of species belonging to family *Convolvulaceae* Juss

Material and Methods:

Field tours were conducted in study area to document the taxa of family *Convolvulaceae* Juss. Collected taxa were identified and confirmed with the help of local floras and available literature (Lakshminarasimhan and Sharma,

1991; Singh and Karthikeyan, 2001a, 2001b). Botanical names and citations were checked with the help of database plants of the world online (POWO). Herbariums of taxa were prepared by following standard method of Jain and Rao (1977). One set of herbarium sheets have been deposited to BSI Pune and SNJB's ACS College Chandwad.

Results and Discussion:

Description of all 15 taxa is given below

Argyreia sericea Dalz. & Gibs. Bombay. Fl. 169. 1861; C. B. Cl. in Hook. f. Fl. Brit. India 4: 188. 1883; Cooke, Fl. Pres. Bombay 2: 326. 1958 (Repr.); Singh et al., Fl. Maharashtra, Dicot. 2: 446. 2001.

Twiner, height 03-05 m. Leaves 04-07 x 03-05 cm, alternate, petiole 02 cm long, densely pubescent above, lower surface silky, apex acuminate, cordate base, margin wavy. Stem twinning, densely white silky, terete. Inflorescence capitate cyme, 04 cm long peduncle, flowers 06 in number, corolla 04 cm long, colour pink, calyx densely silky hairy.

Flowering and Fruiting: Almost throughout the year

Localities: Koldher, Sadetin Rodaga, Indrai

Exsiccata: SDW-1060

Notes: It grows inside bushes as well as spreading on ground.

Cuscuta cassyroides Nees ex Engelm. Trans. Acad. Sci. St. Louis 1: 513 (1859); *Cuscuta reflexa* Roxb. Pl. Cor. 2: 3, t. 104. 1798; C.B.Cl. in Hook. f. Brit. India 4: 225. 1883; Cooke, Fl. Pres. Bombay 2: 292. 1958 (Repr.); Yuncker in Mem. Torr. Bot. Club 18: 259, f. 130 & 130, A–F. 1932; Sant. & Patel in J. Bombay nat. Hist. Soc. 54 :712, f. A, 1-7. 1957; P. K. Bhattacharya & S. K. Mukerjee in Ind. J. For. 1: 162. 1978; Singh et al., Fl. Maharashtra, Dicot. 2: 492. 2001.

Parasitic twiner, stem terete, colour yellow, with red marks on surface, flowers pedicellate, 06-09 mm in length, bracteate in cymose clusters, pedicels 02-03 mm in length, somewhat fleshy, corolla white in colour, infundibuliform, length 06-09 mm, margin of corolla somewhat wavy, stamens short in length than corolla tube, seeds suborbicular, 01-02 in numbers.

Flowering and Fruiting: December-April

Localities: Indrai

Exsiccata: SDW-1208

Notes: It twinning on *Bauhinia* sp & *Ficus* sp.

Dinetus racemosus (Roxb.) Sweet. Brit. Fl. Gard. 2: t. 127. (1825); *Porana racemosa* Roxb. Fl. Ind. 2:41. 1824; Sharma et al. in Bio. Mem. 2 (1 & 2) : 97. 1977. *P. malabarica* C. B. Cl. in Hook. f. Fl. Brit. India 4: 223. 1883; Cooke, Fl. Pres. Bombay 2: 294. 1958 (Repr.); Singh et al., Fl. Maharashtra, Dicot. 2: 480. 2001.

Twiner, height 30-40 cm. Leaves 03-06 x 02-04, alternate, ovate, margin entire, acuminate apex, base deeply cordate, slightly pubescent above, petiole 02 cm long. Stem twinning, terete, pubescent. Inflorescence panicle, leafy bracts. Flower pink in colour, pedicel 01 cm in length, capsule 0.8 cm long.

Flowering and Fruiting: November-December

Localities: Sadetin Rodaga, Indrai

Exsiccata: SDW-1045

Notes: It grow on soil rich moist places on hill slopes.

Evolvulus alsinoides (L.) L. Sp. Pl. ed. 2, 2: 392. 1762; C.B.Cl. in Hook. f. Fl. Brit. India 4: 220. 1883; Cooke, Fl. Pres. Bombay 2: 297. 1958 (Repr.); Austin & Ghazanfar in Nasir & Ali,

Fl. W. Pak. 126: 32, f. 5, A–B. 1979; Austin in Dassan. & Fosb. Rev. Handb. Fl. Ceylon 1:309. 1980. *Convolvulus alsinoides* L. Sp. Pl. 157. 1753; Singh et al., Fl. Maharashtra, Dicot. 2: 453. 2001.

Herb, height 15-20 cm. Leaves 01-1.8 x 0.4-0.5 cm, alternate, elliptic, obovate, pubescent on surface, apex acute, base acute, petiole 0.1 cm long, margin entire & ciliate. Stem sub erect or prostrate, quadrangular, silky pubescent. Flowers solitary, axillary, pedicel 1.5 cm long, colour blue.

Flowering and Fruiting: July-December

Localities: Baladya, Sadetin Rodaga, Indrai, Chandreshwari, Koldher

Exsiccata: SDW-23

Notes: It grows on gravelly hill slopes and in rock crevices.

Ipomoea biflora (L.) Pers. Syn. Pl. 1. 183. 1805; *Ipomoea sinensis* (Desv.) Choisy in Mem. Phys. Soc. Geneve 6: 459. 1834. *Convolvulus chinensis* Desv. in Lam. Encycl. 3: 557. 1791. *Ipomoea calycina* C. B. Cl. in Hook. f. Fl. Brit. India 4: 201. 1883; Cooke, Fl. Pres. Bombay 2: 311. 1958 (Repr.); Singh et al., Fl. Maharashtra, Dicot. 2: 471. 2001.

Annual herb, prostrate or twining, stem pilose, 2.4 cm in length. Leaves simple, triangular to ovate, petiole 02-04 cm in length, margin entire, cordate at base with round basal lobes, 01 to 03 flowered cymose inflorescence, corolla funnel shaped, white in colour, 06-08 mm long, ovary conical type, style short, stigma purplish capsule globose, glabrous.

Flowering and Fruiting: October-December

Localities: Indrai, Sadetin Rodaga, Rawalya, Chandreshwari

Exsiccata: SDW-1010

Notes: It grows inside bushes

I. cairica (L.) Sweet, Hort. Brit. 287. 1827; Sant. in Rec. Bot. Surv. India 16(1): 193. 1953; Naik, Fl. Marathwada 1: 586. 1998. *Convolvulus cairicus* L. Syst. ed. 10: 922. 1759. *Ipomoea palmate* Forssk. Fl. Aeg.–Arab. 43. 1775; C.B.Cl. in Hook. f. Fl. Brit. India 4: 214. 1883; Singh et al., Fl. Maharashtra, Dicot. 2: 485. 2001.

Twiner, height 30-40 cm. Leaves 03-06 x 04-06 cm, alternate, palmately compound, cut into 05

deep lobes. Stem twinning, angular, branched. Flowers colour violet, corolla funnel shaped, 4.5 cm long. Capsule 01 cm across.

Flowering and Fruiting: September-October

Localities: Chandreshwari, Baladya

Exsiccata: SDW-325

Notes: It grows on middle plateaus near old walls.

I. eriocarpa R. Br. Prodr. 484. 1810; C. B. Cl. in Hook. f. Fl. Brit. India 4: 204. 1883; Cooke, Fl. Pres. Bombay 2: 312. 1958 (Repr.); Ooststr. in Steenis, Fl. Males. 1, 4: 462, f. 35. 1953; Austin & Ghazanfar in Nasir & Ali, Fl. W. Pak. 126: 41, f. 6, A–B. 1979; Singh et al., Fl. Maharashtra, Dicot. 2: 463. 2001.

Twiner, height 0.5-01 m. Leaves 03-06 x 01-2.5 cm, pubescent on both surface, apex acuminate, base cordate, petiole 01-03 cm long, margin entire. Stem twinning, pubescent, terete. Inflorescence axillary cyme, flowers white in colour. Capsules 0.4 x 0.3 cm, densely hairy at apex.

Flowering and Fruiting: September-October

Localities: Rajdher, Sadetin Rodaga, Chandreshwari, Baladya

Exsiccata: SDW- 890

Notes: It grows inside bushes.

I. hederifolia L. Syst. Nat. ed. 10. 925. 1759; Austin & Ghazanfar in Nasir & Ali, Fl. W. Pak. 126: 43. 1979. *I. coccinea* auct. non L. 1753; C.B.Cl. in Hook. f. Fl. Brit. India 4: 199. 1883. *Quamoclit coccinea* Moench. Method. 453. 1795; Cooke, Fl. Pres. Bombay 2: 330. 1958 (Repr.); Singh et al., Fl. Maharashtra, Dicot. 2: 463. 2001.

Twiner, height 0.5-1.3 m. Leaves 2.5-4.5 x 03-05 cm, alternate, ovate, acuminate at apex, cordate at base. Stem twinning, angular. Flowers in lax cyme, red in colour, corolla 03 cm long. Capsules 0.4 x 0.4 cm.

Flowering and Fruiting: October-November

Localities: Chandreshwari

Exsiccata: SDW- 335

Notes: It twinning on branches of *Acacia* sp.

I. nil (L.) Roth, Cat. Bot. 1: 36. 1797; Ooststr. in Steenis, Fl. Males. 1, 4: 465. 1953; Austin in Dassan. & Fosb. Rev. Handb. Fl. Ceylon 1: 332. 1980. *Convolvulus nil* L. Sp. Pl. ed. 2. 219.

1762. *Ipomoea hederacea* auct. non Jacq. 1786; C.B.Cl. in Hook. f. Fl. Brit. India 4: 199. 1883; Cooke, Fl. Pres. Bombay 2: 321. 1958 (Repr.); Singh et al., Fl. Maharashtra, Dicot. 2: 465. 2001.

Twiner, height 01-02 m. Leaves 05 x 04 cm, alternate, ovate, acuminate apex, deeply cordate base, petiole 04 cm long, upper surface hairy, margin entire. Stem twinning, soft, terete, pilose. Inflorescence 03-04 flowered cyme, peduncle 07 cm long, pedicel 01 cm long. Flower colour magenta.

Flowering and Fruiting: September-October

Localities: Rawalya, Baladya, Sadetin Rodaga, Chandreshwari, Rajdher.

Exsiccata: SDW- 175

Notes: It grows inside *Euphorbia* sp.

I. ochracea (Lindl.) Sweet. Hort. Brit., ed. 2: 371 (1830); *Convolvulus trichocalyx* Schumach. & Thonn. C.F.Schumacher, Beskr. Guin. Pl.: 91 (1827); *I. clarkei* Hook. f. Fl. Brit. India 4: 734. 1885; Cooke, Fl. Pres. Bombay 2: 314. 1958 (Repr.); Billore & Singh in Indian Forester 98: 147. 1972; Singh et al., Fl. Maharashtra, Dicot. 2: 460. 2001.

Twiner, prostrate, height 01-1.5 m. Leaves 1.5-2.5 x 1.5-02 cm, alternate, apex acuminate, cordate base, pubescent on both surface, petiole 01-1.5 cm long. Inflorescence axillary 01-02 flowered cyme, peduncle 02-3.5 cm in length, pubescent, corolla yellow in colour, 3.5 cm long, funnel shaped.

Flowering and Fruiting: July-August

Localities: Baladya

Exsiccata: SDW-488

Notes: It hanging on cliffs.

I. obscura (L.) Ker–Gawl. Bot. Reg. 3, t. 239. 1837; C.B.Cl. in Hook. f. Fl. Brit. India 4: 207. 1883; Cooke, Fl. Pres. Bombay 2:317. 1958 (Repr.); Naik, Fl. Marathwada 1: 591. 1998. *Convolvulus obscurus* L. Sp. Pl. ed. 2: 220. 1762. *Ipomoea curassavica* All. Auct. Syn. 10. 1773; Dandy in Taxon 19: 622. 1970; Singh et al., Fl. Maharashtra, Dicot. 2: 466. 2001.

Climbing herb, 01-1.5 m. Leaves 02-04 x 02-04 cm, alternate, orbicular, cordate at base, acuminate at apex, hairy on both surfaces, petiole 01-04 cm long, hairy. Stem erect, branched, angular, hairy. Flowers axillary,

peduncle 02-06 cm long, corolla white.

Flowering and Fruiting: August-January

Localities: Sadetin Rodaga, Koldher

Exsiccata: SDW- 721

Notes: It grows under shady places.

I. parasitica (Kunth) G. Don in Cooke, Fl. Pres. Bombay 2: 294. 1958 (Repr); *Convolvulus parasiticus* Kunth. F.W.H.von Humboldt, A.J.A.Bonpland & C.S.Kunth, Nov. Gen. Sp. 3: 163 (1819); *Pharbitis parasitica* (Kunth) V.M. Badillo H.F. Pittier & al., Cat. Fl. Venez. 2: 321 (1947).

Twiner, stem woody at base & herbaceous at upper portion, cylindrical, hollow. Leaves simple, alternate, 04-20 x 02-18 cm, shape ovate, acuminate at apex, base cordate, flowers axillary, inflorescence few flowered cyme, peduncle hairy, up to 25 cm long, capsules ovate to globular, seeds black in colour, 04.

Flowering and Fruiting: September-October

Localities: Chandreshwari Plateau

Exsiccata: SDW- 268

Notes: It grows near seasonal ponds.

I. triloba L. Sp. Pl. 161. 1753; Ooststr. in Steenis, Fl. Males. 1, 4: 468, f. 41. 1953; Fernandes et al. in J. Bombay Nat. Hist. Soc. 52: 661. 1954; Austin in Dassan. & Fosb. Rev. Handb. Fl. Ceylon 1: 341. 1980; Singh et al., Fl. Maharashtra, Dicot. 2: 472. 2001.

Herb, height 01-02 m. Leaves 2.4-5.4 x 2.5-04 cm, alternate, triangular, three lobed, apex acute, base cordate, margin entire. Stem angular, twinning, hairy. Inflorescence axillary cyme, flowers pink in colour, corolla 01-1.5 cm in length. Capsule 0.4 cm in length.

Flowering and Fruiting: September-December

Localities: Chandreshwari Plateau.

Exsiccata: SDW- 571

Notes: It grows in open grasslands

Rivea hypocrateriformis (Desr.) Choisy in Mem. Soc. Phys. Geneve 6: 408. 1834; C. B. Cl. in Hook. f. Fl. Brit. India 4: 184. 1883; Cooke, Fl. Pres. Bombay 2: 323. 1958 (Repr.); Austin & Ghazanfar in Nasir & Ali, Fl. W. Pak. 126: 60, t. 8, D-E. 1979. *Convolvulus*

hypocrateriformis Desr. in Lam. Encycl. 3: 561. 1792; Singh et al., Fl. Maharashtra, Dicot. 2: 480. 2001.

Climber, height 02-03 m. Leaves 1.5-3.5 x 02-03 cm, alternate, upper surface glabrous, lower surface pubescent, obtuse apex, cordate base, undulate margin, petiole 01-02 cm

long. Stem stout, hairy, terete. Flower single, white, calyx ovate-oblong in shape, apex obtuse. Capsule 0.9-0.11 cm in diameter.

Flowering and Fruiting: September-October

Localities: Chandreshwari, Rahud Ghat

Exsiccata: SDW- 662

Notes: It grows inside *Euphorbia* sp.

Stictocardia tiliifolia (Desr.) Hallier. f. Bot. Jahrb. Syst. 18: 159 (1893); *I. campanulata* L. Sp. Pl. 160. 1753; Cooke, Fl. Pres. Bombay 2: 316. 1958 (Repr.); Austin et al. in Brittonia 30: 196. 1978. *I. campanulata* var. *illustris* C. B. Cl. in Hook. f. Fl. Brit. India 4: 211. 1883. *I. illustris* (C. B. Cl.) Prain, Bengal Pl. 2: 735. 1903; Ooststr. In Steenis, Fl. Males. 1, 4: 485. 1953; Naik, Fl. Marathwada 1: 589. 1998.

Twiner, height 02-03 m. Leaves 07-10 x 05-08 cm, alternate, orbicular, acuminate apex, base cordate, petiole 2.5 cm long, undulate margin, leaf surface glabrous. Stem twinning, terete, woody. Inflorescence axillary cyme, flowers 06-08 in number, corolla purple in colour with dark centre, pedicellate, peduncle 06 cm long.

Flowering and Fruiting: September-October

Localities: Sadetin Rodaga, Koldher

Exsiccata: SDW- 1064

Notes: It grows near seasonal streams

References:

Cronquist A, (1988). "The Evolution and Classification of Flowering Plants", 11nd Ed. NYBG, New York, U.S.A

Jain, S.K. and Rao, R.R. (1976). "A Hand Book of Field and Herbarium Methods". Today and Tomorrow's Printers and Publishers, New Delhi. pp. 157

Lakshminarasimhan, P. and B.D. Sharma. (1991). "Flora of Nasik District". Botanical Survey of India, Calcutta. pp. 644

Oudhia P. 2001. "Major *Ipomoea* species of